UNIVERSITY OF CALIFORNIA SAN DIEGO

Toward Precise Statistical Inference in Spatial Environmental Epidemiology

A Dissertation submitted in partial satisfaction of the requirements
for the degree Doctor of Philosophy

in

Biostatistics

by

Kristen Antonia Hansen

Committee in charge:

Professor Tarik Benmarhnia, Co-Chair
Professor Armin Schwartzman, Co-Chair
Professor Yoav Freund
Professor Wendy Meiring
Professor Loki Natarajan
Professor Xinlian Zhang

2022

The Dissertation of Kristen Antonia Hansen is approved, and it is acceptable in quality and form for publication on microfilm and electronically.

University of California San Diego

2022

DEDICATION

This dissertation is dedicated to my parents and my husband Alain, a rock-solid support system with a dash of tough love. Teaching me to apply myself and learn independently but recognize my weaknesses as changeable with hard work. And that it is not a wrong

TABLE OF CONTENTS

LIST OF FIGURES

LIST OF TABLES

ACKNOWLEDGEMENTS

Chapter 1, in full, is in revisions at Environmental Research Letters, Kristen Hansen Lara Schwarz, Anais Teyton, Armin Schwartzman, Tarik Benmarhnia. The dissertation author was the primary investigator and author.

Chapter 2, in full, is a reprint of the material as is appears in PNAS 2021. Kristen Hansen, Lara Schwarz*, Anna Alari, Sindana Ilango, Nelson Bernal, Rupa Basu, Alexander Gershunoc, and Tarik Benmarhnia. The paper title is "Spatial variation in the joint effect of extreme heat events and ozone on respiratory hospitalizations in California". Kristen Hansen was the co-primary contributor and writer to this paper along with Lara Schwarz.

Chapter 3, in full, is currently being prepared for submission for publication of the material, Kristen Hansen; Armin Schwartzman; Tarik Benmarhnia. The dissertation author was the primary researcher and author of this paper.

Chapter 4, in part is currently being prepared for submission for publication of the material. Kristen Hansen; Armin Schwartzman; Tarik Benmarhnia. The dissertation author was the primary researcher and author of this material.

VITA

2017 Bachelor of Arts in Statistics and Psychology, University of Minnesota, Morris

2022 Doctor of Philosophy in Biostatistics, University of California San Diego

PUBLICATIONS

Hansen, K., Hasenstab, K., & Schwartzman, A. (2021). Estimating Mountain Glacier flowlines by local linear regression gradient descent. *IEEE Transactions on Geoscience and Remote Sensing*, *59*(12), 10022–10034. https://doi.org/10.1109/tgrs.2020.3035513

Hansen, K., Schwarz, L., Alari, A., Ilango, S. D., Bernal, N., Basu, R., Gershunov, A., & Benmarhnia, T. (2021). Spatial variation in the joint effect of extreme heat events and ozone on respiratory hospitalizations in California. *Proceedings of the National Academy of Sciences*, *118*(22). https://doi.org/10.1073/pnas.2023078118

Aguilera, R., **Hansen, K**., Gershunov, A., Ilango, S. D., Sheridan, P., & Benmarhnia, T. (2020). Respiratory hospitalizations and wildfire smoke: A spatiotemporal analysis of an extreme firestorm in San Diego County, California. *Environmental Epidemiology*, *4*(5). https://doi.org/10.1097/ee9.0000000000000114

Baxter, S. L., Lander, L., Clay, B., Bell, J., **Hansen, K.,** Walker, A., & Tai-Seale, M. (2022). Comparing the use of dynamed and uptodate by physician trainees in clinical decision-making: A randomized crossover trial. *Applied Clinical Informatics*, *13*(01), 139–147. https://doi.org/10.1055/s-0041-1742216

Eyler, L. T., Aebi, M. E., Daly, R. E., **Hansen, K**., Tatsuoka, C., Young, R. C., & Sajatovic, M. (2019). Understanding aging in bipolar disorder by Integrating Archival Clinical Research Datasets. *The American Journal of Geriatric Psychiatry*, *27*(10), 1122–1134. https://doi.org/10.1016/j.jagp.2019.04.003

Alari A, Schwarz L, Chen C, **Hansen K**, Chaix B, Benmarhnia T. The role of ozone as a mediator in the relation between heat waves and mortality in 15 French urban agglomerations. American Journal of Epidemiology [In Press]

ABSTRACT OF THE DISSERTATION

Toward Precise Statistical Inference in Spatial Environmental Epidemiology

by

Kristen Antonia Hansen

Doctor of Philosophy in Biostatistics

University of California San Diego, 2022

Professor Tarik Benmarhnia, Co-Chair
Professor Armin Schwartzman, Co-Chair

Climate change has been identified as one the main public health challenges of this century and quantifying how different communities are affected is crucial to inform local adaptation strategies. While the number of empirical studies reporting the harmful health effects of climate-sensitive exposures has drastically increased in the past few years, methodological discussions and developments have mostly focused on time trends as a source

of bias. However, other methodological challenges remain. One particular source of bias that received little attention in this area of research is related to spatial confounding. Furthermore, while most communities are exposed to climate-sensitive exposures such as extreme heat or ozone peaks, an important spatial heterogeneity regarding such exposures and related effect estimates may exist but approaches to handle such challenges remain underused or underdeveloped in this field. In the past decade, there has been growing interest in developing causal inference methods to answer various etiological questions such as mediation analyses to understand the mechanisms which through a given exposure may lead to a health outcome. Yet, little effort has been dedicated to incorporating spatial techniques when implementing such causal inference methods. Finally, an important mismatch can exist in regards to the scale at which environmental exposures and health data may be available which prevents an optimal identification of environmental-health patterns at a fine scale. Downscaling methods are quite common in many fields including climate sciences but have not been adapted yet to environmental health issues so empirical evidence can be available at the finest spatial resolution.

In this dissertation we work toward precise analysis in this setting to advance spatial statistics in the context of climate and health research questions. First, we employ the combination of within-community matched design and Bayesian Spatial Hierarchical models to estimate at the zip code level the hospitalization burden of extreme heat events of varying definitions. Then we take a step into spatial causal inference to develop a procedure to estimate spatially varying estimates of mediation effects. And finally, we work toward a more ideal data setting through downscaling approaches coupled with machine learning algorithms,

making the use of and adapting methods from Remote Sensing research to perform these tasks.

INTRODUCTION

Climate is one of the biggest public health issues facing the world in this century (Romanello et al 2021). Still, not enough is understood about the effect of climate and human health especially in regard to how such impacts may vary over space. Although climate-sensitive exposures and health are interrelated in diverse ways, the public is mostly familiar with only the health effects of extreme weather and heat due to climate change. Air pollutants, temperature and humidity are examples of environmental exposures that are changing rapidly and in divergent ways in different areas of the world. It is important to not only understand impacts of the extremes of climate but to estimate the synergistic and compounded impacts on our communities at a local scale. These effects are spatially heterogeneous across different communities and thus need to be studied spatially.

First, and perhaps foremost there is a need for effect estimates of extreme weather events and compounded impacts at as low a spatial scale as possible. To get these spatial estimates spatial confounding must be accounted for within the modeling procedure. Spatial confounding has different definitions depending on the field of study. In this field, spatial confounding is a type of unmeasured confounding that can bias effect estimates. It arises due to spatial variability in the covariates, both measured and unmeasured, that are not adequately accounted for in the modeling paradigm for a particular research question. In particular, the spatial nature of a covariate cannot be ignored within any predictive or inferential model as the spatial covariance of those variables will introduce bias to the effect estimates. Thus, for any model in

environmental epidemiology the spatial covariance of the dependent and independent variables must be included. This means that the models that are used cannot be the same models that are used for individual level data but must be spatial statistical models if we want accurate effect estimates at a small scale.

In addition to the need for small scale effect estimates there is an increased interest in causal inference for these data. The emergence of spatial causal inference as a subfield is ongoing, but in causal inference for epidemiology, mediation is especially popular. Mediation analysis is the study of effect decomposition of an exposure into two effects. A direct effect of an exposure on an outcome of interest and an indirect effect of an exposure on that outcome through a mediator. This is an important causal graph to estimate in climate change and health studies because we expect effects of environmental exposures to be mediated by spatially varying variables. For instance, the effect of extreme heat on hospitalizations can reasonably be expected to be mediated by ozone. Simplistically, ozone (O_3) is created when heat and NO_2 mix. Furthermore, NO_2 is spatially varying because it is a common pollutant of gasoline powered cars. Thus, spatial confounding could be a problem when using mediation analysis methods that do not account for spatial covariance. To date, this spatial problem has not been addressed. Mediation analysis must be extended to the use of spatial statistical models such that spatial confounding does not bias the effect estimates.

Beyond the need for small-scale effect estimates and spatial causal inference in environmental epidemiology, there is a spatial data problem. Using spatial statistical models for public health data is not as simple as implementing these models and current literature does not

address this. Spatial data for public health problems is at a scale that is far from ideal. Though most public health studies are conducted on an individual level, observational environmental health studies must be conducted in an aggregate. Health data for spatial environmental epidemiology is provided from government agencies that must adhere to privacy constraints set forth by HIPAA (Health Insurance Portability & Accountability Act). This means the data is not truly even spatial when provided. Zip codes are the only georeferencing in the data. This is a complication for two reasons. Not only is zip code data not truly spatial because zip codes are merely road maps and have only been assigned geographic meaning because of post processing from Tigris, but also, zip codes are not regular in any sense. Zip code population numbers vary widely, they are not continuous over space and are incredibly variable in size. Although, there are a plethora of problems with spatial health data, it does not change the fact that this data is what researchers have access to without millions of dollars to study a small subset of people in a single place, which would disadvantage those communities that do not have universities or agencies funding research therein. This means that methods like downscaling prove to be important techniques to consider. Downscaling is the process of taking non-ideal spatial scale data and decreasing the scale by fitting predictive models. Downscaling as a method exists in a variety of fields but has not been adequately explored with data of this type in epidemiology and public health as it relates to climate-sensitive exposures.

The combination of these spatial data problems showcases that methods development in spatial environmental epidemiology is incredibly important and not addressed adequately. This perfectly highlights the disconnect that exists between the relevant fields to these problems. Particularly between public health researchers and statisticians. Statisticians have been

developing spatial statistical methods for decades but not with this type of data. Statisticians have made great strides in Random Field theory, Image Processing, and climate modeling among other fields, but these subfields all rely on gridded and regular datasets or point processes like disease case locations, which just isn't possible in Public Health observational studies. Data scientists, as well, decree that zip code data should never be used for a geostatistical study. But the spatial nature of the environmental epidemiology data cannot be ignored either.

Therein lies the big question: if these public health researchers are to not utilize the spatial information in the data they have because it is not good enough for a spatial statistical study, but also not treat it as if it were independent samples, as that will bias the results of any model, what are they to do?

In this dissertation, I step into this maelstrom. I adapt and extend existing methodology from other fields as well as produce novel approaches to deal with some of these issues because these research problems need to be solved if we are to produce high quality estimates of effects of climate-sensitive exposures on the health of those individuals in our communities locally, across regions, and the world. This dissertation serves as a start and continuation of a long research process. This work is important to explore even if the research at this stage lacks elegance or provability, the way mathematicians and theoretical statisticians prefer. To get to that stage, research must start with messy problems and deficient data.

In Chapter 1, we will discuss a novel extension of the Bayesian hierarchical model framework to the spatial domain to get estimates of heat effects on hospitalizations. This method

extends within-community matched designs for observational studies combined with Bayesian modeling as well as classification through rank and meta-regression to understand the effects of this environmental exposure on the people in California communities on a fine scale. Chapter 2 shows an application of this combined method for the estimation of joint ozone and heat effects in California. Chapter 3 extends the causal inference mediation literature to a spatial domain for the first time using the combination of existing methods and a simulation study to determine the effectiveness of said approach on current data. Chapter 4 takes on the challenge of downscaling public health data. Downscaling has its origins in climate science. Downscaling in public health is more complex because we do not have historical data or any health data on a desired scale. Therefore, in Chapter 4, we descriptively downscale data using decision tree-based ensemble methods borrowed from Remote Sensing.

CHAPTER 1: The spatial distribution of heat related hospitalizations and a local classification of the most dangerous heat events in California

Introduction

Extreme heat has a substantial public health burden (NOAA 2018; Whitman et al 1997) (Robine et al 2008; Nitschke et al 2011). Many epidemiological studies have found that extreme heat events (EHE) increased risk of hospitalizations for many diagnoses including hospitalizations from cardiovascular, respiratory, diabetes, fluid and electrolyte disorders, and renal failure (Bunker et al 2016; Li et al 2015). However, EHEs do not affect populations equally, and some individuals and communities are more vulnerable to their effects (Jänicke et al 2018; Uejio et al 2011; Smargiassi et al 2009). Health risks associated with heat can vary across space (Hondula et al 2014; Hondula et al 2012; Vaneckova et al 2010), including within cities or counties (McElroy et al 2020). Identifying such spatial heterogeneity on the impacts of EHEs can be particularly useful to target vulnerable areas and communities as well as to guide warning systems that can, in turn, greatly reduce the health impacts of heat waves. However, there are important methodological considerations to the study of spatial heterogeneity of the effects of extreme heat, including the handling of spatial information, the classification of extreme heat events and the scale of estimated effects.

There are many ways to classify heat events such as considering different temperature metrics, for example minimum, maximum or diurnal (representing the nighttime-daytime difference). In addition to the several temperature metrics, various lengths of heat exposure (single day versus multi-day heat events) must be considered. Finally, different thresholds (e.g. 95^{th}, 99^{th} etc.) must be used to define extreme heat events. While it is expected that higher

thresholds be associated with higher risks (on a relative scale), examining the occurrence of such events is critical when estimating the total burden (e.g. total number of attributable hospitalizations) associated with different heat events (McElroy et al. 2020).

Moreover, while it is important to quantify spatial variation as to the risks associated with heat on a relative scale (expressed through risk ratios, or standardized mortality ratios for instance as typically done in previous spatial studies), it is also critical to quantify such risk on an absolute scale to identify the spatial variability of heat-related number of cases. In this context, the absolute scale is represented by the number of increased cases attributable to heat for each region with no regard to population size. An additional challenge when assessing the spatial variability of heat impacts is related to the precision of estimates. In previous studies, uncertainty in risk estimates has been either ignored or obtained through the assessment of significance of a statistical test alone.

The relative scale allows us to see where people are more (or less) vulnerable to heat, whereas the absolute scale determines where the greatest number of people affected reside. These two scales can be used in combination to be complementary in the process of designing adaptation strategies. The absolute scale allows governments to design policy to proportionately target those areas with highest burden to reduce the total number of hospitalizations due to heat. The relative scale allows policymakers to identify areas composed of vulnerable populations (for positive residuals) that are not typically found when focusing on the state or county levels or when using traditional spatiotemporal methods.

Spatial heterogeneity in the type of heat events that drive the health burden can be notably explained by differences in population composition (Hondula et al. 2014; Benmarhnia et

al. 2017), local meteorological conditions (Guirguis et al. 2018), or landscape characteristics (Schinasi et al 2018). California constitutes an ideal region to study the spatial variation of the impact of heat on hospital admissions due to the high burden, high variation in population distribution and high variance in climate throughout the state (Mann and Gleick 2015). Heat-related health impacts are well studied in California (Guirguis et al 2014; Sherbakov et al 2018; Green et al 2009); however, to the best of our knowledge, there is no small region spatial estimation or statewide estimate of spatial variability of heat-related health impact across California.

We applied a comprehensive spatio-temporal approach, an extension of a within-community matched design, to study the spatial variability in the health impacts of heat events in California for unplanned hospitalizations for cardiovascular disease (CVD), respiratory disease, acute renal failure, dehydration, and heat illness. We extended this methodology by using Bayesian models to account for spatial autocorrelation, improve precision and explore the drivers of small-scale vulnerability to extreme heat including the heat metric, heat event length and extremity (Aguilera et al 2020, Schwarz et al 2021). Identifying what heat event characteristics drive the greatest health burden on the relative and absolute scale can be used to prioritize specific areas and neighborhoods in policy planning to best protect populations from the effects of extreme heat.

Methods

Hospitalization Data

We obtained all unscheduled hospitalization data in California for the years 2004 – 2013 from the Office of Statewide Health Planning and Development (OSHPD). The following primary diagnoses were evaluated, as listed in the International Classification of Disease codes,

9th Revision, Clinical Modification (ICD-9): acute myocardial infarction (MI) (410), acute renal failure (584), cardiac dysrhythmias (427), cardiovascular disease (CVD) (390–459), dehydration/volume depletion (276.5), essential hypertension (401), heat illness (992), ischemic heart disease (410–414), ischemic stroke (433–436), and all respiratory diseases (460–519). These diseases were chosen because they have previously been linked to extreme temperatures (Bunker et al, 2016; Li et al., 2015, Sherbakov et al 2018). For this analysis, all cardiovascular hospitalizations were grouped, leaving five hospitalization outcomes of interest. Data were aggregated into daily counts for each zip code, with data provided by the Census Bureau 2010 Census. Mapping of these data was reduced to the use of Zip Code Tabulation Areas (ZCTAs). Where ZCTAs are the geographic representation of zip codes provided by *tigris*.

Meteorological Data and Heat Wave definition

Daily minimum and maximum temperature data were downloaded from a publicly available data set that collects data from approximately 20,000 National Ocean and Atmosphere Administration Cooperative Observer (NOAA COOP) stations across the US (Cal-Adapt 2015). Daily maximum and minimum temperatures (°C) were derived from 1/16° (~6 km) gridded observed data from this data set for all of California (Livneh et al. 2015). Population-weighted centroids for each Zip Code Tabulation Area (ZCTA) were linked to the nearest temperature measurements using the *geonear* function in Stata15 SE.

There are many possible definitions for a heat event as evidenced by warning systems across the world. In this study, we considered 27 EHE (extreme heat event) definitions. These include different metrics: maximum and minimum temperatures, and the difference between the maximum and minimum temperature for each day. We considered duration with 1, 2 and 3 days

of heat exposure as well as considering extremity with percentiles 95%, 97.5%, 99% for minimum and maximum temperatures and 1%, 2.5%, and 5% for difference in temperature. As an example, consider a 95% maximum temperature, 1-day event. An EHE day is defined as an as one in which the daily maximum temperature is greater than or equal to the 95th percentile of the distribution of maximum temperatures during the warm season (May-September) for each zip code. The observed temperature threshold for a heat wave (HW) is displayed in Figure 1 in degrees Celsius. Figure 1 displays temperatures for the four main geographic regions in California, showing that the Central Valley and southeastern desert are warmer, and the coast and eastern mountain ranges are generally cooler. The same procedure is applied to all 27 different definitions of EHE.

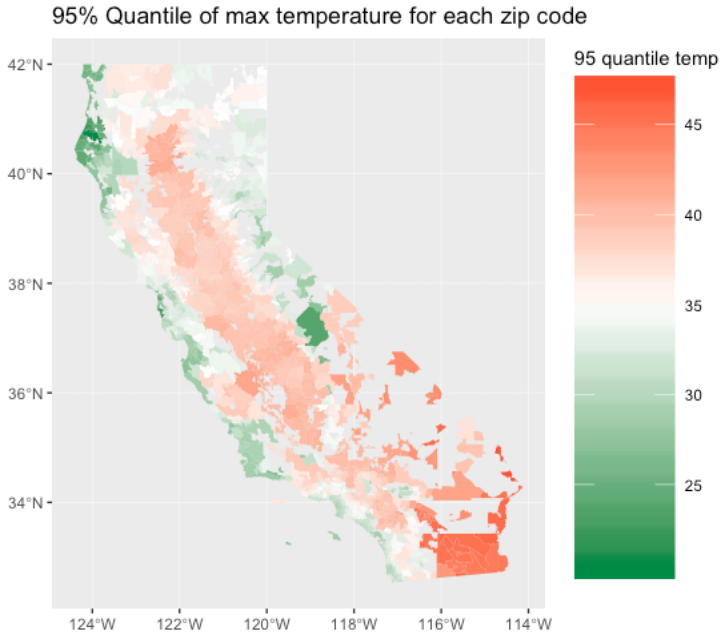

Figure 1 Display of the heat wave threshold in Celsius used in our analysis for each zip code in California. The mean threshold of 35 Celsius is shown in white.

Data Analysis

The Spatial Within-Community Matched Design

We used a spatio-temporal approach, which can be seen as a spatial within-community temporally matched design (Goin et al 2019) that we applied to other environmental exposures in previous work (Aguilera et al 2020, Schwarz et al 2021). This approach allows us to control, for any time-fixed, measured or unmeasured, confounders at the zip code level. Our approach includes four sequential steps to quantify the heat impacts on both relative and absolute scales, a schematic can be found in Figure 2. First, we adopted a procedure to match EHE days in each zip code to similar non-EHE days, and we produce a contrast from a weighted average based on distance in time from the EHE day, given that the control non-EHE days fall within the same calendar year. This is a temporal version of an Inverse Distance Weighting (IDW) procedure, where our bandwidth is a single calendar year. Second, we calculated the absolute difference between EHE and the weighted average of non-EHE days for each zip code. Third, we modeled the relationship between excess counts of hospitalizations and the population size of each zip code using a linear model, where the residuals represent the heat impacts relative to the population size.

$$Y = X\beta + \epsilon$$

In this equation, Y is the excess count of hospitalizations (henceforth referred to as absolute scale estimates), X includes only an intercept and the population value for each zip code in the 2010 census, ϵ is the error term and β is the estimate of the population effect. We will not

consider the effect estimate, but rather the difference between the predicted Y and the observed Y.

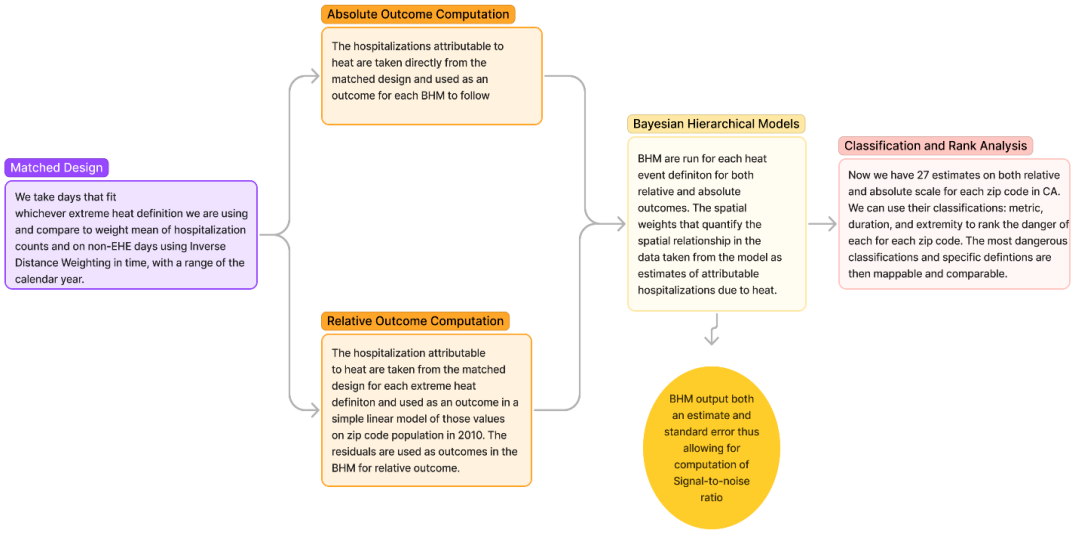

Figure 2 Schematic of the methods procedure for within community matched design and Bayesian extension.

Bayesian Hierarchical Models

To consider spatial autocorrelation and improve precision in our estimates for our fourth step, we used a spatial Bayesian Hierarchical model (BHM). Spatial modeling leverages information from surrounding areas to improve the precision of the estimate at any point in space. We used the within-community matched design absolute scale estimates for each zip code as the response value in linear BHMs and for relative scale estimates we used the residuals from the linear models described above, using the *spBayes* package in R. Population weighted centroids provided by the US Census Bureau are used as the spatial unit for this analysis as this type of modeling requires a SpatialPointsDataFrame. We fit an empirical semi-variogram to estimate the starting prior for the parameters: sill (σ^2), nugget (τ^2), and range(ϕ). Due to the

shape of the empirical semi-variogram, we chose a Spherical correlation structure. The model was formulated as a two-stage model:

1st: $\mathrm{Y}|\theta, \mathrm{W} \sim \mathrm{N}(\mathrm{X}\beta + \mathrm{W},\ \tau^2 I)$

2nd: $\mathrm{W}|\sigma^2, \phi \sim N(0, \sigma^2 H)$

Where W is the vector of spatial weights, and θ is the vector of estimated spatial parameters. The Y_i are our outcome values, which are independent but conditional on W. H represents the structure of the spatial covariance and X represent just an intercept. The second stage model captures the spatial process of the data. We completed model specification by adding prior values and distributions to β and τ^2, and the hyper parameters ϕ and σ^2.

Prior distributions of parameters to reduce sensitivity to the priors during the sampling process were used. We apply 1000 Markov chain Monte Carlo (MCMC) samples, with the final 250 kept after the burn-in period. The final recovered spatial weights were utilized as the estimates for excess hospitalizations in each zip code. We interpolated across space using multi-level B-splines to create a surface of estimates. Though the above methodology assumes isotropy, we acknowledge that the spatial correlation may not be stationary. Isotropy is the assumption that the spatial correlation has the same range in all directions at all points in a data set. Lastly, to represent the precision of the BHM estimates, we estimated the signal-to-noise ratio (SNR) using the resulting model output (weights for each ZIP code and standard deviations). An SNR is the estimated spatial prediction from the BHM divided by the standard error estimated from that BHM. The SNR was mapped for each ZCTA as an indication of areas where estimates are more (or less) precise. We accept that these SNR values are artificially large

because of the violation of the isotropy assumption and thus the traditional cutoff for significance (which is 2.0) would be too small.

We also included randomly generated data and R syntax for reproducibility purposes [https://github.com/KristenHansen/SpatialHeatWaves].

Heat wave definition classification and rank

For the above analysis each heat event definition is considered in isolation. But we want to understand whether the definitions of EHE are correlated with each other or whether the locations where a definition is most affective are located closely together. For both the relative and absolute scales we can form a dataset with our BHM estimates of excess hospitalizations. Thus, we have 27 columns and rows correspond to our zip codes. Thus, we can rank the extremity of the EHE for each zip code relative to those other events in the same zip code. This will allow the exploration of patterns for all our heat event classifications: metric, duration, extremity. We explore the spatial heterogeneity of metric as a contributing factor to hospitalization due to heat.

Results

We observed 131,461 total hospitalizations during EHE days for the five disease subgroups, and 98,562 matched non-EHE day hospitalizations. Cardiovascular disease (CVD) hospitalizations accounted for most of the total hospitalizations on both day types (EHE and non-EHE days) with 58% and 66% on EHE and non-EHE days, respectively (see Table 1).

Table 1 Descriptive statistics describing the hospitalizations on HW days and matched non-HW days in California, 2004-2013.

	Type of Day	Total observed	Mean observed per day	Standard deviation
All-Cause Hospitalizations	HW	131,461	0.95	1.446
	Matched non-HW	98,562	0.72	1.148
Respiratory Disease	HW	40,900	0.2968	0.647
	Matched non-HW	29,551	0.216	0.498
Cardiovascular Disease	HW	76,644	0.559	0.967
	Matched non-HW	65,394	0.477	0.803
Acute Renal Failure	HW	7,918	0.057	0.251
	Matched non-HW	2,421	0.0176	0.135
Dehydration	HW	5,215	0.038	0.200
	Matched non-HW	1,171	0.0085	0.093
Heat Illness	HW	784	0.0057	0.077
	Matched non-HW	25	0.00018	0.0135

Spatial Bayesian Model Results

Figure 3(a) displays the results from the Bayesian Hierarchical model on all-cause hospitalization count differences computed via a within community matched design (results for each ICD (International Classification of Diseases) code separately are presented in Figure A4). Figure 3(a) only displays the results for the example EHE definition (95^{th} percentile in maximum temperature for one day). In the image we see areas of high effect specifically in the Central Valley and the southeastern desert highlighted as having the highest associations with extreme heat. Extending to the relative framework, accounting for population, we used population in a linear model of the absolute hospitalizations, took the residuals from that model and used those as the outcome in the Bayesian model, the spatial effects of which are displayed in Figure 3(b). Similar patterns are found on both risk scales; however, the relative model does display more detail and positive estimates for less populated regions, although the estimates are close to zero, as would be expected for a model where population is included. SNR plots are shown for the same EHE definition on both relative and absolute scales in Figure 4. We have higher precision in the absolute case as opposed to the relative. This is to be expected because relative case estimates are lower in magnitude. For the other EHE definitions a shiny application can be viewed by running *runGitHub("benmarhnia-lab/SpatialHeat", "KristenHansen")* in your R console.

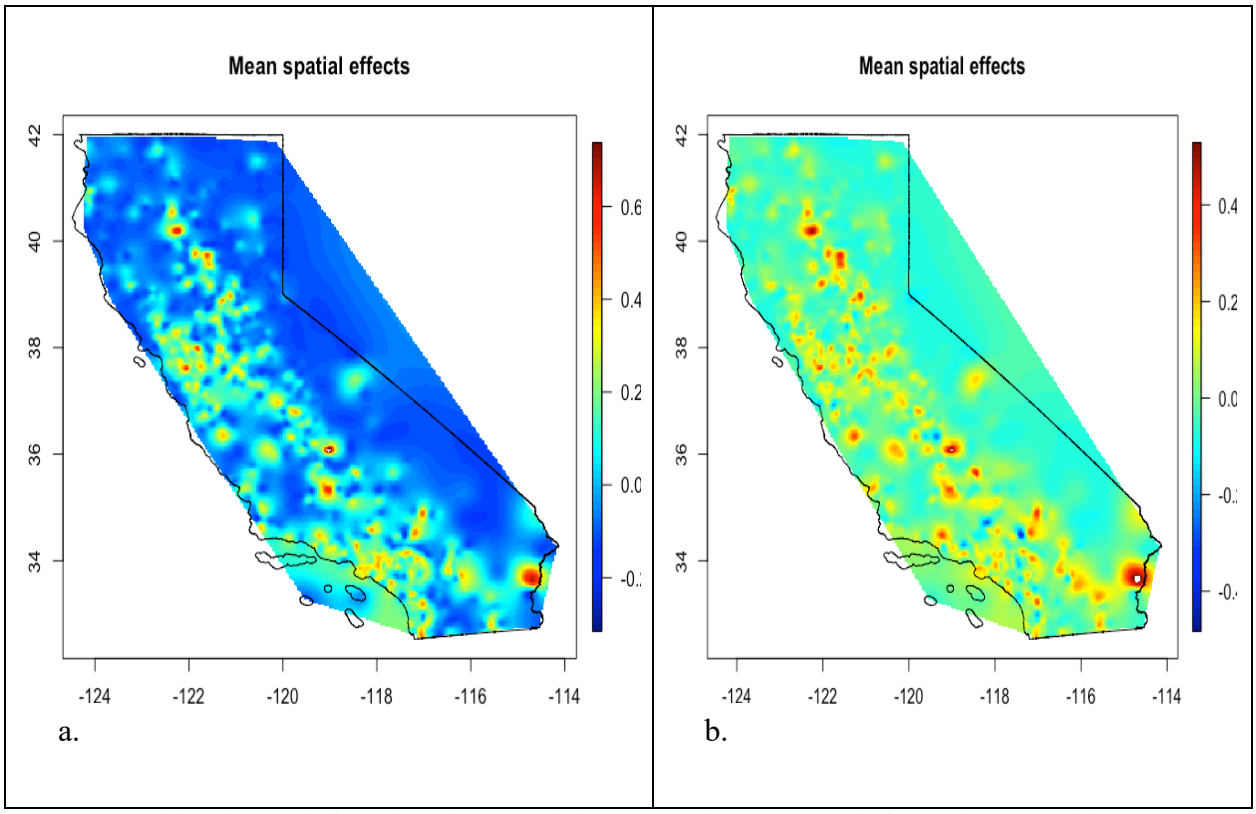

Figure 3 Spatial distribution of effects of one heat event definition (>95th Tmax percentile for one day) on total hospitalization on the absolute (left) and the relative (right) scales.

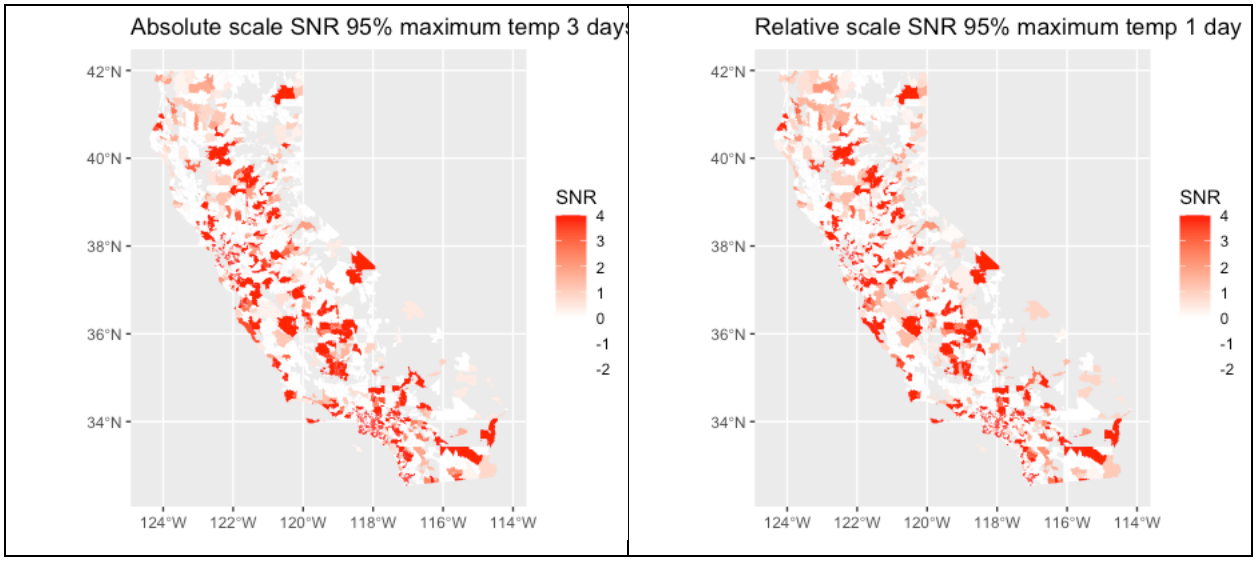

Figure 4 SNR values on both the relative (right) and absolute (left) scale effects of one heat event definition (>95th Tmax percentile for one day).

Heat wave definition rank results

In Table 2, the highest ranked heat event definitions are shown by type for both the absolute and relative risks scaled to the population. We observed that the most hospitalizations occurred in EHEs of the diurnal type where the temperature difference between day and night is very small, especially for ranks 1 and 2 on both the absolute and relative scales. However, in the third and fourth ranks, on the absolute scale, diurnal and maximum temperature EHEs are most common. In the relative case, minimum temperature EHEs are most commonly found in the fourth rank. This is because the low population desert regions of the state are highly affected by minimum temperature extreme heat events. We can see the spatial pattern of the top rank in Figure 5 (a), the metric is displayed for the entire state. Figure 5 (b) shows a more detailed map with all 27 definitions for the greater Los Angeles area. One can see that minimum temperature EHEs are the most dangerous in the desert regions, diurnal EHEs are the most dangerous in the Central Valley and the maximum temperature EHEs are often the most dangerous in urban regions and the mountains. However, there is considerable variability in urban regions, as can be seen in the Los Angeles plot. Although there is mixing in all these regions the general pattern holds for both relative and absolute scales. We saw that the less extreme HE definitions have higher frequency in the absolute case, suggesting longer duration less extreme heat events may cause a higher number of hospitalizations overall.

Table 2 The number of ZCTAs, for which the four most dangerous heat waves definitions fall within the maximum temperatures, minimum temperatures, and low difference in temperatures definitions of heat waves.

Scale	Rank	**Maximum**	**Minimum**	**Difference**
Relative	**First**	603	409	732
Relative	**Second**	570	538	636
Relative	**Third**	591	569	584
Relative	**Fourth**	585	645	566
Absolute	**First**	575	474	695
Absolute	**Second**	531	535	678
Absolute	**Third**	578	539	627
Absolute	**Fourth**	598	567	579

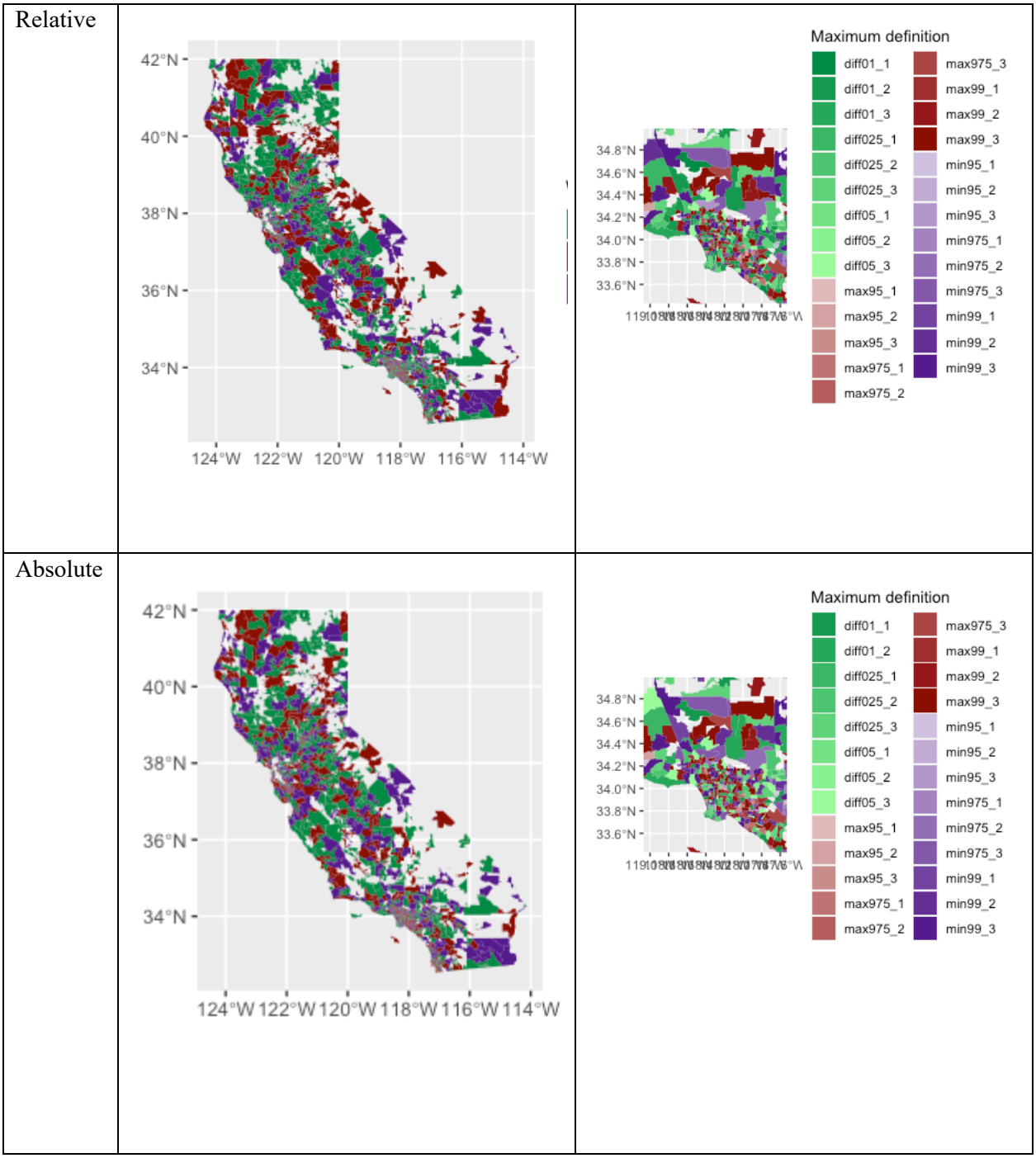

Figure 5 The most impactful metrics for each ZCTA for both absolute and relative-to-population risk scales. Green for diurnal, Red for maximum temperature and purple for minimum temperature heat events. Zoomed in portion on the right for Los Angeles. Darker colors represent the more extreme heat wave definitions and longer in length in days.

Table 3 presents the distribution of the four heat event definitions that are commonly ranked as most dangerous on both relative and absolute scales. For the relative scale all four of

the toperanks are from the most extreme definitions (99%-ile) included in the analysis, whereas for the absolute scale ranks 3 and 4 represent the less extreme long duration HE definitions. Table 3 also shows that the metrics that are causing the most hospitalizations, namely diurnal HEs, are not necessarily the most consequential with finer stratification, adding duration and extremity. Furthermore, we found the 99th percentile maximum temperature, 1st percentile difference between maximum and minimum temperature and 99th percentile minimum temperature long duration heat events caused the most hospitalizations overall. Thus, as we would expect, the most extreme long duration heat events lead to the most hospitalization.

Table 3 Distribution of the four heat wave definitions most commonly ranked as most dangerous on relative and absolute scales.

	Scale	Rank 1	Rank 2	Rank 3	Rank 4
Definition	Relative	99th percentile of Maximum temperature for 3 days	99th percentile of Maximum temperature for 2 days	99th percentile of Maximum temperature for 2 days	99th percentile of Minimum temperature for 2 days
Number of ZCTAs with this rank	Relative	282	143	112	115
Definition	Absolute	99th percentile of Maximum temperature for 3 days	99th percentile of Minimum temperature for 3 days	Difference in Max/min temperature 2.5 percentile for 3 days	Difference in Max/min temperature 5th percentile for 3 days
Number of ZCTAs with this rank	Absolute	228	191	179	131

Discussion

From the study results, we wished to determine where the areas of health burden associated with extreme heat and which extreme heat definitions have the greatest impact for different regions in California to understand the spatial variation of this heat burden on both the relative and absolute scales. Areas including the Central Valley region experience higher burden throughout the studied outcomes. Highest spatial variability can be seen within urban areas: Los Angeles, San Diego, and San Francisco, as some of the highest and lowest estimates of heat effects are found there.

Similarly, the heat event definitions that led to the most hospitalizations are highly varying across zip codes in California. In general, of the three EHE types, the diurnal heat events have the greatest effect in the Central Valley, the minimum temperature heat events are most detrimental in the desert and the maximum temperature heat events are the most common in coastal and mountainous regions with considerable variability in urban areas. This pattern holds true on both the relative and absolute scales. Using rankings, we estimated the small-scale variability in the drivers of the heat-related hospitalizations regardless of the metric, extremity or duration of heat events. We do find that the more extreme and longer heat events are especially prevalent in high rankings on the relative scale with duration being the driver on the absolute scale.

Previous studies have considered or accounted for spatial variation in impacts of extreme heat by adjusting for spatial location, conducting geographic weighted regressions, or applying cluster analysis methods (Song et al 2021). Adjusting for spatial information in models by using a Gaussian smoother to account for spatial autocorrelation is also common (Chen et al 2015;

Chien et al 2016). Other studies have stratified by spatial units without considering spatial autocorrelation or spatial structure (Ingole et al 2020; Murage et al 2020). One of the most common methods for estimating spatial variation in heat related impacts is based on cluster analysis methods, the most readily used being Kulldorf (Benmarhnia et al 2017; Hondula et al 2012; Vaneckova et al 2010). Kulldorff analysis identifies a significant excess of cases within a moving circular window, providing a measure of how unlikely it would be to encounter the observed excess of cases in a comparison region across space. However, such an approach, which is based on significance testing, dichotomizes the spatial units and identifies "significant" clusters where most of the cases occur. Thus, a significant cluster can be driven by the cluster-specific susceptibility to heat or the population size or density. It becomes difficult to get a contrasted and comprehensive assessment of the spatial variability regarding heat-related health impacts for this reason.

Other spatial approaches have been used, such as spatial point pattern analysis, or to estimate relative risks across the study region at a fine scale (e.g. Chen et al. 2015). Bayesian hierarchical models can also be particularly useful to account for spatial variation in heat vulnerability in data rich regions like large cities (Hondula et al 2014). For large geographic areas, such as countries or states, existing studies generally consider only large spatial units like US metropolitan areas (Anderson et al 2013; Bobb et al 2014) or UK districts (Bennett et al 2014). Yet, our approach is the only currently available approach that ranks heat events according to their impacts on a fine spatial scale. Obtaining a classification of the types of heat events that are associated with the highest health burden by zip code are particularly useful in informing tailored interventions to optimize benefits associated with heat action plans and early warning systems.

There are some limitations in our study that should be highlighted. We are restricted to the zip code level, which have high variability in population size, geographic area and are not regularly shaped. Additionally, plotting is restricted to ZCTAs rather than zip codes themselves. ZCTAs do not change when new zip codes are added, thus the visually represented zip codes may not be appropriate in some locations. There are also low rates of hospitalizations on each day for all zip codes, leading to low precision because some of our regions have a very low population. We used Bayesian Hierarchical modeling which has high precision in estimation because it utilizes spatial autocorrelation. The Bayesian hierarchical modeling improves precision over other types of modeling, but has a restrictive isotropic assumption, which under scrutiny may not hold. In order to account for this, we used priors that were not terribly restrictive and ended with acceptance rates around 15%, which, although small, are not worrisome. Spatial correlation structure will be affected by topography and climate. For this reason, we also took a relatively small distance as our range parameter. In future work, it would be important to further explore the use of Bayesian Hierarchical models with covariates for topography, elevation, and climate as well as to explore anisotropic models for spatial data. Here, we consider spatial dependency in the hierarchical models; however, with the isotropy assumption, we are enforcing unfulfilled assumptions into the modeling paradigm, thereby increasing bias of the estimation. Further analysis will strive for higher precision in estimation without using incorrect assumptions, perhaps a Bayesian framework that allows for anisotropy. Future studies may also focus on why we observe this spatial variation, namely whether it's due to population characteristics, environmental factors, or the existence of implemented heat action plans.

Conclusion

In this study, we used a novel spatio-temporal method of analysis to detect areas with highest heat-related burden and to determine the heat wave definitions that drive heat related hospitalizations in different regions of California. We observed high heterogeneity and by elucidating those areas with the worst effects, we can improve current warning systems and guide policy toward those locations and vulnerable subgroups that are most adversely affected by specific types of extreme heat events.

Acknowledgements

Chapter 1, in full, is in revisions at Environmental Research Letters, Kristen Hansen, Lara Schwarz, Anais Teyton, Armin Schwartzman, Tarik Benmarhnia. The dissertation author was the primary investigator and author.

CHAPTER 2: Spatial variation in the joint effect of extreme heat events and ozone on respiratory hospitalizations in California

Introduction

Early warning systems for air pollution (Kelly et al 2012; Wang et al 2017) and heat (Toloo et al 2013; Lowe et al 2011) have been implemented in various areas to limit the health impact of these increasingly prevalent environmental stressors (Gershunov and Guirguis 2012; Mahmud et al 2008). Extreme heat events and some air pollutants such as tropospheric ozone have similar meteorological drivers, as they result from chemical reactions between volatile organic compounds (VOCs), nitrogen oxides (NOx) and sunlight leading them to regularly coincide (Schnell and Prather 2017). However, no joint early warning systems have been implemented to combat the dual-burden of these environmental health risks. An improved understanding of these risks and the interaction between these hazards is important to inform the development and use of early warning systems that consider these joint exposures.

The adverse health effects of heat are well documented. For example, exposure to high ambient temperature has been shown to increase the risk of mortality and morbidity for a range of diseases (Phung et al 2016; Xu et al 2016). High ambient temperature causes heat stress and decreases ability to thermoregulate efficiently, which can produce heat-related inflammation and cardiac stress (Bouchama et al 2017). Several studies have found impacts of heat on respiratory hospital admissions, such as chronic obstructive pulmonary disease and an increase in respiratory infections leading to increased hospitalizations (Michelozzi et al 2009; Green et al 2010; Anderson et al 2013; Gronold et al 2014).

Ozone is a reactive, oxidative gas that is absorbed by the upper respiratory tract; epidemiological studies show a robust relationship between acute exposure to ambient ozone and

morbidity (Nuvolone et al 2018). Ozone pollution is associated with a range of adverse health effects induced by oxidative stress and increased risk of respiratory disease, such as acute respiratory illnesses and asthma (Magzamen et al 2017; Malig et al 2015; Liu et al 2018). In 2015, it was reported that globally, 4.1 million disability-adjusted life years (DALYs) were attributable to ozone exposure alone (Forouzanafar et al 2016).

Ambient ozone increases under high ambient temperature and blazing sunlight, characteristics of extreme heat events (Nuvulone et al 2018). Due to the comparable meteorological patterns, heat and ozone are co-occurring risk factors, and a number of studies have considered the potential concurrent risks and interaction of these exposures in driving the health burden (Filluel et al 2006; Atkinson et al 2016; Madrigano et al 2015). Studies in Brisbane, Australia and in the Netherlands suggested that both ozone and heat play a role in increasing excess deaths during a heat wave (Fischer et al 2004; Tong et al 2010). Interaction between both exposures suggests that the effect of both ozone and heat drive an increased burden compared to each exposure individually. Findings differ between these studies, some revealing a strong relative interaction (Filluel et al 2006; Ren et al 2008; Shi et al 2020) while others demonstrating a weaker signal (Pattenden et al 2010; Scortichini et al 2018) or no joint effect (Jhun et al 2014). For example, high temperature enhanced the effects of ozone on all-cause mortality in France (Filluel et al 2006) and cardiovascular and respiratory deaths in China (Madrigano et al 2015). In contrast, no relative interaction between ozone and heat was observed in all but one city in England (Fischer et al 2004).

Although several studies have considered joint effects of temperature and ozone (Filluel et al 2006; Shi et al 2020; Pattendon et al 2010), few have considered the fine spatial variation in these effects (Wilson et al 2014). Consideration of fine spatial variation is important because it

can provide location-specific thresholds that are most effective in revealing this health burden. Studying spatial variation across diverse regions is vital because it can reveal the heterogeneity of this interaction that can be used to inform warning systems. One study applied a spatial semi-parametric model to estimate joint effects of ozone and temperature risk in urban areas in the United States (Wilson et al 2014). Although that paper finds evidence of ozone-temperature interaction at high temperature thresholds and ozone concentrations, the study focused on urban areas and the relationship varied by city studied. Therefore, we were motivated to consider this interaction at the zip code level in various geographical and socio-demographic contexts.

Some vulnerable groups are known to be especially susceptible to the effects of ozone and heat. For example, the ozone-related excess attributable risk was found to be almost two times higher for black compared to white residents in California for air pollution exposure above federal standards (Hackbarth et al 2011). Racial discrimination plays a role, as decreased access to primary care, private insurance and preventive medication of black residents when compared to their white counterparts likely drive this health disparity (Hackbarth et al 2011). Furthermore, racial minorities and communities of a low socio-economic status are also more susceptible to heat-related health effects; this is associated with poorer physical health, lower access to air conditioning and greater neighborhood level exposure that may increase risk (Gronold 2014). Green space, for example, has been shown to be a modifier of heat-related health effects (Gronold et al 2014). Although these contextual variables are known to play a role in the effect of these exposures, no study to our knowledge has considered the role of socio-demographics and neighborhood level factors in driving the interactive effect between ozone and heat.

We examined the potential heterogeneity in joint effects between heat and ozone resolving fine geographical scales. The majority of studies considering joint effects have not used heat waves or extreme heat events as a binary variable to study temperature effects. We argue that studying the effects of temperature exceeding thresholds is a policy-relevant measure that can be used to activate early warning systems (Xu et al 2016). Moreover, most studies focus on mortality and very few have considered the burden on hospitalizations, a more moderate signal that could reveal broader health impacts. Lastly, the majority of studies investigated heat-ozone interactions based on the relative scale by including a product term in multiplicative models (Analitis et al 2014; Li et al 2017). In this study, we investigate interaction on the additive scale that constitutes a more relevant public health measure (Rothman et al 1980; Vanderweele and Knol 2014) since it directly quantifies the absolute number of hospital admission cases that could be prevented by a joint intervention on both heat and ozone exposures as compared to independent interventions. Focusing on the highly diverse state of California, we explore the role of socio-demographics and environment characteristics at the zip code level in predicting these joint effects to identify factors that can be used to prioritize areas for joint warning systems.

Materials and Methods

Data sources

Environmental data

Temperature data from the National Oceanic and Atmospheric Administration's vast Cooperative Observer and First Order stations were used for this study (Cal-Adapt 2015). The minimum and maximum daily temperature (°C) observations at these stations spanning 1950 through 2013 had been interpolated onto a 1/16° (~6 km) grid (Livneh et al 2018). Population-weighted centroids for each Zip Code Tabulation Area (ZCTA) were linked with the nearest temperature measurements using the *geonear* function in Stata15 SE. The distance from each centroid to a temperature grid cell center thus did not exceed 6 km. Unpopulated areas such as national parks are excluded from the ZCTA delineations, so no data are provided for these areas.

Various extreme heat events were defined when the daily maximum or minimum temperature exceeded the 99^{th}, 97.5^{th}, or 95^{th} percentile of the temperature distribution for each ZCTA for one day and two consecutive days during the warm season of May to September. We considered a total of six extreme heat event definitions during the warm period (Table 1). Each of these definitions were examined using maximum and minimum temperature to consider daytime and nighttime- accentuated extreme heat events, as nighttime accentuated heat typically occurs in anomalously humid conditions (Gershunov et al 2009), which hold special health risks.

Ozone data were estimated at the daily level using 8-hour maximums sampled and analyzed by the US EPA Air Quality System (EPA). Measured concentrations from fixed-site monitoring stations within a 20km radius of each population-weighted zip code centroid were used for interpolation (see figure S9 for the spatial distribution of ozone estimates missingness). To capture acute exposure to high ozone levels, five definitions of ozone peaks were estimated at

various percentiles of the ozone distribution for each ZCTA. The 99th, 95th, 90th and 75th percentiles of the May through September period were considered, as well as a standard threshold of 70ppb, which corresponds to the EPA National Ambient Air Quality Standard for ozone (EPA 2018).

Hospitalization data

Unscheduled hospitalizations in California from 2004 through 2013 were obtained from the Office of Statewide Health Planning and Development Patient Discharge Data. This included all hospital visits that were not prearranged, including emergency department visits and hospital admissions; these together will be referred to as hospital visits in the remainder of this manuscript. Variables of interest included ZCTA of the patient's residence, day of the week, and hospitalization outcome, which was aggregated into daily counts for each ZCTA in California. Respiratory disease (ICD-9 code: 460–519) hospital visits were considered as the outcome of interest due to the well-documented association with both ozone and extreme heat.

Statistical analysis

Case-crossover methodology for the California overall effect

A time-stratified case-crossover design was used to study the association between each extreme heat event definition, ozone peak and hospital visits for respiratory disease (Basu and Ostro 2008; Basu et al 2008; Tong et al 2012) to understand average joint effects in California as a whole. Controls were identified for each case in the study population and selected based on the same day of the week of the hospital visit within the same month and year that the case occurred. Only time-varying variables were considered as covariates in models. A relative excess risk due to interaction (RERI) was then calculated to consider the overall joint effect of ozone and

extreme heat events for California as whole (Vanderweele and Knol 2014). We first assessed the average joint effect of ozone and extreme heat across the entire state.

Within-community matched design analysis

A within-community matched design was then used to study the association between extreme heat events and ozone exposure and hospital visits for respiratory disease at the zip code level to further understand whether spatial variation played a role in average overall effect. This novel approach offers benefits over previous approaches by allowing the investigation of interactive effects at the zip code level. For each exposed day, we identified all possible controls based on two criteria: 1) matches must be in the same zip code and 2) matches must be in the same year. We used an inverse time weighting scheme to calculate comparison averages of hospitalizations on those control days for the contrast. For example, control days closer in time to the exposed day were given a stronger weight than those that were further in time. An RERI was calculated for each ZCTA to consider the joint effects of ozone and extreme heat events at the zip code level (Richardson and Kaufman 2009; Hosmer and Lemeshow 1992). Three relative risks (RRs) were computed for each zip code using the control day weighted averages mentioned above where we compared rates in joint extreme heat events (HW)/O_3 days RR_{11} (RR_{joint}), HW only RR_{10}(RR_{hw}) and O_3 only RR_{01}(RR_{ozone}) days to days without any HW nor O_3 event RR_{00} ($RR_{neither}$), where HW is extreme heat event and O_3 is ozone. For each independent occurrence of ozone peak and extreme heat event, we calculated RR by taking the total number of respiratory hospitalizations in a zip code on a case day versus the weighted average on all control days for that particular case day (extreme heat event, ozone peak), then similarly RRs for the joint heat and ozone days were calculated. When all RRs were calculated for a zip code, we used the

average to produce zip code level RR estimates. Thus, RERI was calculated by the following equation:

$$\text{RERI} = \left(RR_{joint} - 1\right) - \left(RR_{HW\overline{ozone}} - 1\right) - \left(RR_{ozone\overline{HW}} - 1\right)$$

This quantifies the joint-effects at this fine spatial domain on the additive scale (Richardson and Kaufman 2009). The within-community matched design focused on extreme heat events using 95th percentile of maximum temperature and ozone peaks at the 75th percentile to capture sufficient joint-effect days for analysis.

With an outcome of interest such as hospital visits, we expect there to be many days in low population zip codes where there are zero hospital visits. For this reason, some of the RRs are very small for small population zip codes on case days. Due to the weighted average being used as a denominator for our RRs, we do not encounter many zeros in the denominator. The few case days where there was a zero-value denominator, the numerator was also zero. Thus, scarcity of data did not pose a significant problem for our analysis however for the smallest population zip codes, we do not observe precise estimates. Incorporating information from surrounding zip codes can improve precision, thus a spatial analysis is beneficial.

Analyses were conducted on Stata 15/SE and R. For reproducibility purposes, a co-author that was not involved in the analysis reviewed the code for the study. Additionally, the code and a sample dataset for reproducibility purposes is provided at the following link: https://github.com/KristenHansen/JointOzoneHeatWaves.

Bayesian Hierarchical Model Extension

We expect there to be spatial autocorrelation in our RERI estimates. Due to data scarcity, leveraging this spatial information can increase precision in our estimates. Similarly to Aguilera et al., (2020), we used a spatial Bayesian Hierarchical model (BHM) for this purpose (Aguilera

et al 2020). BHMs provide a decrease in variance of estimates by using information spatially near any point. The RERI estimates for each zip code obtained from the within-community matched design analysis were used as the response variable in a spatial linear model. The Bayesian model was fit using the spBayes package in R (Finley et al 2007). This package requires the use of point-referenced data rather than areal regions, for this we used population-weighted centroids from the US Census Bureau (Census Bureau). We fit an empirical semi-variogram to estimate the starting values for the spatial parameters, sill (σ^2), nugget (τ^2), and range (ϕ). Based on the shape of the semi-variogram, a Spherical covariance structure fit the most closely to the data. The Spherical covariance function is commonly used in spatial analyses and has the following form:

$$C_{sph}(h) = \begin{cases} \sigma^2(1 - \frac{3}{2}\frac{|h|}{\phi} + \frac{1}{2}\frac{|h|^3}{\phi^3}), & 0 \le |h| \le \phi \\ 0, & |h| > \phi \end{cases}$$

The covariance structure is specified in the model implementation, which forces the covariance matrix to hold this form. All covariance structures for this type of model are isotropic.

The model forms a hierarchical model with two stages:

First stage: $Y|\theta, Z \sim N(X\beta + Z, \tau^2 I)$

Second stage: $Z|\sigma^2, \phi \sim N(0, \sigma^2 H)$

Where θ is the vector of parameters including β, sill, nugget, and range and Z is the vector of spatial random effects. Conditionally, $Y_i|Z$ are independent. H represents the spatial correlation structure, which we set as Spherical in this case. The second stage model, called the process model, is introduced to capture spatial dependence in the outcome variable. Model specification finally includes adding starting, tuning, and distribution values for our priors of parameters τ^2, and the hyper parameters ϕ and σ^2. The

model captures the spatial process underlying the distribution of RERI in California from 2004 through 2013. This model generally can be considered a spatial Bayesian extension to a general linear model (GLM).

The prior distributions and tuning parameters we used allowed for minimal impact on the final values. Monte-Carlo Markov chain (MCMC) samples are used to estimate parameters. We used 10,000 samples, 75% for burn-in. An 800x800 raster grid was produced by interpolating the recovered sample weights using multi-level B-splines. This methodology assumes isotropy although that may not hold in the case of environmental variables.

To represent the precision of the point estimates, we computed the signal-to-noise ratio (SNR) from the model output, which includes weight and standard errors. The SNR was mapped for each ZCTA to represent significance. This gives a visual representation of areas where estimates of RERI from the BHM are precise. We use the traditional cutoff when $|SNR| > 2$ to represent precision. Additionally, as acclimation and adaptation can modify the effects of heat (Marmor 1975) and ozone (Gong et al 1997), respectively, a sensitivity analysis was conducted considering stratified estimates for each month of study, to consider the potential differing effect of these exposures throughout the summer.

Meta-regression

Once spatial estimates from the BHM were output, we used them in a meta-regression to understand the factors influencing these joint effects of ozone and heat over space. Demographic and environmental variables were retrieved from the U.S. Census American Community Survey (Census Bureau), and the Healthy Places Index (Delaney 2018). The variables we considered for this analysis were neighborhood and demographic variables that have been shown to be related to ozone and heat effects. These include population density, the percentage of residents that are non-white, black, over 65 years of age, female, unemployed, without health insurance, foreign born, race and environmental variables such as the percentage of the zip code with tree canopy,

access to parks, and concentrations of other pollutants ($PM_{2.5}$, PM_{10}, NO_2). We additionally included variables about lifestyle, including accessibility of parks, percentage of commuters who walk or ride a bike, and automobile ownership. Finally, we create a composite score from the eigenvectors of the first principle component derived from PCA, we use this composite score as another variable. Each variable was considered in a univariate linear model, with the spatial estimates output from the BHM as the outcome. Effect estimates and confidence intervals were taken from each model to represent the significance of each variable in the spatial distribution of joint ozone and heat effects.

Results

Study population and summary of exposures

A total of 817,354 unscheduled respiratory hospitalizations occurred from 2004 to 2013 in 543 hospitals (map shown in Figure S8) in California (Table 1). Temperature and ozone thresholds for various extreme heat event and ozone peak definitions are also described in Table 1. For example, extreme heat events defined by the 99th percentile using maximum temperature across all ZCTAs have an average threshold of 38.95ºC, ranging from 22.5 ºC at the coast of Northern California to 49.8 ºC in the Southern desert, and a total of 28,616 ZCTA-days are considered extreme heat event days using this definition (Table 1). There is coherent spatial variation in what temperature value corresponds to specific percentiles throughout California; the variation in maximum temperature threshold is shown for the 95th percentile of the temperature distribution in Figure 1, ranging between 20ºC in the coastal redwood forest of Humboldt County in far Northern California as well as in the high southern Sierra Nevada mountains, to greater than 45ºC in the Mojave and Colorado/Sonoran Deserts in the far southeast. For ozone peaks,

whose spatial distribution largely reflects that of temperature, but locally modified by the distribution of population centers and industrial activity around the State, the overall average concentration is 79.9 ppb with a standard deviation of 15.3 for the 99th percentile definition; 23,126 ZCTA-days fall within these concentration levels (Table 1). In subsequent results, ozone peaks were considered at the 75th percentile to ensure sufficient ozone days could be analyzed.

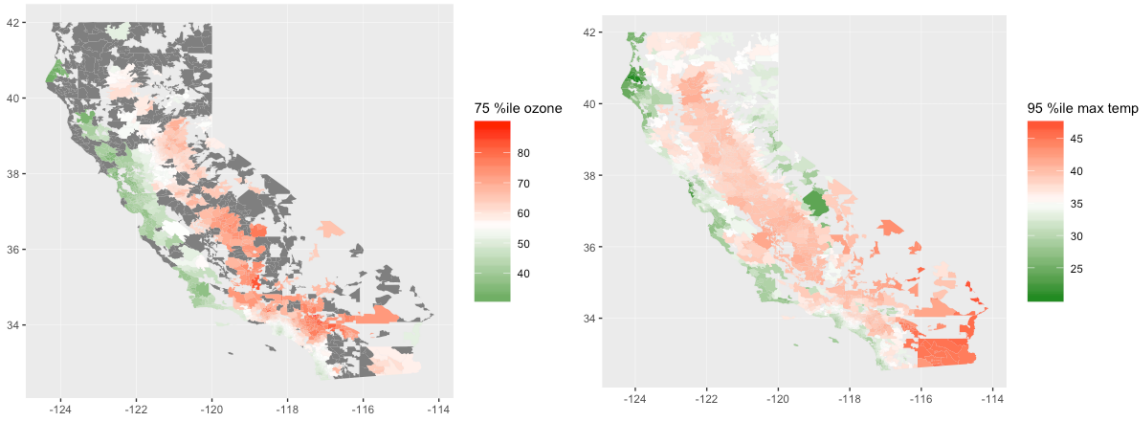

Figure 6 Spatial distribution of exposure values that corresponds to a 75th percentile of ozone (ppb) and 95th percentile of maximum temperature (ºC) during the warm season (May-September) for each ZCTA, 2004-2013 in California. Light gray areas indicate no population and dark grey indicates missing environmental data.

Table 4 Characteristics of respiratory hospital visits and summary of daily temperature and ozone pollution in California, May-September, 2004-2013.

Health Outcome	***n***	***Mean daily cases (SD)***
Respiratory hospital visits	817,354	677 (195)
Environmental exposures	***Threshold***	***# ZCTA-days exceeding threshold for 2,863 ZCTAs***
Heat waves (°C)	Mean ±SD	
Maximum temperature		
97.5th 1-day	37.75±4.11	69,692
99th 1-day	38.95±3.85	28,616
97.5th 2-day	38.37±3.98	34,612
99th 2-day	39.57±3.78	11,391
Minimum temperature		
97.5th 1-day	20.29±4.21	69,783
99th 1-day	21.27±4.22	28,679
97.5th 2-day	21.08±4.00	33,394
99th 2-day	22.10±3.88	12,105
Ozone waves (ppb)		
99th	79.92±15.36	23,126
95th	71.58±15.00	110,122
90th	67.49±14.87	217,272
75th	61.67±14.41	534,519
70 ppb	78.07±7.81	187,227

Isolated effects of extreme heat events and ozone exposures

Figure 7 shows the association between extreme heat events and ozone peaks separately and respiratory hospital visits for California. Extreme heat events defined using maximum temperature revealed greater health impact than extreme heat events defined using minimum temperature (Figure 7). Therefore, maximum temperature extreme heat events were emphasized in the following analyses. Overall, the majority of thresholds used for ozone peaks appear to be associated with increased hospital visits (Figure 7). Overall, results showed that ozone and extreme heat events were independently associated with respiratory disease hospital visits in some areas of California, but this association is not consistent.

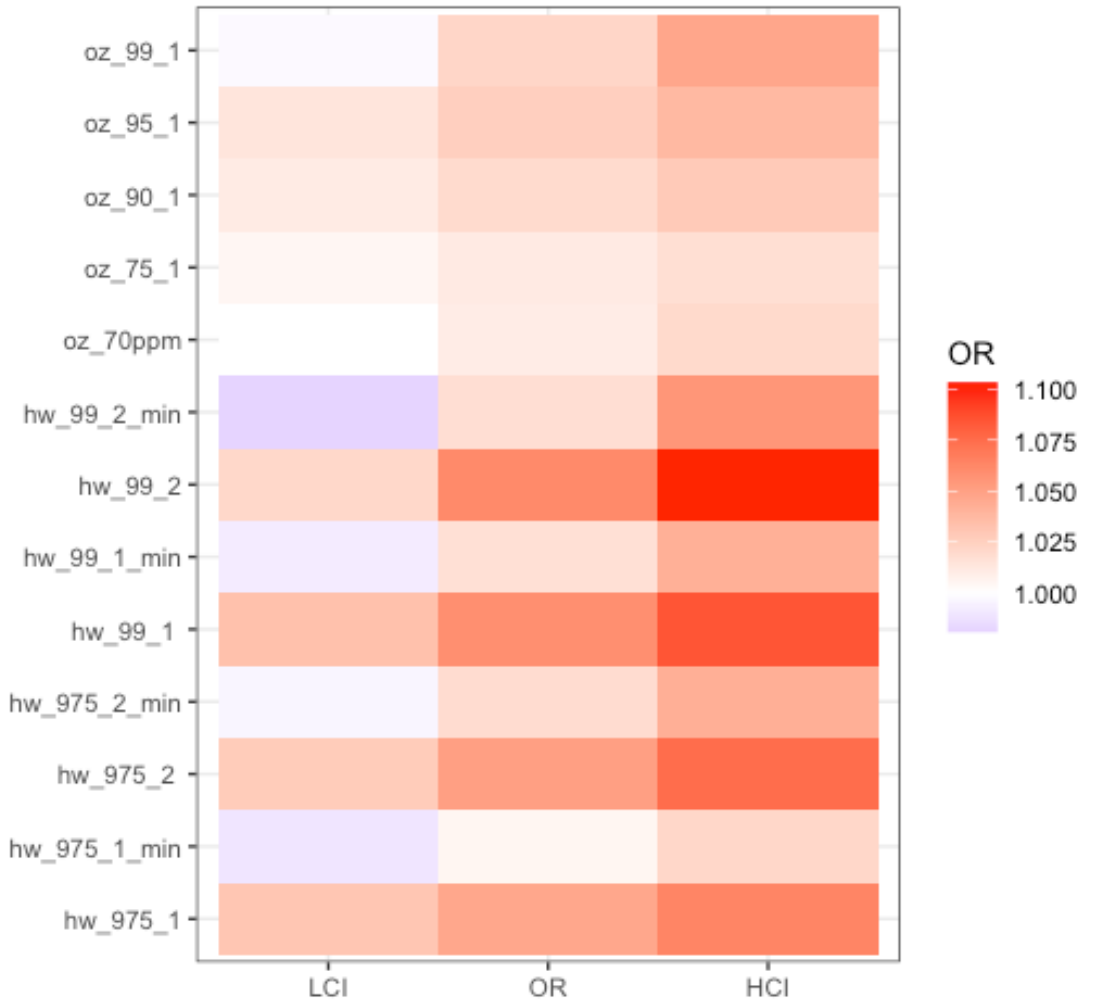

Figure 7 Odd ratios and 95% CI of the bivariate association between heat waves (99th 1-day, 99th 1-day, 97.5th 1-day, 97.5th 2-day), ozone peaks (99th, 95th, 90th,75th, 70ppm) and respiratory hospital visits in California, 2004-2013.

Joint effects and spatial variation

When considering average joint effect in all of California, the RERIs revealed no effect for any combination of extreme heat events and ozone peak definition (Supplementary Table 1). However, when considering spatial differences in effect at the zip code level within California, the variation is revealed (Figure 8). Differences in RERI estimates considering extreme heat events at the 95th percentile and ozone at the 75th percentile within California demonstrated that

some areas showed a strong joint-effect with RERIs exceeding values of 2, and other areas indicate negative interaction of values lower than -2 (Figure 8). Hotspots that show strong joint effects are sparse, peppering the state here and there. Examples of these hotspots include a spot along the US-Mexico border area and a sizable are in the western Central Valley along the San Joaquin River. It is important to note that the high variation leads to imprecise estimates of joint effects through RERI; precision of estimates can be seen in the Supplementary Material (Figures S1 and S2). Results of spatial heterogeneity in RERI when ozone peak is defined by an absolute threshold of 70 ppb are shown in Figure S3 and S4. However, some information is missing for this definition due to many ZCTAs never reaching 70 ppb for ozone. Definitions of both extreme heat events and ozone peaks analyzed showed distinct spatial differences.

We consider the lagged effect of these joint days by considering the average hospitalizations on the two following days after an event. Figure S5 displays the Bayesian surface of the RERI estimates. Overall, we find lower effect sizes and significance for this analysis. The sensitivity analysis considering stratified estimates for each month of study showed some variation in spatial patterns throughout the summer, indicating that acclimation may play a role in some ZCTAs (Figure S6). However, we did not identify a strong attenuation of effect and acclimation does not seem to be a major driver of our observed results.

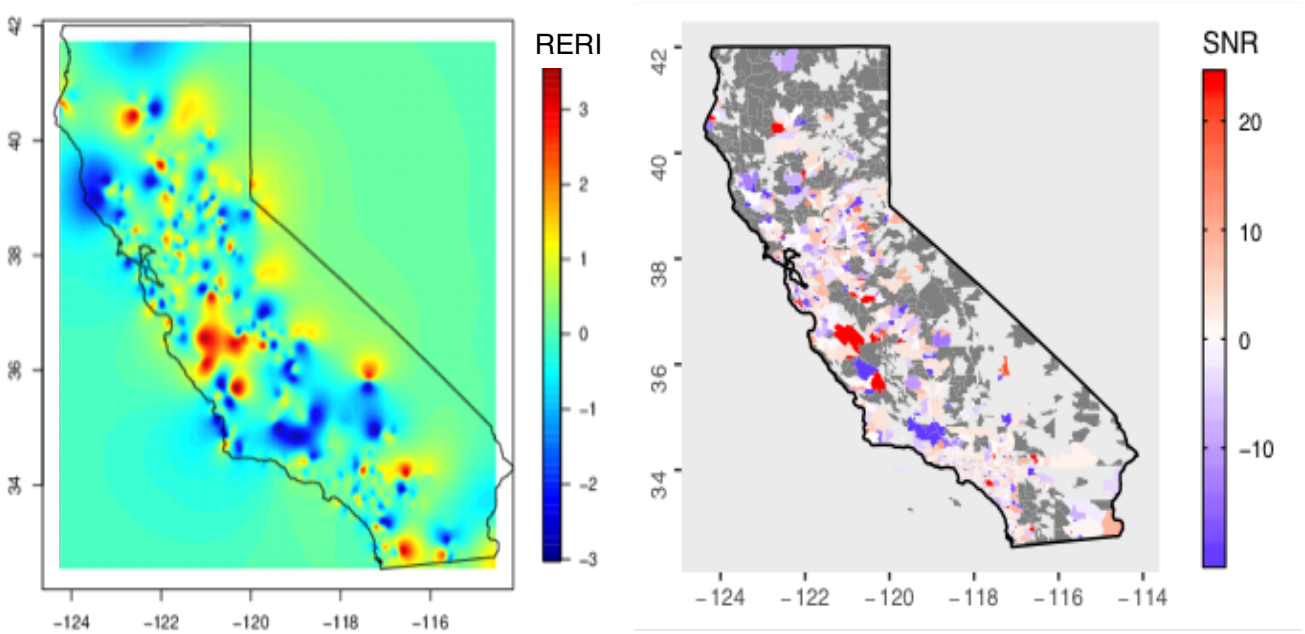

Figure 8 Interpolated spatial distribution of joint-effects of heat waves at the 95th percentile of maximum temperature (ºC) and ozone peaks (ppb) at the 75th percentile on respiratory hospital visits using RERI in California, 2004-2013 from Bayesian Hierarchical Model (BHM).

Prediction of joint effects using neighborhood-level socio-demographics

Descriptors of variables included in the meta-regression for all California zip codes are shown in the supplementary material (Table S3). Results of the meta-regression showed that zip codes with a higher percentage of non-white residents, unemployed residents and population with no health insurance were associated with stronger joint effects (Figure 9). However, these variables are correlated with other demographic variables considered (Figure S7). After accounting for median income, percentage non-white is no longer significant (Table S4) due to the high correlation between these two variables leading to a model that is less reliable for identifying effects. Zip codes with higher concentrations of other pollutants were also associated with stronger effects, while a higher percentage of commuters who walk or ride a bike was associated with decreased joint effects, although this effect was attenuated after adjusting for socio-economic status (Table S4). Park accessibility, tree canopy the percentage of female residents, percentage of residents with air conditioning, and those over 65 years of age showed imprecise predictions. The composite score produced from PCA showed high influence from the variables for NDVI, no

health insurance percentage, percent non-white and mean NO_2. The PCA score was significant and relatively high in magnitude as we would expect.

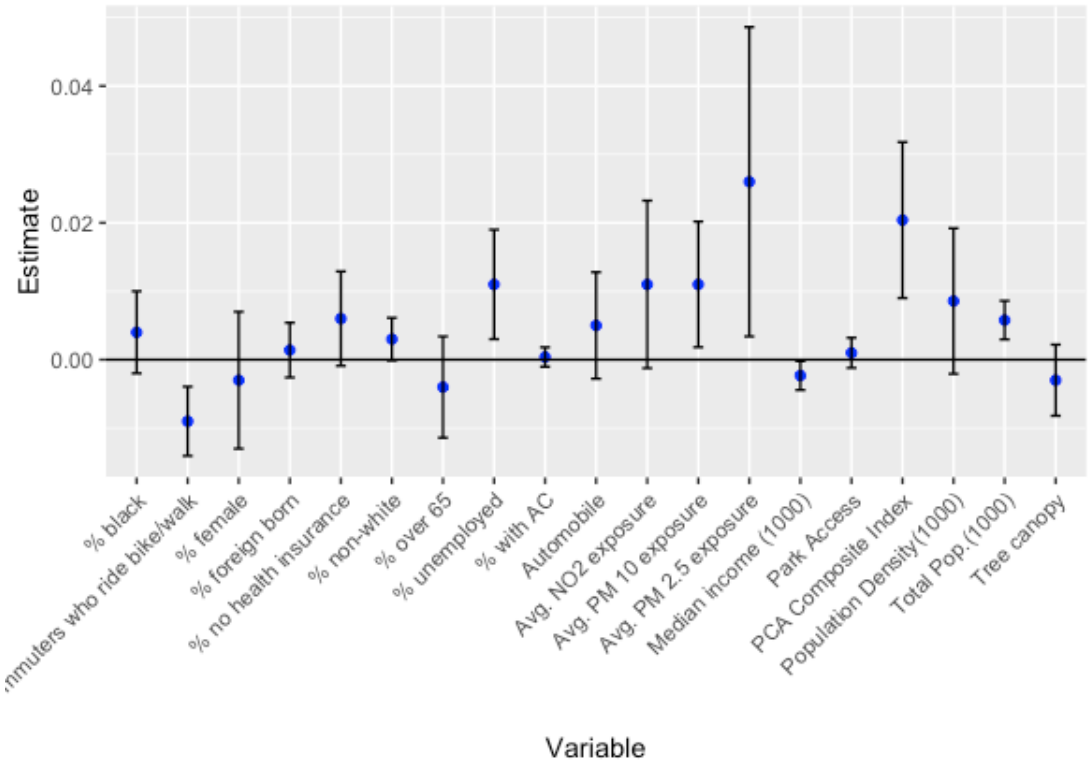

Figure 9 Results of meta-regression showing the association between standardized socio-demographic characteristics at the zip code level and joint-effects of heat waves at the 95th percentile of maximum temperature (ºC) and ozone peaks (ppb) at the 75th percentile on respiratory hospital visits in CA, 2004-2013.

Discussion

Results of this study indicate that the effects of ozone and heat are highly heterogeneous throughout California; some areas show strong joint effects while other parts of the state suggest no interaction, or negative interaction, between ozone and heat. This validates the importance of considering the effects of these exposures at a local scale. Understanding which spatial units (ex: ZCTA) have joint heat and ozone effects in a large geographically and demographically complex region such as California can inform warning systems and provide motive for considering thresholds of both ozone and heat exposures to activate these warning systems in specific

geographical areas. More specifically, understanding how zip-code level demographic and environmental information is associated with these joint effects can be used to prioritize resources.

In California, the forecasting system includes extreme heat events; the National Weather Service uses an early warning system to identify potential heat risks at a local scale, which provides guidance to decision makers to take action (NWS 2019). This resource forecasts potential threats of dangerous high heat year-round, but to our knowledge does not take into account joint-effects of ozone and heat. Our results highlight an opportunity to identify spatial heterogeneity to inform joint warning systems at this localized scale. Interestingly, no large-scale spatial pattern was observed, but "hotspots", such as strongest positive joint effects were observed in certain areas such as the Central Valley and the southern border region (Figure 3). When considering a smaller scale, what appeared to be large-scale noise showed local signals at the ZCTA level. Results of the meta-regression show that specific demographic and zip code level information are drivers of these interactive effects. By identifying these areas that experience joint effects of ozone and heat, interventions considering thresholds of both exposures have the potential to prevent more cases of respiratory disease when implemented in addition to two independent interventions.

Heat warning systems have been shown to be effective at decreasing the deleterious effects of heat exposure (Toloo et al 2013; Benmarhnia et al 2019; Benmarhnia et al 2016). In particular, the thresholds of local heat emergency plans can be adapted based on evidence from epidemiological studies, which have been shown to increase the health benefits of activating heat action plans (Benmarhnia et al 2019). Warning systems can be adapted to consider the joint-effects of air pollutants such as ozone, which our results show would be beneficial in specific

areas throughout California. This study and others considering fine spatial variation in the effect of environmental exposures can be valuable to define and target these specific regions.

A literature review was conducted for studies investigating the joint effect of ozone and heat on health (Table S2). Most of the literature considering the joint effects of heat and ozone have presented assessments of average exposures in specific geographic areas such as cities or counties, primarily in Asia and Europe (Scortichini et al 2018; Analitis et al 2014; Li et al 2017). Studies have found conflicting results, ranging from indications of strong interaction (Qian et al 2008; Pascal et al 2012), to no interaction (Jhun et al 2014). Another study found a negative association between ozone exposure and mortality on hot days (Lin and Liao 2009). Two papers considering different cities or geographical areas found spatial variation in their results; Pattenden et al., (2010) found ozone-heat interaction in only one conurbation in England (London) out of the 15 studied (Pattenden et al 2010). Similarly, Ren et al., (2008) found synergistic associations in communities in the northeast but not in the southeast of the United States (Ren et al 2009).

Our results shed light on some of the variation in the findings of previous studies, some of which may be explained by differences in socio-demographics and environmental factors at the local level. Figure 3 shows the spatial distribution of the effect of extreme heat events on respiratory hospital visits, which is highly heterogeneous (Basu et al 2012; Guirguis et al 2014). When considering joint-effects, the overall results for the entire state of California showed no interaction between ozone and extreme heat events (Table S1). However, there is a wide spatial variation in the effects of heat, ozone and interaction of both, as observed in Figure 3. Some areas show negative interaction. There is evidence to suggest that reductions in NOx are associated with increase in ozone concentrations (Jhun et al 2015); these ozone precursors, such

as nitrogen dioxide, could therefore be higher on low ozone-days, acting as a competing risk in this association and potentially driving negative interaction in some ZCTAs. Additionally, the perceived risk of air pollution and high heat events may alter behaviors and decrease exposure when there is a dual threat of ozone and heat exposure (Semenza et al 2008); this may vary based on capacity of populations to adapt which may be related to resource and socioeconomic factors.

As shown in the meta-regression results, neighborhood-level environmental characteristics modify the vulnerability of specific ZCTAs to ozone and heat joint exposures. Previous research has shown that high settlement density and sparse vegetation can increase the human thermal comfort index, an indicator of heat stress (Harlan et al 2006). In our results, population density was found to have a slight positive association with ozone-heat interactive effects, but this estimate was not precise (Figure 4). Tree canopy, a measure of green space at the ZCTA level, was not found to be a strong predictor of joint-effects either, although it did have a slight protective effect (Figure 4). Although the interaction hotspots we observe are not consistently concentrated in the highly urbanized areas of California, total population showed a strong positive association with observed interactive effects in meta-regression results. This heterogeneity may be explained by neighborhood-level demographic differences within highly urbanized areas.

Minority populations and those of a low socio-economic status are particularly vulnerable to heat (Gronold 2014) and ozone (Bell et al 2014) due to the range of associated individual and neighborhood level factors that increase risk in these specific populations. Racial microaggressions and racism experienced by individuals from minority groups may also hinder their comfort in seeking care (Babla et al 2021). Our results are consistent with this finding, as zip codes with a higher proportion of non-White populations showed a stronger joint-effect of

ozone and heat (Figure 4). Interestingly, such effect is no longer observed after adjusting for median income (Table S4). As discussed recently, race/ethnicity (both for individual level self-reported race/ethnicity or neighborhood race/ethnicity composition) in environmental epidemiological studies operates through various pathways such as differential socio-economic status to generate observed environmental health disparities of interest (Benmarhnia et al 2021). As described in the social epidemiological literature (Vanderweele and Robinsom 2014), such patterns can be interpreted as mediated inequality measures which correspond to what would happen to race/ethnic inequalities for a given health outcome if certain socioeconomic status (like income) distributions were set to something other than what they in fact were across racial/ethnic sub-groups. In the context of our findings, it means that if we were able to (hypothetically) reduce income inequalities between race/ethnic groups (at the neighborhood level) to zero, observed race/ethnic disparities regarding the joint impacts of extreme heat and ozone would disappear. Interestingly, such patterns have been found in other studies in environmental epidemiology (Benmarhnia et al 2021) or in the context of COVID-19 test positivity and risk of hospitalization (Gershengorn et al 2021).

That being said, the positive association between median income and the role of the proportion of unemployed residents in driving joint effects also exemplifies differential susceptibility to environmental determinants and demonstrates the strong role of neighborhood socio-economic status in driving this increased vulnerability to joint effects of heat and ozone exposure. Exposure to multiple environmental risks, such as other toxins and poor housing quality (Evans and Kantrowitz 2002), as well as social deprivation from lack of access to proper healthcare and education can increase the vulnerability of populations from a lower socio-economic status (Schnittker 2004). Older populations are considered to be more vulnerable to

both heat (Benmarhnia et al 2015) and ozone exposures (Medina-Ramon and Schwartz 2008), although our results do not indicate that zip codes with a higher elderly population have increased vulnerability. Our results can be used to prioritize specific neighborhoods that are considered at higher risk for joint ozone-heat effects, such as those with lower income and with a high rate of unemployment.

Certain commuting and travel behaviors can also play a role in the joint health effects of ozone and extreme heat events. In our results, the percentage of workers commuting by walking, cycling or transit was shown to be associated with decreased joint-effects and automobile ownership showed the opposite, indicating that car usage may a predictor of joint effects. Reduced car travel has been shown to have health benefits through reduced air pollution exposure and increased exercise (Grabow et al 2012). Specifically, using bicycles for urban travel has been found to drive health benefits from decreased emissions (Lindsay et al 2011). Increased walking and bicycling in California has been shown to contribute to disease reduction (Maizlish et al 2017). However, accessibility to walking and bicycling for commuting is also strongly correlated with neighborhood socio-economic status (Zahran et al 2008), which is partially driving the association we observe. Although a higher percentage of workers commuting by walking, cycling or transit remains associated with decreased joint effects after adjusting for income (Table S4), there may be various other factors related to the socio-economic context of the ZCTA that may explain this association.

Lastly, concentrations of other air pollutants were found to be associated with increased joint effects, indicating that there may be multi-pollutant effects. This may be related to environmental injustices, as low-income areas and communities of color have disproportionate exposure to air pollutant concentrations (Su et al 2009). The Central Valley, where we observe a

large hotspot of strong interactive effects has some of the worst air quality in the nation; this has been shown to be associated with the highest rates of asthma in California (Meng et al 2010). These findings indicate the importance of considering neighborhood-level characteristics in understanding the vulnerability of specific areas to interactive ozone and heat effects.

Our results demonstrate the importance of going beyond an overall regional measure to consider fine spatial heterogeneity in the effects and thresholds for early warning systems. Without considering these effects at a local scale, positive associations may be concealed. In the future, it would be important to assess the spatial variation in effects in other studies which found limited or no joint-effects of ozone and heat in other regions. Additionally, this methodology can be applied to other exposures to understand their spatial heterogeneity and identify susceptible areas that can be used to inform targeted interventions.

There are a few limitations to this study that should be acknowledged. Missing values for ozone left some gaps in our understanding in certain areas of California (23.4% of zip codes do not have ozone information, missing data shown in Figure S9); zero values for hospital visits also led to some difficulties in examining this association at the at the ZCTA level. Existing methodologies for the use of spatial effects do not allow for anisotropy in spatial processes. The assumption of isotropy does not hold for data across complex geographies of regions and climates such as that of California, where, for example heat wave expressions at the highly populated coast are modulated by coastal marine-layer clouds (Clemesha et al 2018). There is room for methodological development in this area, and we plan to explore more flexible methodologies. Lastly, heat waves are expected to become more humid in California (Gershunov and Guirguis 2012); understanding the role of humidity in driving ozone and heat interaction is an important area for future work.

Climate change projections show that the frequency, intensity and duration of extreme heat events as well as days of high ozone concentration are expected to increase (Gershunoa and Guirguis 2012; Mahmud et al 2008; Gershunov et al 2009)[,]. This study helps understand predictors in the spatial distribution of these effects and can be used to inform and target joint early warning systems to protect populations from the deleterious effects of both ozone and heat.

Acknowledgments

Chapter 2, in full, is a reprint of the material as is appears in PNAS 2021. Kristen Hansen, Lara Schwarz*, Anna Alari, Sindana Ilango, Nelson Bernal, Rupa Basu, Alexander Gershunov, and Tarik Benmarhnia. The paper title is “Spatial variation in the joint effect of extreme heat events and ozone on respiratory hospitalizations in California”. The dissertation author was the co-primary contributor and writer to this paper along with Lara Schwarz.

CHAPTER 3: Spatially varying effect estimates of mediation in the presence of spatial autocorrelation

Introduction

Many research questions in epidemiology require more than estimating the total effect of an exposure. Instead, such questions involve decomposition of the total effect into separate causal pathways. The most common strategy is to break down the total effect into a direct effect of the exposure and an indirect effect of the exposure through a mediator. Recently, mediation can be found in environmental epidemiology in relation to the role of air pollution on ethnic health disparities (Benmarhnia et al, 2021), analyses of psychological outcomes like academic burnout (Ye et al, 2011), social epidemiology research on socioeconomic status and mortality (Hossin et al 2019), epidemiological research on blood pressure and tooth loss (Mendes et al 2021), and cancer prognosis (Syriopoulou et al 2021). Mediation analysis is used frequently and widely in many fields and diverse research contexts.

The first and most common approach to mediation analysis comes from Baron and Kenny (1986). This approach works in special circumstances but is marred by many restrictive assumptions. Over the past decade mediation analysis methods to assess the importance of different pathways and mechanisms has experienced incredible growth. Although traditionally used in the social sciences, many recent methodological developments have been born from public health and epidemiology. The Baron and Kenny approach, henceforth referred to as the Product method, does not apply in most observational studies because the assumptions are intractable (Kaufman 2004). Developments in the methodology of mediation attempt to alleviate required assumptions and broaden the contexts in which mediation can be used. The

counterfactual framework has been a large part of this development. A formal counterfactual approach to mediation analysis was developed in 1992 (Robins 1992; Pearl 2001). It was shown that the total effect can always be decomposed into natural direct and indirect effects, regardless of the underlying statistical model. One of the initial developments has been to allow for interactions between the exposure and mediator (Lange et al 2012; Vanderweele et al 2014). Furthermore, early developments included allowing for binary outcomes (Vanderweele et al 2010) and binary mediators. There has been extensive evolution in the estimation of these effects in time-to-event outcomes (Aalen et al 2019; Cho et al 2018) as well as time varying confounders, mediators, and exposures (Lin et al 2017). In addition, progress has been made to allow for multiple mediators (Bellavia et al 2017). Furthermore, there has been growth of methodology to deal with collider-stratification bias and confounders of the mediator-outcome relationship induced by the exposure (Vanderweele et al 2014). Finally, expansion to the use of additional estimators that are robust against misclassification has been researched more recently (Wodtke et al 2020; Rudolph 2018; Rudolph 2020).

The literature handles measured confounding of many types and different techniques for modeling. There is however one methodological gap in the literature. Spatial variability in causal inference is beginning to be explored (Reich et al 2021). As far as we know mediation literature does not address spatial heterogeneity nor does it allow for spatial exposures, mediators, or outcomes. This is especially pertinent for problems relating to environmental or social epidemiology or in any field where data is spatially structured. In addition, mediating relationships can be reasonably expected to vary over space due to confounders and spatial covariance or due to distribution of the exposures and mediators. To ignore the spatial relationships when considering mediating relationships is ill-advised as it allows for bias in

estimation as well as not accounting for spatial variation. Understanding the spatial heterogeneity of direct or indirect effects can help refining targeted interventions.

In this paper, we propose a novel analytical framework for this type of data. We propose to combine the use of regression-based mediation analysis with spatial regression techniques; specifically, spatially varying coefficient models. This allows us to explore spatial heterogeneity in direct and indirect effects. In our simulation study we will explore data contexts of both regular grid data and zip code level data, which is very common in epidemiological research. We investigate different covariance scales, total effects sizes, and varying proportions mediated to account for diverse data contexts. Finally, we include a case study with real data to show how results of this methodological framework could be presented in practice.

Mediation

Traditional Mediation Analysis

Statistical mediation analysis is used to estimate how an independent exposure variable (A) affects an outcome variable (Y) through a mediator (M). There are many examples of mediation published in fields from psychology to public health. Numerous studies use the regression approach to mediation analysis, where there is a single mediator and the direct and indirect effects are estimated through the use of three regression models (Baron et al 1986). This is also referred to as the Product method (or Baron and Kenny).

$$Y = \beta_0 + \beta_1 A + \epsilon \quad (1)$$

$$M = \eta_0 + \eta_1 A + \epsilon_m \quad (2)$$

$$Y = \theta_0 + \theta_1 A + \theta_2 M + \epsilon_{full} \quad (3)$$

The Product method uses the product of two model coefficients to estimate the indirect effect of *A* on *Y* through *M*. Equation (1) estimates the total effect of *A* on *Y* (β_1). The controlled direct effect is estimated from θ_1 in Equation (3). Finally, the indirect effect is estimated by multiplying η_1 from Equation (2) and θ_2 from Equation (3), with the assumption that *Y* and *M* are both continuous variables. The indirect effect can also be equivalently estimated as the difference of the total effect and the controlled direct effect when all relationships are linear and without interaction.

Recent developments proposed a formal causal framework for mediation analysis using this Product method, but these enhancements are applicable to any form of outcome, mediator and exposure (continuous, binary, counts etc..) and also allow for exposure-mediator interaction. As with any modeling approach we assume there is no unmeasured confounding of any of the relationships (exposure-mediator, exposure-outcome and mediator-outcome). An additional assumption for this method is that there is no confounder measured or unmeasured of the mediator-outcome relationship induced by the exposure (A). We will henceforth refer to this type of confounding as intermediary confounding.

Modern Mediation Analysis: Counterfactual Framework

Modern mediation analysis has built upon the Product method using causal inference literature and counterfactual frameworks (Rubin et al 2005). The counterfactual framework

provides notation for fixing relevant variables in non-randomized studies (Rubin 1974). For further details on this notation see *Causal inference: For statistics, social and biomedical sciences: an introduction* by Imbens and Rubin (2015).

The individual causal effect of an exposure on an outcome is the hypothetical contrast between the outcome under the exposure and in the absence of the exposure. The notation for this includes Y_a, which is the potential outcome under the exposure, $\mathrm{A} = \mathrm{a}$. Then Y_{a^*} is the potential outcome under the counterfactual exposure, $\mathrm{A} = a^*$ where $\mathrm{a} = 1 - a^*$ when there is a binary exposure. It is only possible to observe either Y_a or Y_{a^*}, this is known as the fundamental problem of causal inference (Holland 1987). Then the causal effect is defined as $\mathrm{E}(\mathrm{Y_a} - \mathrm{Y_{a^*}})$ (Richiardi et al 2013; Rubin 1974).

In mediation analysis specifically, this framework defines natural direct and indirect effects that sum to the total effect (Pearl 2001). Here $Y_{a,m}$ is the potential outcome under exposure $\mathrm{A} = \mathrm{a}$ and mediator $\mathrm{M} = \mathrm{m}$. The natural direct effect is the difference between the outcome if exposed to $\mathrm{A} = \mathrm{a}$ and the value of the counterfactual outcome if the same realization of all confounders, were exposed instead to $\mathrm{A} = a^*$ and the mediator set to the value it would take with exposure $\mathrm{A} = a^*$. The natural direct effect is thus defined as $\mathrm{E}\left(Y_{a,M(a^*)} - Y_{a^*,M(a^*)}\right)$. It is also possible to estimate controlled direct effects (which is equivalent to natural direct effects in the absence of exposure-mediator interactions), but in this paper we focus on natural direct effects as our estimand of interest. Finally, the natural indirect effect is defined as $\mathrm{E}\left(Y_{a,M(a)} - Y_{a,M(a^*)}\right)$. This is the difference in the outcome if exposed to $\mathrm{A} = \mathrm{a}$ and $\mathrm{M} = \mathrm{M}(a)$ and the value of the counterfactual outcome, if exposed to $\mathrm{A} = \mathrm{a}$ but $\mathrm{M} = \mathrm{M}(a^*)$ takes on the value M would take if the exposure was $\mathrm{A} = a^*$, under the same realization of all confounders under $\mathrm{A} = \mathrm{a}$.

Assumptions and Confounding

The four major assumptions in mediation analysis are in a class of confounding based assumptions (Vanderweele 2010).

1 No unmeasured confounders of the relation between A and Y

2 No unmeasured confounders of the relation between A and M

3 No unmeasured confounders of the relation between M and Y

4 No measured or unmeasured confounders of M and Y that are affected by A

Through use of the counterfactual framework various weighting and standardization methods have been developed to address assumptions including the fourth and most restrictive assumption. Weighting methods such as Inverse Probability of Treatment Weighting (IPTW), Inverse Odds Ratio Weighting (IORW) and others handle multiple mediators, interactions, and measured intermediary confounding. Additionally, use of G-Computation, a standardization method, can address time-varying confounding, time-to-event outcomes, and exposure induced mediator-outcome confounding and multiple mediators. Stochastic mediation (Rudolph 2018) can allow for exposure induced mediator-outcome confounding and multiple mediators. Thus, there are many methods for handling assumptions in this context that are not available in the spatial domain.

Spatially Varying Coefficient Models

In most settings, mediation analysis uses regression models to estimate direct and indirect effects. Fortunately, there exist various methods for spatial regression as well, but not in the context of mediation. Thus, we can extend the use of linear regression in mediation to the spatial

domain through the use of spatial regression. We will consider two methods within a single class of models referred to as Spatially Varying Coefficient (SVC) models, which allow model coefficients to vary over space. We chose these two methods as they are computationally tractable and analogous to linear modeling with no spatial dependence.

SVC modeling is a popular method for spatial regression in many applied science fields including physics, marine biology, geography, climatology, atmospheric sciences and urban planning (Paulson & Jiang 1995; Zang et al 2021; Wang et al 2008; Gan et al 2022; Jiang et al 2021). As a brief introduction consider that a response variable is sampled at N sample sites distributed across a study region. The simple linear SVC has the following form:

$$y_i = \Sigma_{p=1}^{P} x_{pi}\beta_{pi} + \epsilon_i \tag{4}$$

$$\mathrm{E}[\epsilon] = 0$$

$$\mathrm{Var}[\epsilon] = \sigma^2$$

where, x_{pi} represents the p-th explanatory variable at the i-th sample site and β_{pi} represents the k-th SVC, where K is the number of sample sites multiplied by the number of explanatory variables. Finally, σ^2 is a variance parameter. The two methods we will consider are the representative SVC, Geographically Weighted Regression (GWR) and Moran based SVC for large data sets (M-SVC).

Geographically Weighted Regression

GWR extends Ordinary Least Squares (OLS) linear regression models by accounting for spatial structure and estimates a separate model and local parameter estimates for each geographic location contained in a data set. This local model is based on a subset of the data around the location or the neighborhood of the point. These points are utilized by adopting a differential weighting scheme. Introduced by Brunsdon et al (1998), this method of modeling is very similar to kernel regression (Ruppert et al 1995), in that we have a kernel function. However, in GWR the kernel is not based on similarities in predictor variables, but is instead spatial, considering physical distance.

GWR can be considered a kernel-weighted method of regression. In any kernel regression, there are two major choices to be made. We must choose a kernel function and choose a bandwidth for our 'circle of inclusion'.

Kernel Function

The regression model centered at each x_i can be thought of as a weighted OLS regression where the weights for points within the neighborhood follow a particular kernel function and those outside the neighborhood are weighted at 0. The simplest case of a kernel function gives uniform weights to all observations within the neighborhood.

$$w_{ik} = \begin{cases} 1 & d_{ik} < h \\ 0 & otherwise \end{cases} \quad (5)$$

Where h is the radius of the neighborhood and d_{ik} is the distance from a point x_k to the point x_i. This weighting is overly simplistic and restrictive as a step function. Continuous kernel functions are more common. A kernel function, K(d), which is a function of distance, should have the following properties (Brunson et al 1998):

1) $K(0) = 1$
2) $lim_{d\to\infty} K(d) = 0$
3) K is a monotone decreasing function for positive real numbers

The kernel function we will consider for our analysis and simulation will be the Gaussian decay kernel.

$$w_{ik} = e^{-d_{ik}^2/(2h^2)} \tag{6}$$

The Gaussian decay kernel allows for the weight to gradually decay with distance. The constant bandwidth, h, in a continuous decay function only provides a measure of the rapidity of decay. Using this weighting scheme, each resulting β estimate in model (4) will be continuous on $R^{\mathbb{2}}$.

There are several other common Kernel functions including the Exponential function.

$$w_{ik} = e^{-d_{ik}/(h)}$$

and the bi-square function.

$$w_{ik} = \begin{cases} 1 - \left((d_{ik})^2/(2h^2)\right)^2 & d_{ik} < h \\ 0 & Otherwise \end{cases}$$

Ideally, the choice of a Kernel function will depend on the spatial covariance of the observed data. However, in my experience the bandwidth is more important than the shape of the kernel. There are many approaches to choosing a kernel function apart from the spatial covariance but in the literature a Gaussian kernel is the most commonly used in practice for continuous data (Lu et al 2011).

Choosing the Bandwidth

Choosing the bandwidth is a more important and influential choice in our experience. There are two common ways to choose the bandwidth h. The first uses a cross validation method to choose the optimal fixed bandwidth. Here we find the h that minimizes the sum of squared errors at all locations, i:

$$\mathrm{CV} = \Sigma_i[y_i - \widehat{y_{\neq 1}}(\beta)]^2$$

Where $\widehat{y_{\neq i}}(\beta)$ is the fitted value of y_i with the observation for the i^{th} site omitted from the calibration. This method is the method we will use when choosing a bandwidth. However, it

should be noted that leave one out cross validation can change the spatial dependence structure in an areal data setting.

There is an additional method for bandwidth choice that minimizes the Akaike Information Criterion (AIC), but this involves the computation of n × n matrices where n is the number of sample sites and therefore is not ideal for large spatial datasets. However, AIC can be more exact in smaller spatial settings.

Computation

Having chosen a weighting function and bandwidth our β estimates can be computed with the following:

$$\beta = (X^T W X)^{-1} X^T W y \tag{7}$$

The matrix W_i is the diagonal matrix of the w_{ik} weights.

$$W_i = \begin{pmatrix} w_{i1} & \cdots & 0 \\ \vdots & \ddots & \vdots \\ 0 & \cdots & w_{in} \end{pmatrix} \tag{8}$$

The β in Equation (7) is a matrix containing all β_{ij} for each sample site i and predictor j (from 1 to p). This is the main output from GWR. A row corresponds to all the β estimates for

each location. The matrix of β's can be extracted as an n × p matrix where p is the number of predictors.

Moran Spatially Varying Coefficient Model

Moran SVC (M-SVC) is an approach developed and based on the Moran coefficient (Moran 1950). This coefficient is a diagnostic statistic of spatial dependence. MC when $\boldsymbol{y} = [y(s_1), \ldots, y(s_N)]'$ is:

$$\mathrm{MC}(y) = \frac{N}{\mathbf{1}'\mathbf{D}\mathbf{1}} \frac{\boldsymbol{y}'C\boldsymbol{D}C\boldsymbol{y}}{\boldsymbol{y}'C\boldsymbol{y}} \tag{9}$$

Where the w are the spatial weights, D is a symmetric spatial proximity matrix with 0 diagonals and C is a centering matrix of the form $C = \boldsymbol{I} - \mathbf{1}\mathbf{1}'/N$, and N is the number of sample sites. When the $\mathbf{y}_s$ are positively spatially dependent values then $\mathrm{MC(y)} > \frac{-1}{N-1}$. And when negatively dependent, $\mathrm{MC} < \frac{-1}{N-1}$ (Griffith 2003). D is a proximity matrix where the $(i,j)^{th}$ element is defined by $e^{-d(s_{ij})/r}$ where the range parameter r is given by the maximum distance in the minimum spanning tree connecting all sample sites (Dray et al 2006; Murakami et al 2015).

Modeling

Moran eigenvector SVC (M-SVC) is a modeling approach (Griffith 2008), which is an extension of the Moran eigenvector spatial filtering approach (Griffith 2014). While

instability of this approach was alluded to by Helbich and Griffith (2016) and Oshan and Fotheringham (2018), Murakami et al. (2017) extended it to approximate the Bayesian-SVC model, and Murakami et al. (2017; 2018) demonstrated its estimation accuracy through Monte Carlo experiments with a fast computation approach introduced in 2019 (Murakami 2019).

Let V = CDC, take $\boldsymbol{E} = [e_1, \dots, e_L]$ to be an N $\times$ L (< N) matrix of eigen vectors of the CDC matrix. Furthermore, $\boldsymbol{\Lambda}$ is the diagonal L $\times$ L matrix of the L leading eigenvalues of V $\{\lambda_1, \dots, \lambda_L\}$, these explain the highest proportion of spatial dependence. This method applies L eigen-pairs corresponding to positive eigenvalues from $\boldsymbol{E}$ and Λ. This method like other SVCs assumes positive spatial dependence by only taking L eigen-pairs corresponding to positive eigenvalues.

The M-SVC coefficients are formulated with a fixed and varying portion with an eigenvector Moran Coefficient (MC) based model of spatial dependence. The overall model for an outcome, Y, is as follows:

$$\boldsymbol{y} = b_1\mathbf{1} + \Sigma_{k=2}^{K}\boldsymbol{x}_k{}^{\circ}\boldsymbol{\beta}_k + \boldsymbol{E}\boldsymbol{\gamma_1} + \boldsymbol{\varepsilon}, \boldsymbol{\gamma_1} \sim N(0, \tau_1^2\Gamma^{\alpha_1}),\ \varepsilon \sim N(0, \sigma^2\boldsymbol{I}) \quad (10)$$

Where $\mathbf{y}$ (N $\times$ 1) is a vector of response variable values at each sample site and x_k ($N \times 1$) is the vector of the k^{th} covariate for all the spatial sample points, i. The $\mathbf{E\gamma_1}$ captures residual spatial dependence, Murakami and Griffith (2018) showed that the term $\mathbf{E\gamma_1}$ with L = 200 greatly reduces residual spatial dependence.

The β_k is made from two components, $\beta_k = b_k + \boldsymbol{E\gamma_k}$, where b_k is a constant mean and $\mathbf{E\gamma_k}$ is the spatially varying component, composed of eigenvectors and random coefficients, $\boldsymbol{\gamma_k} \sim N(0, \tau_k^2 \Gamma^{\alpha_k})$. $\mathbf{E\gamma_k}$ has 2 properties, it is interpretable in terms of the Moran Coefficient and the eigenvectors have zero means. Both properties are important to make the $\mathbf{E\gamma_k}$ values identifiable and model the spatial dependence.

The $\boldsymbol{\gamma_k}$ vector is a vector of random coefficients depending on two shrinkage parameters, τ_k^2 and α_k. The τ parameter controls the variance of the spatial variation of $\boldsymbol{\beta_k}$. The α parameter guides the spatial scale, thus estimating the spatial scale parameter of the SVC rather than using a range parameter, which is treated as fixed in a GWR model. This accelerates model estimation and estimation error remains small (Murukami and Griffith 2018).

We additionally have an error term ϵ, which we assume is Gaussian with mean 0 and variance σ^2, that captures non-spatial variance. We assume all spatial variation is captured in the other terms of the model.

Parameter Estimation

The M-SVC model is estimated by the Type II restricted likelihood (empirical Bayes) method that maximizes the log-likelihood of the shrinkage parameters $\Theta = \theta_1 \ldots \theta_k$, where $\theta_k = \{\tau_k^2, \alpha_k\}$ and the log-likelihood of y conditional on b and Θ. If the probability density functions for y and the random coefficients u are Gaussian, the log-likelihoods have an analytical expression. Using this restriction, the parameters can be estimated (Bates 2010). Thus, since $\mathbf{u}$ represents the random coefficients, $\mathbf{V}(\boldsymbol{\theta_k})\boldsymbol{u_k} = \boldsymbol{\gamma_k}$ as defined previously.

$$loglik(\Theta) = -\frac{1}{2}\ln|\boldsymbol{P}| - \frac{N-K}{2}\left(1 + ln\left(\frac{2\pi d(\Theta)}{N-K}\right)\right)$$

(11)

$$\boldsymbol{P} = \begin{bmatrix} \boldsymbol{X'X} & \boldsymbol{X'E_1V\,(\theta_1)} & \dots & \boldsymbol{X'E_kV\,(\theta_k)} \\ \boldsymbol{X'E'_1V\,(\theta_1)} & \boldsymbol{V\,(\theta_1)E'_1E_1V\,(\theta_1)\ +\ I} & \dots & \boldsymbol{V\,(\theta_1)E'_1E_kV\,(\theta_k)} \\ \vdots & \vdots & \ddots & \vdots \\ \boldsymbol{V\,(\theta_k)E'_kX} & \boldsymbol{V\,(\theta_k)E'_kE_1V\,(\theta_1)} & \dots & \boldsymbol{V\,(\theta_k)E'_kE_kV\,(\theta_k)\ +\ I} \end{bmatrix}$$

The derivative $\mathbf{d}(\boldsymbol{\theta})$ is equal to:

$$d(\theta)\ =\ \left\| y\ -\ X\widehat{\boldsymbol{b}}\ -\ \sum_{k=1}^{K} \boldsymbol{E_kV\,(\theta_k)\widehat{u_k}} \right\|^2\ +\ \sum_{k=1}^{K} \|\widehat{\boldsymbol{u_k}}\|^2$$

The b and the u values are estimated by Equation (12).

$$\begin{bmatrix} \widehat{\boldsymbol{b}} \\ \widehat{\boldsymbol{u_1}} \\ \vdots \\ \widehat{\boldsymbol{u_k}} \end{bmatrix} = \boldsymbol{p^{-1}} \begin{bmatrix} \boldsymbol{X'y} \\ \mathbf{V(\theta_1)E'_1y} \\ \vdots \\ \boldsymbol{V(\theta_k)E'_ky} \end{bmatrix}$$

(12)

This combination balances the accuracy and complexity of the model. The values for Θ can be estimated by maximizing (11). This is followed by the estimation of the $\{b,u_1, \dots, u_K\}$with Equation (12). The SVCs are estimated by Equation (13).

$$\boldsymbol{\beta_k = b_k + E\gamma_k\ =\ \widehat{b_k}1\ +\ EV(\widehat{\theta_k})\widehat{u_k}}$$

(13)

Finally the residual variance must be estimated as $\widehat{\boldsymbol{\sigma^2}}\ =\ \widehat{\frac{1}{N-K}}\,\hat{\boldsymbol{\varepsilon}}'\hat{\boldsymbol{\varepsilon}}$ where $\hat{\varepsilon}\ =\ y\ -\ \widehat{\boldsymbol{b_1}}\,\mathbf{1}\ -\ \sum_{k=2}^{K}\boldsymbol{x}_k{}^{\circ}\boldsymbol{\beta}_k\ -\ \boldsymbol{E\gamma_1}$ as defined in equation (10). The variance of the $\hat{\beta}$estimates are used to evaluate statistical significance. This variance is estimated analogously to a linear mixed effects model.

Likelihood maximization is computationally inefficient especially due to the high number of parameters that must be estimated under a high number of predictors, K. Thus, matrix tricks

can be employed to speed the processing time of this type of model (Murakami 2019). For the purposes of computational efficiency, there is a fast M-SVC (Murakami 2019). Using the Nystrom extension (Drineas 2005) based approximation of the Moran eigenvectors and eigenvalues (Murakami 2018), this avoids the high computational cost of eigenvalue decomposition. And instead of using every sample point for the development of the proximity matrix a C matrix is computed using L knots where $L \ll N. L = 200$ is sufficient to model spatial dependence (Murakami 2018).

Combining Mediation Analysis and SVC modeling

Spatially varying coefficient models are analogous to linear regression or mixed models both of which are employed for traditional mediation analysis (Bind 2016). For this reason, under similar assumptions to the Product method, we can extend this to a spatial setting. We can fit two SVC models with the forms from Equations (2) and (3) using either GWR or Moran SVC modeling. From there the Product method can be employed to provide local estimates for NDE and NIE.

GWR requires the selection of a bandwidth, for which we will employ a cross-validation (CV) procedure to select for both models (2) and (3), however M-SVC does not require this step. The modeling procedure employed the use of two packages *spmoran* (Murakami) for the M-SVC modeling and *GWModel* for the GWR modeling.

Thus, the procedure has the following form:

1) Choose the bandwidth for the y model of the form of Equation (1), this is required only for GWR models.

2) Fit a model of the form of Equation (1):

$$\mathrm{E[Y]} = \theta_0 + \theta_1 \mathrm{A} + \theta_2 \mathrm{M} + \theta_{3-p} B$$

, where A is the exposure, M the mediator and B are any confounders.

3) Choose bandwidth for the M model (Equation (2)) in GWR.

4) Fit a model of the form of Equation (2),

$$\mathrm{M} = \eta_0 + \eta_1 \mathrm{A} + \eta_{2-p_m} B_m$$

where B_m are the measured confounders of the causal pathway from $\mathrm{A} \rightarrow \mathrm{M}$.

5) Estimate errors in estimation of Y using RMSE and squared errors at each location.

6) Estimate spatially varying estimates of NDE and NIE by extracting coefficients from each model and using the procedure outlined in the traditional mediation section to multiply coefficients.

7) Estimate the coverage probability using the standard errors from the SVC models and the true median NDE and NIE values.

There are a few advantages and disadvantages to these two SVC models that are worth mentioning prior to the presentation of simulation studies or empirical example. The main difference between the two methods comes in the form of a trade-off, we must choose whether we prefer computational efficiency over estimation accuracy. The M-SVC method is much more computationally efficient as N increases due to the approximation of the eigenvector-eigenvalue decomposition. Although under most situations, the data will not be large enough to cause GWR to take longer than an hour. However, GWR has the potential to be more accurate due to no

approximation or restrictions on the maximum likelihood estimation. However, GWR does introduce human bias by the choice of spatial covariance function as well as having no adaptive scale parameter.

Validation

To validate this method of spatial mediation we will use RMSE to estimate bias, and standard error estimates from the two SVC models to give coverage probability of our NDE and NIE estimates for each setting.

Simulation Study

Design

To test the efficacy of combining the traditional Product method of mediation analysis and spatial regression techniques, M-SVC and GWR, we must perform a simulation study in a variety of settings. We want to test in different mediation scenarios and across different values of the range parameter for spatial auto-correlation.

In Table 5, we present the 12 simulation settings to be considered. We will consider scenarios where the total effect is both high and low and when the proportion mediated is high and low, with a distribution across space that has scale (range) that takes on three values. We use the terms range and scale here, interchangeably, referring to the extent of the spatial correlation. We consider range as a proportion of the size of the image due to the multiple different spatial domains used in this simulation study: both small and large. We consider range parameters that are small compared to image size (1/20), where the range is about 1/5 of the image size and when range is high at about 1/2 of the image size.

We consider baseline spatial confounders, but no confounders that are unmeasured. We, additionally, do not consider confounders that effect the mediator and outcome that are affected by the exposure variable, i.e. intermediary confounders.

We study three different data scenarios in addition to our 12 simulation settings. We examine a small setting, with just a 20×20 pixel image. We consider a large regular grid setting, in which we use the shape of California and a grid system that has $0.1° \times 0.1°$ cells. And finally, we aggregate the regularly gridded data into ZCTA areas, like how most epidemiological data is provided to test efficacy in that setting.

Small grid simulation results

In Table 6,we can see the RMSE for the outcome and mediator models in the small 20x20 grid simulation. When our total effect is low, universally the RMSE in the mediator model is much higher than the RMSE for the outcome model. When total effect is high and proportion mediated is high we have the most favorable results of the models with lowest bias. However, in the low total effect and high proportion mediated case, when the scale parameter is high the mediator models fail in both GWR and M-SVC. However, a scale parameter this large is not expected in practice and with a spatial covariance with such a large relative scale, a global linear model may perform just as well. In addition, both modeling techniques perform about equally here. We do not present the standard errors and coverage probability because this setting is under powered, and thus the standard errors are larger than the effect sizes.

Table 5 Simulation Settings considered in the simulation study, all are considered in the small grid, regular grid setting and aggregated into regions (zip code).

Total Effect	**Proportion Mediated**	**Range Parameter** (as a proportion of image size)
0.625	4%	1/20
0.625	4%	1/5
0.625	4%	1/2
0.625	36%	1/20
0.625	36%	1/5
0.625	36%	1/2
6.25	4%	1/20
6.25	4%	1/5
6.25	4%	1/2
6.25	36%	1/20
6.25	36%	1/5
6.25	36%	1/2

In Table 7, we can see the counter intuitive result that M-SVC takes longer to fit than GWR suggesting in a small area setting, GWR does not suffer the disadvantage of time.

Table 6 Small simulation RMSE results for both GWR and M-SVC

TE	Prop Med	Scale	RMSE GWR	RMSE GWR	RMSE M-SVC	RMSE M-SVC	RMSE Ratio	RMSE Ratio
		pixels	Outcome	Mediator	Outcome	Mediator	Outcome	Mediator
0.625	4%	1	0.74	1.27	0.66	1.23	1.12	1.03
0.625	4%	3	0.24	0.68	0.26	0.86	0.92	0.79
0.625	4%	10	0.10	0.34	0.57	0.34	0.14	1.0
0.625	36%	1	0.48	1.0	0.46	0.99	1.04	1.01
0.625	36%	3	0.34	0.73	0.41	0.78	0.83	0.93
0.625	36%	10	0.56	16.6	0.43	11.3	1.3	1.46
6.25	4%	1	0.14	0.84	0.48	0.84	0.29	1.0
6.25	4%	3	0.11	0.51	0.41	0.54	0.26	0.94
6.25	4%	10	0.02	0.27	0.03	0.20	0.66	1.35
6.25	36%	1	0.19	0.82	0.38	0.82	0.5	1.0
6.25	36%	3	0.05	0.31	0.11	0.36	0.45	0.86
6.25	36%	10	0.27	0.31	0.66	0.59	0.41	0.52

Table 7 Small simulation time results showing counterintuitive GWR efficiency over M-SVC.

Method	Time (sec)	Standard Deviation (SD)
GWR	4.12	0.64
M-SVC	34.5	10.8

Regular grid simulation results

In Table 8 are shown the RMSE values for both modelling frameworks for all the simulation settings as well as ratios for the GWR RMSE over the M-SVC RMSE. In this setting due to the larger data size, the small total effect settings do not result in significantly higher RMSE values. We see the largest RMSE in settings with the smallest scale parameter. Here in this data setting we also do not suffer when the scale is large, total effect is small ,and proportion mediated high the same way as we do in the small simulation setting.

The ratio columns show that performance for the M-SVC model is better for the outcome model in settings with a high scale parameter. But overall, the GWR model handles the mediator model efficiently. Thus, suggesting in a setting with very large scale we should consider M-SVC, but in most scenarios GWR performs very well.

Overall performance here is very good. The NDE and NIE median estimates for each method are in Table 9. The true median values are displayed in bold columns. Also displayed are the results if you were to run global linear models instead of accounting for any spatial autocorrelation. The global linear models are inconsistent and most often do not fit the data well. The GWR and M-SVC have similarly good performance in inference except in very particular scenarios. For instance, in simulation setting 12 GWR underestimates both the NDE and the NIE, whereas M-SVC performs much better. Additionally, in setting 6, GWR underestimated the NDE and overestimates the NIE. When scale is high and proportion mediated is high GWR tends to underestimate the NDE whereas M-SVC does not suffer from this problem.

The coverage probability and standard errors are displayed in Table 10, we can see from this table that the M-SVC models are more consistent and accurate in estimating the NDE and

NIE, with some underestimation of NIE in settings 10-12. The coverage probability is varying with the GWR model and the standard errors are incredibly high in simulation settings 3 and 8, suggesting high scale may lead to low accuracy or precision for GWR models, where the bandwidth of the neighborhood is chosen through cross validation. Furthermore, the accuracy of the NDE estimates is shown to be low in the high mediated effect simulations because the coverage probability is so low.

Table 8 Simulation settings with Standardized RMSE from both outcome and mediator models for regular grid simulations.

TE	**Prop Med**	**Scale**	**RMSE GWR**	**RMSE GWR**	**RMSE M-SVC**	**RMSE M-SVC**	**RMSE Ratio**	**RMSE Ratio**
		degrees	Outcome	Mediator	Outcome	Mediator	Outcome	Mediator
0.625	4%	0.5	0.32	0.51	0.48	0.67	0.66	0.76
0.625	4%	2	0.36	0.25	0.25	0.32	1.44	0.78
0.625	4%	5	0.27	0.16	0.17	0.21	1.58	0.76
0.625	36%	0.5	0.33	0.53	0.49	0.67	0.67	0.79
0.625	36%	2	0.23	0.26	0.26	0.34	0.88	0.76
0.625	36%	5	0.30	0.15	0.16	0.21	1.87	0.71
6.25	4%	0.5	0.5	0.36	0.51	0.49	0.67	0.76
6.25	4%	2	0.24	0.25	0.26	0.31	0.92	0.80
6.25	4%	5	0.29	0.16	0.17	0.21	1.70	0.76
6.25	36%	0.5	0.32	0.52	0.48	0.69	0.66	0.75
6.25	36%	2	0.41	0.25	0.26	0.34	1.57	0.73
6.25	36%	5	0.33	0.15	0.17	0.20	1.94	0.75

Table 9 The estimated NDE and NIE for the models as well as with a global linear model.

Sim Setting	Global NDE	GWR Median NDE	SVC Median NDE	LM NDE	Global NIE	GWR Median NIE	SVC Median NIE	LM NIE
1	0.60	0.61	0.61	0.74	0.025	0.032	0.037	0.126
2	0.60	0.58	0.62	0.43	0.025	0.025	0.028	-0.01
3	0.60	0.55	0.59	0.42	0.025	0.143	0.021	1.2
4	0.4	0.41	0.39	0.36	0.225	0.32	0.285	0.31
5	0.4	0.36	0.41	0.01	0.225	0.20	0.27	-0.01
6	0.4	0.18	0.39	-0.07	0.225	0.85	0.21	1.54
7	6	5.96	6.0	5.88	0.25	0.26	0.26	0.14
8	6	5.96	6.01	5.69	0.25	0.31	0.27	0.49
9	6	6.35	6.06	6.97	0.25	0.32	0.25	0.9
10	4	4.02	3.98	4.05	2.25	2.21	2.16	2.10
11	4	3.81	3.97	3.28	2.25	2.15	2.09	3.15
12	4	3.40	3.87	3.46	2.25	1.62	2.24	-0.21

In Figure 10 and Figure 11 we see the performance of GWR and M-SVC, respectively in a single instance of simulation scenario 10. The error displayed in subfigures 10c and 11c is

Gaussian while being low in magnitude. The NDE and NIE for both methods have very similar patterns of differences, SVC has lower variance in the estimates as well as higher spatial correlation than the GWR. From the coverage probability we can determine that SVC has better coverage probability and precision in the estimates, while GWR has marginally lower RMSE. Finally, both error plots show roughly a random field, which suggests good model fit in the outcome model.

We do not include any confidence intervals or hypothesis tests here as power was not a consideration in this set of simulations. For the low mediated effect simulations, there is not enough power to have significant estimates of NIE, additionally simulation settings 10 through 12 are over-powered.

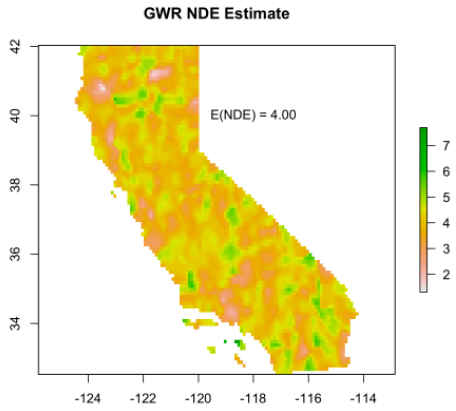

(a) Estimated NDE from GWR models.

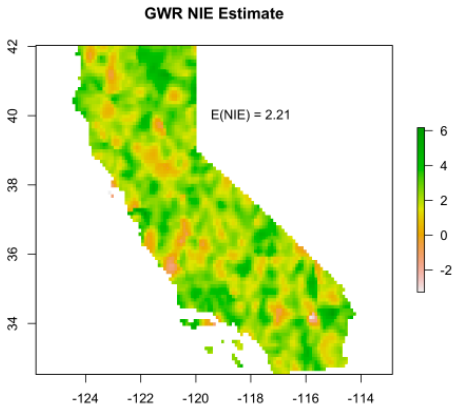

(b) The estimated NIE with GWR models.

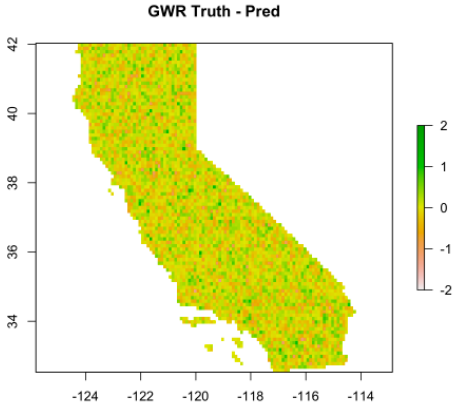

(c) The difference between the true Y and predicted Y.

Figure 10 The estimate plots for using GWR in simulation setting 10. WE expect the median NDE value to be 4 and the median NIE to be around 2.21.

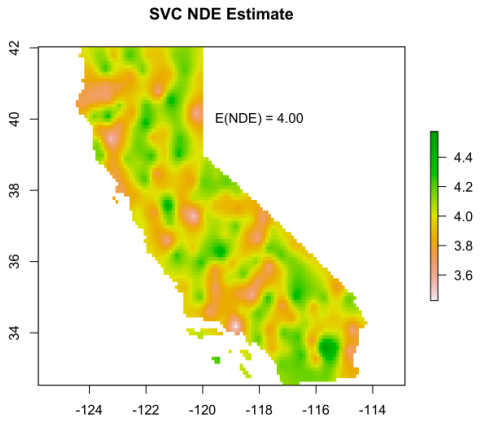

(a) Estimated NDE from Moran SVC models.

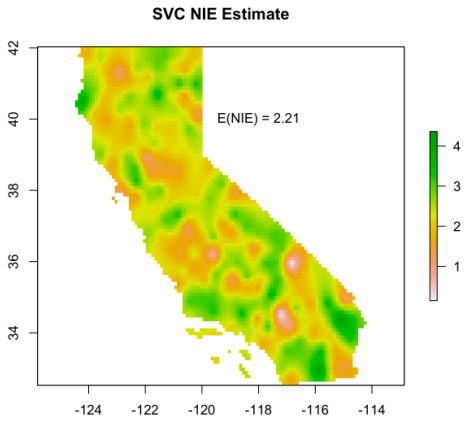

(b) The estimated NIE with Moran SVC models.

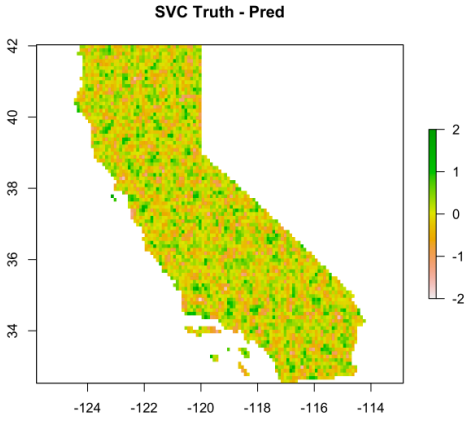

(c) The difference between the true Y and predicted Y.

Figure 11 The estimate plots for using Moran SVC in simulation setting 10. We expect the median NDE value to be 4 and the median NIE to be around 2.21.

Table 10 Coverage Probability from the GWR and M-SVC models for all 12 simulation settings and both NDE and NIE with standard error estimates from the NDE and NIE estimation.

	GWR NDE (SE NDE)	GWR NIE (SE NIE)	M-SVC NDE (SE NDE)	M-SVC NIE (SE NIE)
S1	82.4% (0.29)	98.9% (0.38)	98.6% (0.16)	100% (0.20)
S2	57% (0.19)	92% (0.26)	92% (0.13)	100% (0.13)
S3	100% (6.8)	100% (5.91)	96.5% (0.10)	100% (0.08)
S4	72% (0.22)	87% (0.34)	92.7% (0.19)	98.4% (0.22)
S5	50% (0.20)	71% (0.24)	91% (0.13)	96% (0.14)
S6	33% (0.06)	66% (0.09)	82.4% (0.27)	100 % (0.023)
S7	81% (0.28)	89% (0.36)	93.1% (0.19)	100% (0.05)
S8	100% (27.9)	100% (16.9)	96% (0.15)	98.3% (0.16)
S9	60% (0.10)	78% (0.02)	90% (0.10)	91% (0.09)
S10	81% (0.36)	49% (0.37)	96% (0.20)	65% (0.22)
S11	37% (0.13)	100% (5.0)	93% (0.13)	73% (0.12)
S12	50% (0.12)	34% (0.12)	92% (0.09)	67% (0.08)

The times for running these models are more starkly different than in the small simulation setting. Whereas M-SVC has a strong advantage, taking only 1.7 minutes on average, GWR takes nearly 6 minutes for a single fit of both the mediator and outcome models without fitting the standard errors. Furthermore, when using a GWR model, one must be careful about the implementation they choose. To fit standard errors for each sample site, the modeling computation time increases precipitously with some implementations but not others. In the above grid settings, GWR with fitted standard errors takes about 1.5 hours with the *spgwr* package. We

suggest using the *GWmodel* package instead. This can be incredibly taxing computationally depending on the research question and thus choosing the most efficient implementation is important. For this reason and the increased precision of the M-SVC model, in a big data setting we suggest the use of M-SVC.

Aggregated Areal Region Results

To test the efficacy of this type of analysis on the most common form of spatial data in social or environmental epidemiology, we did the same simulation setting but with data aggregated into ZCTAs in the state of California. This does not represent real data but represents a data situation common for some epidemiology research questions where data is aggregated to preserve privacy.

The RMSE values in Table 11 show much larger values than the non-aggregated case in most settings. In particular, when the total effect is low and proportion mediated is low both model types do not converge to the correct values. However, M-SVC has lower RMSE overall as seen in the ratio columns. When the total effect is large RMSE is similar in value to the non-aggregated case with some bias in the mediator model in simulation setting 7 and 10 suggesting lack of fit when the scale value is too low, which is to be expected because some zip codes are so large relative to the scale.

In Table 12, the NDE and NIE median estimates from both model types are displayed. We can see from the values here that GWR adheres more closely to the true values of NIE but underestimates NDE precipitously. The M-SVC models are severely underestimating both the direct and indirect effects but does a better job in the low total effect settings than GWR.

Furthermore, coverage probabilities are not presented as the standard errors are high in this aggregated setting.

The time differences are negligible, average 1.03 minutes for M-SVC and 1.12 minutes for GWR.

Table 11 Simulation settings with RMSE from both outcome and mediator models for aggregated simulations for GWR and SVC models.

TE	**Prop Med**	**Scale**	**RMSE GWR**	**RMSE GWR**	**RMSE M-SVC**	**RMSE M-SVC**	**RMSE Ratio**	**RMSE Ratio**
		degrees	Outcome	Mediator	Outcome	Mediator	Outcome	Mediator
0.625	4%	0.5	7.39	0.71	6.22	0.78	1.18	0.91
0.625	4%	2	1.18	0.21	0.71	0.12	1.66	1.75
0.625	4%	5	15.69	0.18	8.09	0.08	1.93	2.25
0.625	36%	0.5	1.71	1.07	1.63	1.18	1.05	0.91
0.625	36%	2	0.28	0.24	0.17	0.13	1.64	1.84
0.625	36%	5	0.29	0.21	0.15	0.09	1.93	2.33
6.25	4%	0.5	0.24	1.13	0.23	1.25	1.04	0.22
6.25	4%	2	0.15	0.25	0.13	0.13	1.15	1.92
6.25	4%	5	0.06	0.21	0.04	0.09	1.50	2.33
6.25	36%	0.5	0.22	1.90	0.20	2.01	1.1	0.91
6.25	36%	2	0.33	0.43	0.24	0.25	1.37	1.72
6.25	36%	5	0.13	0.39	0.07	0.16	1.85	1.87

Table 12 The estimated NDE and NIE for the models as well as with a global linear model.

Sim Setting	Global NDE	GWR Median NDE	SVC Median NDE	LM NDE	Global NIE	GWR Median NIE	SVC Median NIE	LM NIE
1	0.60	0.38	0.39	0.74	0.025	0.021	0.011	0.126
2	0.60	0.20	0.39	0.43	0.025	0.013	0.01	-0.01
3	0.60	-0.386	0.39	0.42	0.025	0.08	-0.002	1.2
4	0.4	0.205	0.268	0.36	0.225	0.193	0.135	0.31
5	0.4	-0.02	0.246	0.01	0.225	0.158	0.133	-0.01
6	0.4	-0.43	0.283	-0.07	0.225	0.28	0.06	1.54
7	6	4.35	4.07	5.88	0.25	0.26	0.19	0.14
8	6	4.2	4.17	5.69	0.25	0.25	0.18	0.49
9	6	2.53	3.43	6.97	0.25	0.35	0.08	0.9
10	4	2.60	2.43	4.05	2.25	1.91	1.65	2.10
11	4	2.48	2.43	3.28	2.25	2.05	1.69	3.15
12	4	1.64	2.19	3.46	2.25	2.35	2.38	-0.21

Below similarly to Figure 10 and Figure 11 we have Figure 12 and Figure 13, which are the NDE and NIE spatial estimates for simulation setting 10. Notably, the NDE is underestimated in both models in this setting and the NIE has some outliers in the GWR fit and is slightly underestimated in the M-SVC fit. The errors in the Y models show higher magnitude error than in the non-aggregated and appears more spatially correlated.

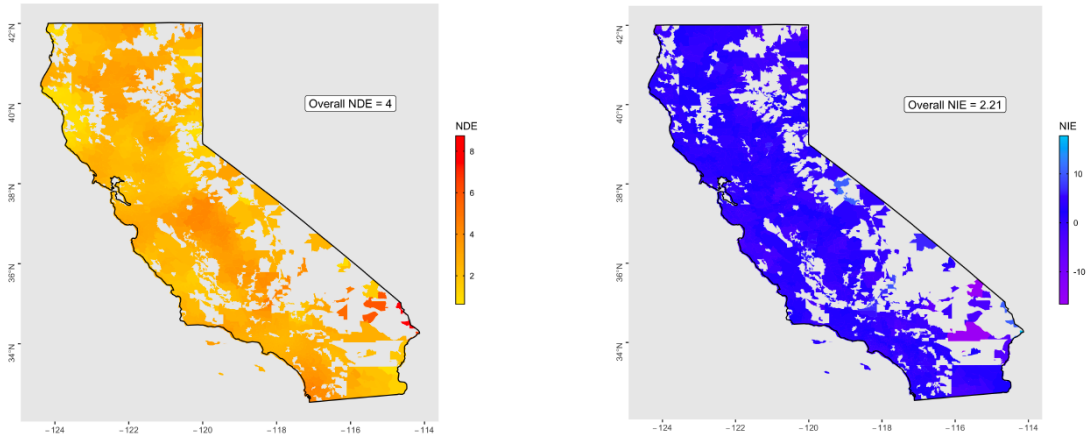

(a) Estimated NDE from GWR models in aggregated setting.

(b) The estimated NIE with GWR models in aggregated setting.

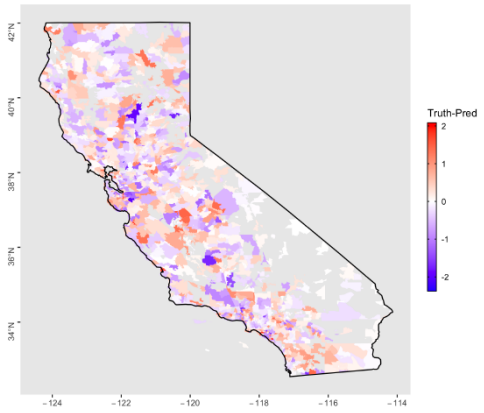

(c) The difference between the true Y and predicted Y in aggregated setting.

Figure 12 The estimate plots for using GWR in aggregated simulation setting 10. We expect the median NDE value to be 4 and the median NIE to be around 2.21.

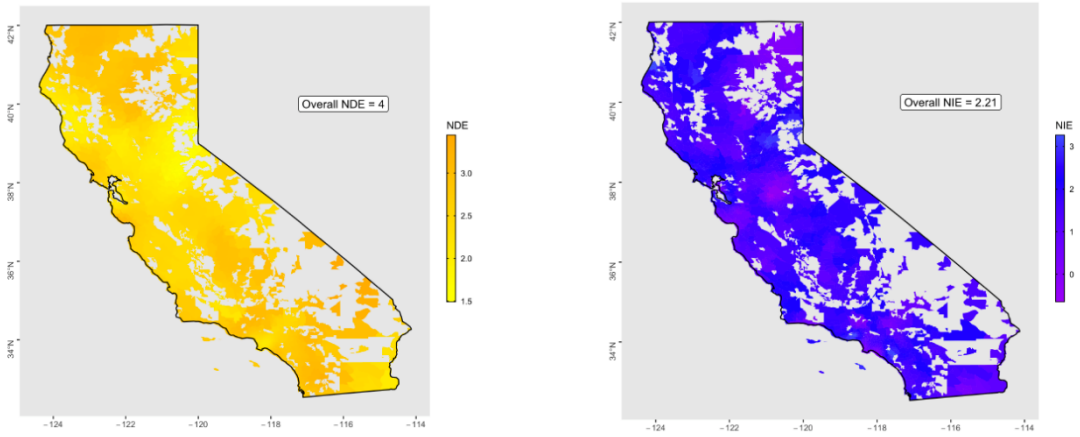

(a) Estimated NDE from Moran SVC models in aggregated setting.

(b) The estimated NIE with Moran SVC models in aggregated setting.

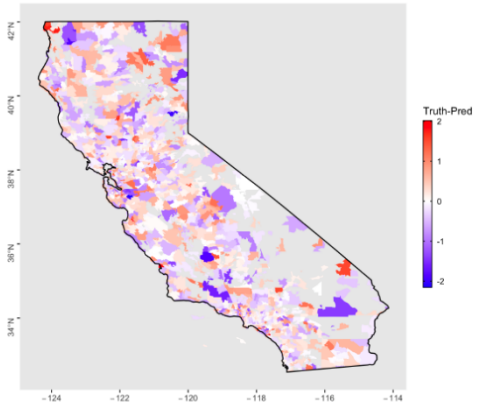

(c) The difference between the true Y and predicted Y in aggregated setting.

Figure 13 The estimate plots for using Moran SVC in aggregated simulation setting 10. We expect the median NDE value to be 4 and the median NIE to be around 2.21.

The results from the aggregated setting show the downfalls to using zip code level data for analysis. The irregularly spaced regions are not geographic regions, but designations for mail delivery by USPS leading to vast areas with no coverage and also low number of neighboring zip codes for many. We see here that GWR and Moran SVC models although they handle the irregularity have some problems, which we expect to be quite common. Overall though M-SVC performs better in most settings even though it underestimates the decomposed effect sizes. In

general, we do not suggest using this method in a zip-code level setting, but if necessary introduce variables to help account for this irregularity, like population and area of each zip code.

Case Study: Modeling Procedure

The modeling framework shown in Section 4 demonstrates that this modeling procedure is viable for use in analysis in environmental epidemiology in some settings. To illustrate the possible use of this methodology in practice a case study with spatial data was undertaken.

For this we use the California Healthy Places Index (HPI 2018) and CalEnviroScreen (2019) data to explore the relationship between income and Cardiovascular Disease (CVD) mediated by PM2.5. We evaluate this relationship because it is understood that income can have an effect on health outcomes like rate of CVD (Mosquera 2016), however, pollution like PM 2.5 can modify this relationship as it is also a predictor of CVD (Hystad 2020), but income can effect PM2.5 exposure as well (Finkelstein 2003).

The data we use to estimate these effects come on the census tract level, this is higher resolution than a zip code and so may lead to better results than the zip code level data. We dichotomize the income variable for simplicity in interpretation by taking the median as the cutoff. We include the education level, proportion white and employed percentage as confounders in our outcome model. We fit the GWR models for the mediator and the outcome and use the Product method to estimate the NDE and NIE.

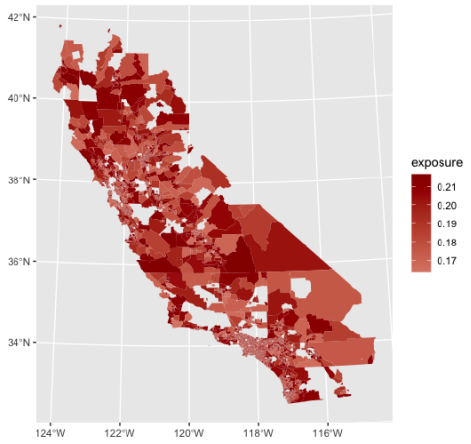

(a) Estimated NDE from GWR models in case stud.

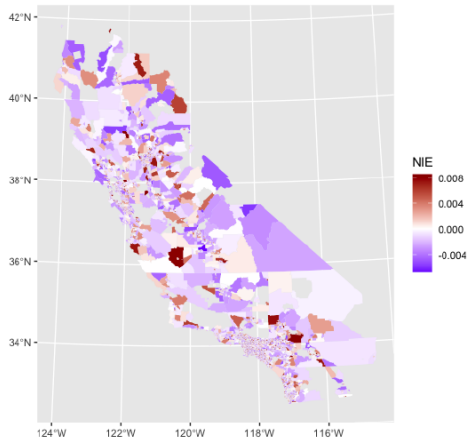

(b) The estimated NIE with GWR models in case study.

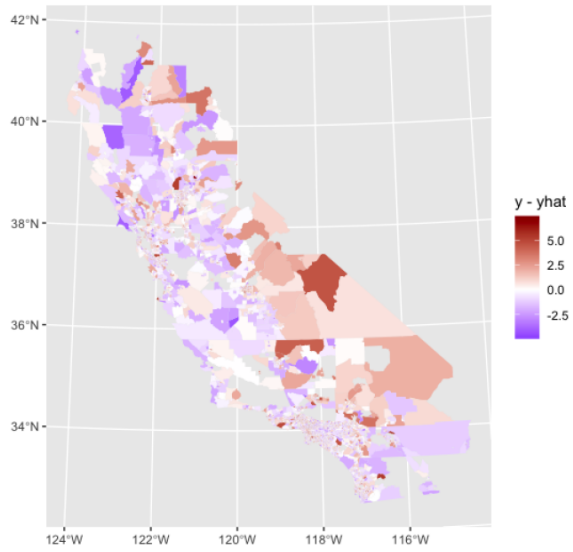

(c) The difference between the true Y and predicted Y from the full outcome model in the case study.

Figure 14 The estimate plots for using GWR with the Case Study data.

Figure 14 shows the results from the case study. We can see that the error and bias ranges between -3 and about 5 with most values falling between -2 and 2, due to the outcome being on a percentile scale from 0 to 100 this is not particularly high. Bias in general can be due to misattribution of the bandwidth or correlation functions, so if one sees high bias in their outcome models a further exploration of the spatial parameters of the data is suggested.

We also can tell that the mediated proportion is quite low, around 5% here. This suggests that the bulk of the total effect of income on CVD percentile is explained by income itself and mediated varying around 5% by PM2.5 exposure. Additionally, in these results we can see that the effect sizes vary over space. The mediated proportion varies from 2 % to 5 % and the NDE varies from $(0.17,0.21)$. However, because this data is on the census tract level, we expect underestimation of the NDE and the total effect is small. This together suggests that this modeling paradigm is not sufficient in this setting.

Discussion

In this paper, we proposed a novel framework for estimating direct and indirect effects of an exposure allowing for spatial heterogeneity. Through simulation we found that this method of combining traditional mediation analysis and spatial regression is accurate on a gridded dataset. We find that with the same assumptions as the Product method in addition to isotropy allow us to accurately estimate natural effects on a spatial domain. We found that on a regular grid, the performance of these analysis methods is far better than when aggregated at the zip code level.

On a gridded dataset in both small and large settings we see very low bias and good coverage. In the small grid setting GWR has lower bias, this was expected because M-SVC is designed for large datasets. In the large regular grid setting we find that although both methods have very low bias in most settings, GWR has lower coverage probability and is more inconsistent in performance than M-SVC. M-SVC is thus suggested as the best model framework for this type of data.

For zip code level spatial data, this analysis method is inadequate in most of the simulation settings. Furthermore, the M-SVC method tends to underestimate effects, particularly when the scale variable is low. But in general, has lower bias than GWR and lower variability in estimates. GWR can even lead to some negative estimates of NIE and NDE in the small total effect settings. If there is a small total effect and large proportion mediated, M-SVC may be sufficient in a zip-code setting with the inclusion of variables to account for irregularity of each zip code.

For these reasons, we advise the use of M-SVC based mediation analysis when gridded data is available. It is ideal to work in the grid setting in any case as the bias is lower and estimates are more precise.

In a zip-code data context we can use special zip-code shapefiles that enforce zip-codes to have neighbors or work in regions without large areas of no population. Additionally, these models, both M-SVC and GWR, are not designed with zip code type data in mind, and so regardless of this research problem, these models are not ideal with epidemiology data, but are continuing to be used. They tend to overestimate the spatial correlation of the data and therefore underestimate the covariates, this is a type of spatial confounding. Furthermore, research must be done to find a modeling framework that works well for zip code level data, however, most spatial models do not estimate on this type of data well.

For these reasons, in principle, statistically we would prefer to work with gridded data. There is precedence for downscaling data from low to high resolution in fields like climatology. Research into the possible downscaling of zip code level data to a grid is ideal and left as an area of future research.

The GWR models can take longer to run but we do not see extreme differences in time to fit the models with the right implementation. For our regular grid simulation, we have around 4000 data points, the GWR models took 6 minutes to fit, and the Moran SVC models just over 1 minute. We do not anticipate time pressure to be a reason to not use GWR, but again M-SVC is preferable in most settings.

The assumptions under this framework are quite restrictive, in addition to the assumptions of the Product method in mediation we also have the assumptions of the GWR and M-SVC models themselves. These assumptions include isotropy, which means that the spatial correlation extends the same distance in the X and Y direction and that same distance from every point in our data set. In our simulations we do present isotropic data. However, in an environmental context we can expect anisotropic data at least in some research contexts. There are a few possible solutions to this. We can include variables that account for environmental anisotropy in the regression equation, like elevation, topography, and population values as covariates, this however will not fully account for anisotropy in all circumstances. We additionally could extend our modeling to the use of anisotropy friendly modeling techniques, GWR has an extension for anisotropy, for instance (Paez, 2004) and M-SVC could be extended

to allow for anisotropic covariance functions. The implementation of these techniques is not built into statistical computing software and left as an area of future work.

In addition to anisotropy this modeling framework cannot estimate accurately in the presence of intermediary confounders. These are the confounders that are affected by the exposure and in turn affect the mediator -outcome pathway. In mediation, this type of confounding can be handled with weighting or standardization techniques like Inverse Probability of Treatment Weighting (IPTW), G Computation, and Stochastic Mediation. Spatial regression with current implementation does not allow for the addition of non-spatial weights along with the geographic weights. Furthermore, G-Computation in a spatial setting has never been done. To allow for G-computation in a spatial setting, there needs to be an extension of time-varying G-computation to two-dimensional space-varying G-computation. This is an area of possible future endeavor.

The limitations discussed are important to consider in the environmental epidemiological context as anisotropy and intermediary confounding could be quite common in this field. For that reason, future work will need to address these concerns. However, this method for estimating spatial heterogeneity in direct and indirect effects of an exposure is an essential step in spatial causal inference for environmental epidemiology. Furthermore, this method allows investigators to explore research questions where spatially heterogeneous effect decomposition can be estimated accurately.

Acknowledgements

This work was supported by the California Environmental Protection Agency Office of Environmental Health Hazard Assessment #19-E0022 and by the National Institutes of Health, National Cancer Institute [grant number R01CA228147]

Chapter 3, in full, is currently being prepared for submission for publication of the material, Kristen Hansen; Armin Schwartzman; Tarik Benmarhnia. The dissertation author was the primary researcher and author of this paper.

CHAPTER 4: Downscaling health outcomes using predictive models of environmental and social exposures

Introduction

In environmental and health research it is incredibly important to have fine scale spatial estimates of health outcomes and effects. This is because in most research problems fine scale heterogeneity can lead to different relationships between variables of interest at different spatial locations. Furthermore, when data is aggregated at a coarse spatial level, important variability within such coarse spatial units can be concealed and opportunities to identify most affected/exposed communities may be missed. Ideally, a researcher or government agency would want the smallest spatial scale possible to target interventions to specific locations where said intervention could be most successful.

However, the data landscape which environmental health research is conducted does not always permit access to the smallest spatial scale. Due to privacy considerations or lack of access to data most health data is only available at a relatively large spatial scale, such as the County or zip code level. In parallel, most environmental exposures, whether they are estimated via remote sensing products, monitoring stations or dynamical models (e.g. chemical transport or dispersion models) can be available at a fine spatial grid. Such spatial mismatch prevents the identification of environmental health issues at a fine spatial scale and optimization of strategies that would prioritize most vulnerable communities. Models when there is spatial scale mismatch exist but are perhaps not ideal for all problems (Gotway & Young 2002).

Yet, it is possible to overcome such issues indirectly by understanding the drivers of the spatial variability of a given health outcome. Indeed, many potential predictors of health outcomes can be available at a fine spatial scale. These can be obtained from various sources of data such as remote sensing products, census data or community-based surveys. Such fine-scale predictors can be leveraged to develop and optimize predictive models that would permit a downscaling of health data to be matched with relevant environmental exposures of interest.

Other disciplines such as climate sciences or hydrology have proposed methods for downscaling a given variable at a finer spatial resolution that are available to borrow (Fan et al 2021; Hanigan et al 2019; Serifi et al 2021; Shen & Yong 2021) and apply to the context of epidemiological studies. There is a standing paradigm in climatology and remote sensing to downscale Global Climate Models (GCM) or satellite imagery to a smaller scale using methods like Neural Networks or Random Forest models (Dibike & Coulibaly 2006; Nicholas et al 2016).

In epidemiology and social research in general, downscaling methods have been barely used (Matisziw et al 2008) to obtain health data at a finer spatial resolution. In previous downscaling work, there is a reliance on either historical data or regularity/continuity in the regions of the original scale of the outcome to downscale. In such cases, population density-based downscaling is possible. However, in a data setting where we expect spatial heterogeneity in populations and the relationship between the variables of interest, a simple downscaling approach such as population density-based resampling will not be fully effective as the correlation between predictor of population density and the outcome of interest may vary by location.

Furthermore, the use of Neural Networks, which is the most popular method in climatological downscaling, is impossible in the social data context because these network models rely on access to historical data on the scale of interest (grid), but we do not have access to that type of health or social data. But contrastingly, in remote sensing there is no reliance on historical data for downscaling, but a use of predictive data that is available on the desired scale (Atkinson 2013). In remote sensing, satellite imagery is downscaled to a finer grid using various machine learning techniques such as decision tree ensemble methods (bagging or boosting); including Random Forest and Gradient Boosting (Nicholas et al 2016; Pouteau et al 2011). Thus, methods in this field can be adapted for the use with irregular regions which is the case for most epidemiological problems. Yet, no previous study adapted such methods specifically to health data nor compared the performance of various machine learning techniques.

In this paper, we propose a new approach and algorithm borrowed and adapted from remote sensing to downscale social and health data from the zip code level to census tracts or gridded setting depending on the available predictive data. We use predictive variables that are available on a smaller scale than our outcome of interest. We fit Random Forest and Gradient Boosting models on the scale of our variable of interest using aggregated predictors. Then we predict from those models at the desired scale. We show a validation example using hospitalization data in California and then apply the method on a case study using Covid-19 Vaccine data in California zip codes.

Methods

Downscaling

Downscaling methodology exists in many fields. Primarily developed for the purpose in climatology of using fine scale historical information to downscale Global Climate Models (GCM) - which predict future temperatures and climate (Dibike & Coulibaly 2006). Our data does not put us into a position much like that of climatology literature, thus recent methods using deep learning and neural networks is not applicable. In downscaling GCM, climatologists have historical data for the outcome on the finer scale, however research in health fields will have no very fine scale health data outcomes at all. We must use the predictive variables that we do have on a fine scale to predict those outcomes.

The field of remote sensing additionally performs downscaling to lower the scale of an outcome using only other variables that are available at the finer scale to predict said outcome. This is a directly analogous situation to the one health researchers and practitioners find themselves. Thus, we will focus on a couple of the methods found therein.

The simple intuition behind downscaling is that an aggregation can be applied to those predictive variables that are available on the fine scale to make them the same -larger- scale as the outcome. Once we have this aggregated data, we can fit a model. For our purposes, those models will be a Random Forest and Gradient Boosting model. Then once the model is fit at the higher scale, we can apply the model to the finer scale predictors to get an estimated outcome on the finer scale.

Random Forest

A random forest is a supervised machine learning algorithm that is constructed from an ensemble of decision trees (another supervised algorithm). This machine learning technique can be used in both regression and classification contexts. To classify or regress a new object from an input vector, we plug this vector into many decision trees. Each tree exports a prediction value or classification. The forest then chooses the classification result with the most trees (majority vote), or a weighted average prediction from the trees.

Within a Random Forest, there is no interaction between the individual trees, but the use of independent trees protects from error within any individual tree. This is because Random Forest uses a bagging approach to ensemble learning and feature randomness. Feature randomness means that the predictors that are used for each individual tree are sampled from the original set of predictors. This decreases the correlation between each tree in the forest. Bagging creates a different training subset from sample training data with replacement and the final output is based on majority voting. This is different from Gradient boosting.

Gradient Boosting

Gradient boosting is another ensemble machine learning algorithm. As the name suggests gradient boosting uses boosting-based ensemble learning. Boosting combines weak learners into strong learners by creating sequential models such that the final model has the highest accuracy.

This method is also generally based on decision trees, but instead of fitting several individual independent trees. Trees are fit sequentially. This is done in an iterative way. The input in this method is a loss function, a type of learner (in this case a decision tree) and an additive model to add trees to the model to account for the specific areas of the domain where the previous tree has the lowest prediction accuracy. For this paper we always use squared loss.

The algorithm can stop in two ways, there can be a fixed number of trees to be added like Random Forest or training will stop once the loss reaches an acceptable level. Thus, when using this algorithm, one inputs a tolerance for the error.

Procedure

The procedure for this method has the following steps. A schematic is included in Figure 15 to understand the steps.

1. Choose outcome variable of interest
2. Collect data for all variables available to the researcher that are expected within the context to predict the value of the outcome variable of interest
3. Aggregate all covariate data into the scale of the outcome variable using a mean, median, or sum aggregation depending on the format of each.
4. Fit a Gradient Boosting or Random Forest model on the data of the same resolution as the outcome (ZCTA based data)
5. Find highest resolution common denominator for all the variables included as predictors in the high scale model

6. Predict from the Gradient Boosting or Random Forest model in 4 on these highest resolution predictors

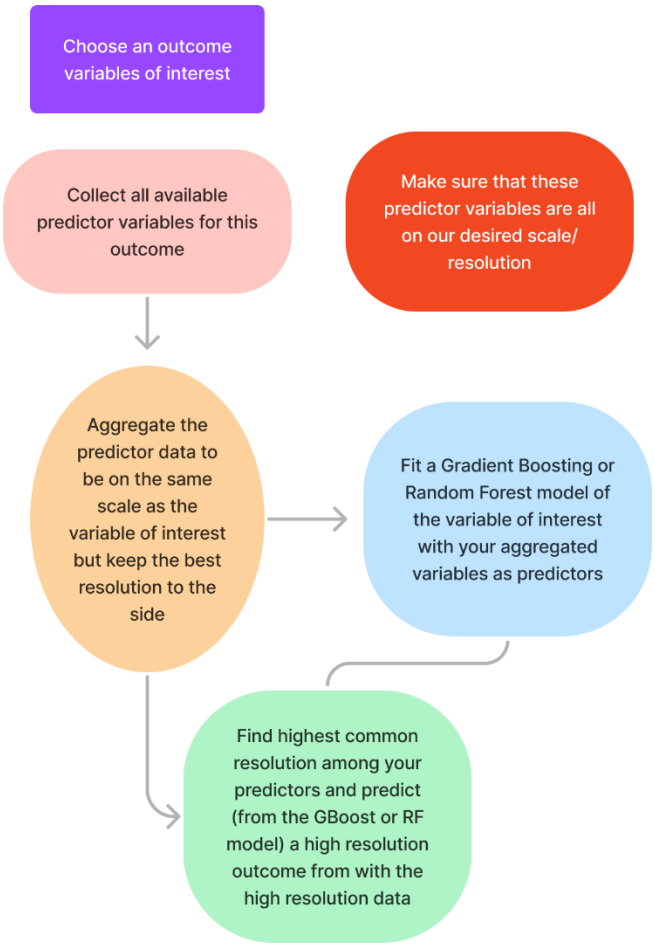

Figure 15 Schematic for descriptive downscaling.

Demonstration and Data

For the purposes of demonstration, we have chosen two examples. One for accuracy estimation of the method proposed and the other for demonstration of possible use. For the determination of accuracy in a health data context, we do not have gold standard data on either a

grid or a census tract and thus had to artificially create groups from zip codes (or Zip Code Tabulation Areas (ZCTAs) for plotting).

Results

We consider a contrived example of yearly unexpected hospitalization rate per 100 people in each zip code in California in 2013 to demonstrate the accuracy of this method. This outcome variable represents an ideal case in this context as in health data in general, outcomes are often skewed right with some outliers depending on the population values in each zip code.

For prediction we will consider various demographic and environmental variables as displayed in Table 13 with their means and standard deviations. As this example is contrived and we do not have census tract level data, we will aggregate our zip codes using a random sample of 100, 200, or 500 zip codes (representing the number of groups we will have to downscale from), and then using a nearest neighbor algorithm to create zip code blocks to then downscale to the original zip code data.

We aggregate the predictor variables from zip codes into our blocks using a mean aggregation for continuous variables. If we had categorical variables, we use a mode and with count variables like population, we use a sum. We fit our models using the *RandomForest* and *gboost* packages in R, respectively. And predict from the results of those models on the zip code level data and compute errors.

Table 13 Descriptive statistics for the hospitalization zip code data.

Variable	Mean	SD	Mean(SD) after aggregation
Hospitalization Rate (year)	0.65	0.24	0.64(0.21)
Median Age	36.7	6.6	37.0(5.9)
Population Density	4911	5940	4603 (5382)
Percent Unemployed	11.6	4.3	11.6 (3.9)
Median Income	66729	27575	67406 (26437)
Percent without Health Insurance	16.6	8.1	16.3 (7.6)
Percent Non-white	34.5	18.4	34.2 (17.9)
Urbanity Indicator	0.87	0.33	0.87 (0.32)
Tree Canopy	9.1	9.6	9.5(9.9)
Park Access	72.3	24.3	71.0 (21.9)
Percent commuting by Bike	8.9	10.5	8.7 (9.5)
NDVI	0.40	0.12	0.40 (0.12)
Mean PM 2.5	11.8	2.6	11.7 (2.6)
Maximum Ozone	0.04	0.006	0.04 (0.006)

As is to be expected, when we have fewer groups to downscale from, we have higher errors than if we use more groups. This intuitively represents a case for downscaling from zip codes instead of downscaling from something like counties.

In Figure 16, we show the errors for the gradient boosting and random forest results with 500 blocks. We define the error as the true hospitalization rate for that zip code minus the predicted value. What we find is that Random Forest is unable to predict in many zip codes because values of the predictor variables are outside those observed within the aggregated blocks, this is a function of the *RandomForest* package and not necessarily of the method itself but does point to a possible reason to steer clear when we have highly skewed predictor variables or variables prone to outliers. To the contrary, Gradient boosting shows an ability to predict in all zip codes with data for each of the predictor variables. Additionally, we see the magnitude of the errors is smaller for Gradient Boosting than Random Forest. There are a few very large errors, but those are for a few zip codes that are incredibly rural and have high hospitalization rates much higher than the mean of 0.65 per 100 people in the year 2013.

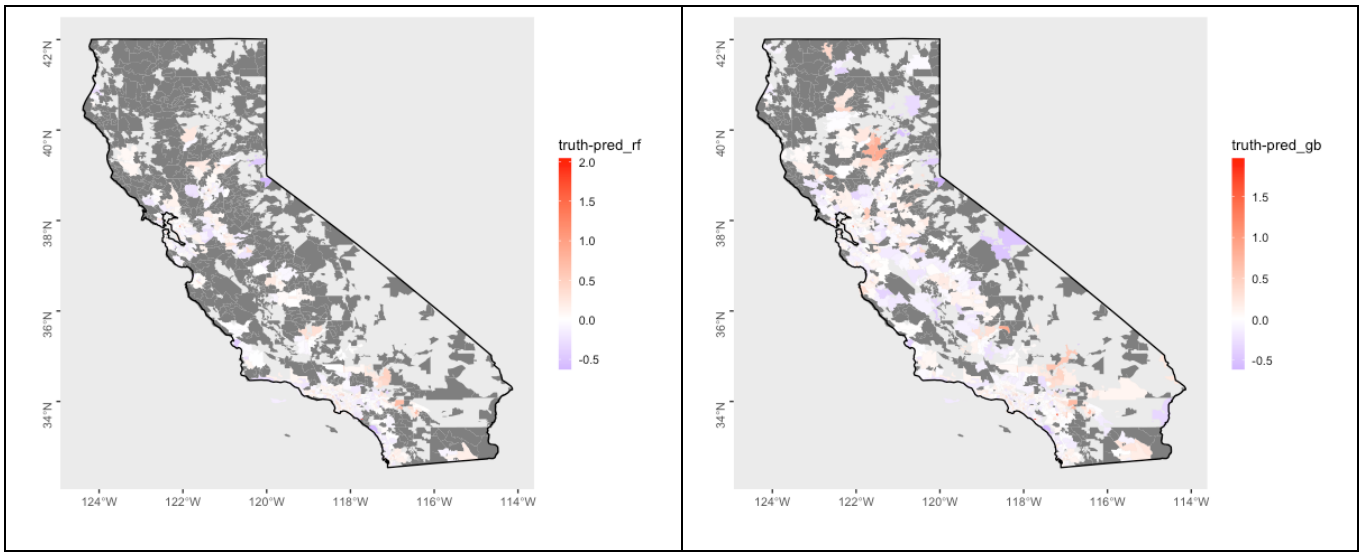

Figure 16 Truth minus predicted value for both the random forest model (left) and the gradient boosting model (right). Dark grey indicated an NA prediction.

In Figure 17, we show the plot of the absolute error values for each model type as a function of the population in each zip code. We can see that as population of a zip code increases the bias goes down. This is to be expected, as we had predicted, because the population values are very skewed allowing for extreme outliers in the hospitalization values. Note that the slope in the Gradient boosting plot is slightly higher in magnitude. This is because of the model predicting at all zip codes, leading to more outliers.

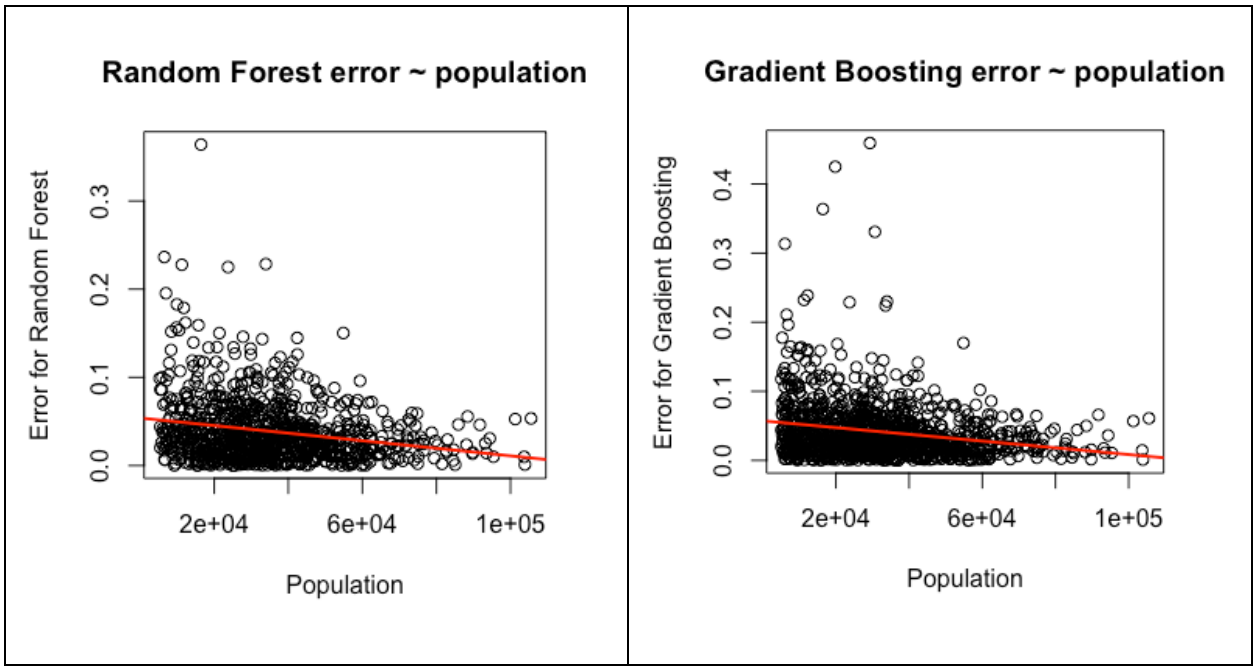

Figure 17 Absolute value of the error from each model (Random Forest, left, Gradient Boosting, right) by the population of each zip code with a least squares line.

Finally, Figure 18 shows the comparison of the error values from both methods on the same zip codes. We can see that the magnitude of the errors are about the same for those zip codes that both methods were able to fit. There is slightly higher error for the Random Forest hence the least squares fit (blue) has a slope slightly less than 1 (slope of the red line). This is due to a few outlier values.. For this reason and those presented previously, we suggest using Gradient boosting.

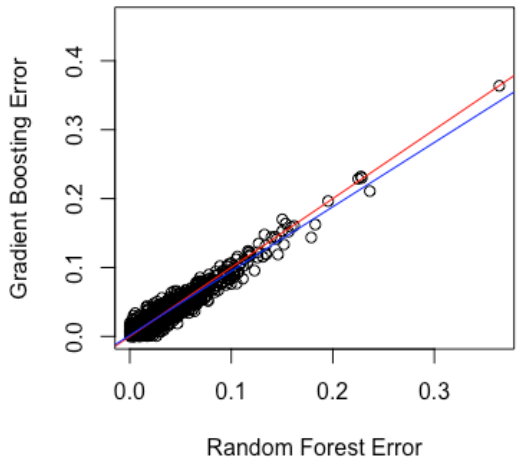

Figure 18 The absolute value of the prediction error for each model against each other. If the models were performing equally as well the blue least squares line should fall on the red line with intercept 0 and slope 1.

Vaccination Rates

Now we show an example of possible use in research. Here we use Covid-19 vaccination data in California through Feb 20, 2022. We use demographic data from the Healthy Places Index to predict the rate of Covid-19 vaccinations in each census tract from the zip code level data provided by the California Government. We retrieved the vaccination data from the https://data.chhs.ca.gov/ website (2022).

We use many variables in the prediction including all 42 percentile-based variables in Healthy Places Index (HPI) and age 5 plus population from the Vaccine dataset to do our predictive models in addition to a region indicator for Southern California and an indicator for the Bay area. The top ten most important variables for the Gradient boosting and Random Forest models are shown in Table 14. The total population and percent of the population which is Native American are found to be the most important followed by bachelor's degree rate,

employed percentile, percent Asian and the Bay Area indicator. We find the general pattern of importance is the same for both models.

Table 14 Most influential variables of the Gradient boosting and Random Forest fits for vaccination rate.

Top Important Variables Random Forest	Top Important Variables Gradient Boosting
Age 5 plus population	Age 5 plus population
Native American Percent	Native American Percent
Bachelor's Education Percentile	Bachelor's Education Percentile
Employed Percentile	Employed percentile
Asian Percent	Asian Percent
Bay Area indicator	Bay Area Indicator
Ozone Percentile	Ozone Percentile
Multiple Race Percent	Multiple Race Percent
Economic Percentile	Alcohol Off Sale Percentile
LEB percentile	Black Percentile

In Figure 19, displayed are the predicted vaccination rates by census tract for both the Random Forest and Gradient boosting models. There is a slight regression toward the mean in the predicted surfaces for each model especially Gradient boosting compared to the true vaccination rate by zip code. Some of this can be explained by census tracts truly covering the entire state whereas zip codes are population dependent and so there are zones where there are no zip codes but there are census tracts. This is most pronounced in the south-eastern portion of the state. This can be handled in a few ways. The zip codes are quite large and the census tracts as well in that region. If we were doing this modeling in practice, we could take the true value in

those places where the downscaled region is about the same area as the lower resolution region. This is a specific solution to downscaling from zip code to census tracts and would not be the case if we were to downscale to a grid. But for instance, if we know that Imperial County has vaccination rates higher than its surroundings, we can use the county as an indicator in the same way we used an indicator for the Bay Area.

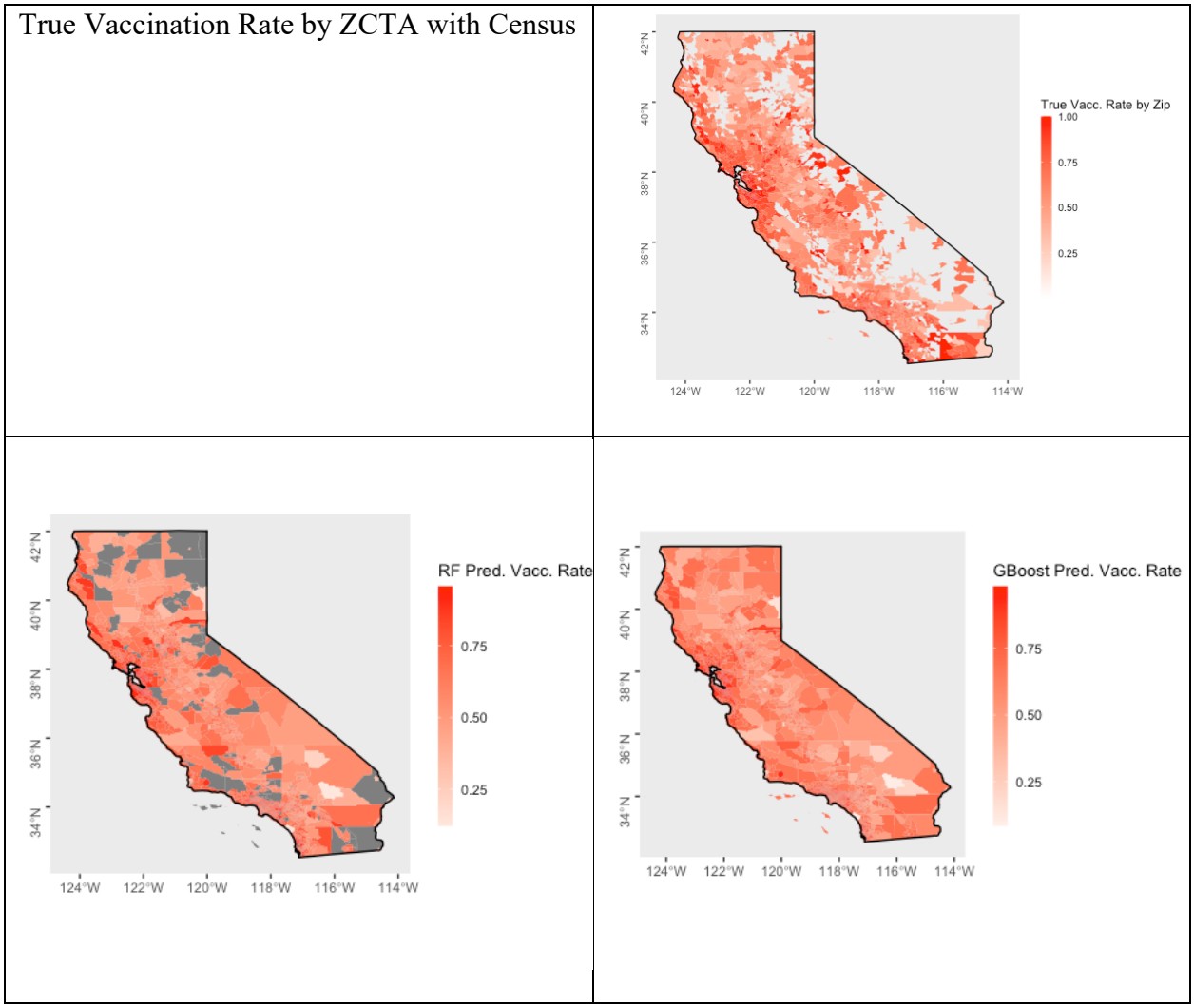

Figure 19 Vaccination Rate in each zip code on top right, and random forest predicted vaccination rate by census tract (bottom left), Gradient boosting predicted vaccination rate by census tract (bottom right).

Discussion

In this paper we introduced a new method for downscaling data in Social and Health Sciences. We used Random Forest and Gradient Boosting to downscale outcome data from a low resolution to a high resolution. In this case either zip codes or census tracts. We find that both random forest and gradient boosting do quite well at downscaling these data accurately. We showed that we have low and varied error values. Especially when the magnitude of the downscaling is as small as 4:1, or 500 blocks to 1700 zip codes. However, upon comparison Gradient Boosting is an improvement over Random Forest because it allows for a prediction from variables outside of the observed range of values leading to no NA values. This is important because with aggregated data, as opposed to individual data, the aggregation strategy is almost always to use the mean or a sum. Using the mean causes outlier values to be shrunk toward the central value.

This approach performs quite well and is novel in many different settings. This is particularly useful in settings where we want to identify small scale areas where further data needs to be collected or areas with a lot of variability. These settings can include anything from finance or housing data as well as social settings outside of the health context. In our application, we looked at vaccine uptake in California across many zip codes and wanted to estimate the vaccine rate in census tracts based on demographic and environmental variables. This approach was able to identify regions where we have high levels of variability and areas of low population that perhaps need more data collection.

This method of downscaling is not the only method of downscaling that exists. In many fields, there are methods of downscaling based on the data that they work with. Downscaling is quite common in climatology, remote sensing, and geography (GIS). Here we will briefly discuss a few methods of downscaling used therein. Perhaps the most prolific use of downscaling occurs in climatology where global climate models (GCM) are downscaled for regional or local future predictions. In this field, Convolutional Neural Networks (CNN) are the most effective predictive procedure currently in use. These are very accurate but rely on access to historical data on the resolution of interest. This allows these models to use this history and the GCM to make the future predictions (Dibike 2006). In a data context, such as that in social or health fields, this will not be possible as none of the variables of interest are available at the desired scale. In Remote Sensing, Gradient Boosting and Random Forests are used much like we introduce here (Atkinson 2013; Pouteau et al 2011; Nicholas et al 2013). However, in Remote Sensing a researcher is almost always downscaling from a grid to another higher resolution grid. This paper shows that Gradient Boosting is effective in an irregular region context. Further, improvements to Gradient Boosting that have already been studied may be worthy additions to this methodology in the context of irregular geographic regions (Bartlett et al 1998). The field of downscaling in these application areas have longer histories and many methods and perhaps the most common predictive variable is the historic data of that variable itself on a high resolution (Fan et al 2021). In a social or health data context, most of these methods would not be useful.

The method presented in this paper has a few limitations. If we have data where we expect extreme outliers downscaling in this way may regress those outliers toward the mean like any modeling procedure where you aren't modeling for extreme values. For this reason, a post

process such as discussed in the results section may be necessary where we look at the places where the model appears to have tempered the signal and adjust our model accordingly and refit. Additionally, these downscaled values cannot be used for further analyses with the same predictor variables that went into the downscaling procedure. Accordingly, this method serves as a purely descriptive first step into the process of downscaling data such that our variables of interest and estimates can be on a higher resolution. Finally, in areas with low population or bad coverage due to zip code size and shape, we have a harder time predicting the outcome value. This is to be expected and is true with most modeling procedures but must be noted.

In the future, we hope to address these limitations by introducing a more systematic method of stepwise modeling or post processing to improve our estimates. Additionally, the inclusion of satellite imagery, Google Street View and even Yelp data products in the analysis can improve predictions greatly without a need to invent new methodology. This in turn would open the door to further analysis with downscaled estimates. Furthermore, this could improve the resolution of our outcome, methods for the use of this data can be taken and adapted from geography and GIS literature.

Finally, in this paper we introduce and adapt a method most used in Remote Sensing to downscale social and health data for the use in descriptive data products. We find Gradient Boosting to be an accurate downscaling technique with a contrived application example of hospitalizations and a demonstration of a possible use case of this method with vaccination data in California.

Acknowledgments

Chapter 4, in full, is currently being prepared for submission for publication of the material, Kristen Hansen; Armin Schwartzman; Tarik Benmarhnia. The dissertation author was the primary researcher and author of this paper.

CONCLUSION

This dissertation presented a set of potential solutions to three problems within spatial environmental epidemiology. These chapters inevitably do not represent an exhaustive description of all the work that went into getting here. We have planned extensions to the methods presented here as well as prep work that would most likely fall into a more applied body of work. This effort however is deserving of notice as it serves as important steps toward inference for Spatial Environmental Epidemiology. With precise inference, we get closer to solving the research problems that are the biggest of this century determining the extent of the adaptability of human health to a rapidly changing climate. The contribution of this dissertation toward that goal is as follows.

First, a novel approach to the modelling of spatially heterogeneous estimates of health outcomes on a fine scale was developed and introduced in Chapter 1 and utilized in Chapter 2. The procedure to implement this modeling framework although composed of existing methodology is unique in that it combines and adapts methods from different fields to create a 2-step modeling procedure that is independent of its forebears. We find, when using this method, that precision in the estimated outcomes are not guaranteed for the entire study region, but this unique combination of methods leads to much better statistical significance in rural areas than a within-community matched design alone as it leverages spatial correlation to reduce variance in the estimates. Although this method performs well, it does have some limiting circumstances particularly when working with environmental data. The Bayesian model that serves as step 2 in the procedure relies on hyper parameters estimated from a semi-variogram, which assumes isotropy in the data. This can be violated in this field. The relaxation of the distribution of the

spatial parameters input into the model reduces the impact of this violation but does not remove it entirely. But this method could possibly be adapted to include anisotropic correlation functions which have been explored in Bayesian modeling but not implemented. This serves as a future endeavor but is made easier with this method as a scaffold.

The second problem that is addressed in this dissertation is the question of mediation analysis in the presence in the spatial autocorrelation. We extend traditional mediation analysis with the use of spatial regression techniques developed in geostatistics to account for the spatial covariance and structure of environmental and health data. We find that if the data of interest is gridded that this method performs just as well as the Product method of mediation in the one-dimensional setting. Although this method does require restrictive assumptions, the Product method remains one of the most popular implementations of mediation analysis in epidemiology and social science literature. Further work must address these assumptions through the extension of standardization techniques like G-Computation to the spatial domain, which has never been addressed. Regardless of these developments the method employed in Chapter 3 is an important extension of the mediation literature in epidemiology and social research to allow for spatially varying decomposed effect estimates. It fits well within the spatial causal inference body of literature and begins to fill a gap in the field of spatial environmental epidemiology.

The spatial mediation problem does not fully account for the spatial nature of epidemiology data however because much epidemiology data is only available on a zip code level. Our method of spatial mediation does not perform well on an aggregated zip code scale in most simulation settings. This leads to the third and final problem tackled in this dissertation.

Namely the downscaling of health and social data to a smaller spatial scale, ultimately a grid setting.

In Chapter 4, a descriptive downscaling technique is borrowed and adapted from Remote Sensing literature. This method of downscaling and furthermore most methods of downscaling have never been employed in epidemiology or social research. This is because downscaling methods have been developed in mostly unrelated fields and for grid-to-grid downscaling. This method that is presented in Chapter 4 performs well to downscale from irregular regions to irregular regions and from a zip code to a grid if the predictive data allows for it. This method is best for descriptive downscaling and not for the downscaling of effect estimates or downscaling the data to be used in modeling at the smaller scale with the predictors that were used to downscale the data originally, but it serves as a great first step.

In the future, there are opportunities to extend the methodology in this dissertation in a few key ways. Mediation in a spatial context is promising as a way to produce causal estimates on a fine spatial scale. For that reason, a concerted effort into the extension of G-computation spatially is important. G-Computation is a standardization method that allows mediation effects to be estimated in the presence of intermediary confounders and with time varying exposures and mediators. This is a natural method to extend to a spatial context as time-varying data, where G-computation is used currently for mediation, has autocorrelation. This autocorrelation in temporal data is one-dimensional, however it may be possible to extend this use of G-computation with two-dimensional autocorrelation. This is not a simple research problem as G-Computation involves making data replicates while maintaining the autocorrelative structure,

which would be incredibly difficult in a spatial context especially when a point in space has no more than a singular row of data.

Continuing with spatial causal inference, Chapter 4 has an extension in progress. Instead of downscaling outcome values we can leverage transportability and data fusion methodology research in recent years to estimate the heterogenous effect modifiers of a particular causal pathway. Then apply these results on the smaller scale, thus it is the case that a downscaled effect estimate for that causal pathway of interest is estimated. This would be referred to as vertical transportability. Transportability research estimates heterogeneous effect modifiers in one research area and uses those effect modifiers to estimate the same coefficient in another area without outcome data. I refer to the existing methodology as horizontal transportability, taking modeling coefficients from one place and transporting it to another location with the collection of effect modifier data. Vertical transportability would use a model from a higher scale to estimate the effects of an exposure on an outcome on the smaller scale which has only aggregated outcome data.

Even with said extensions, the field of spatial causal inference and in turn spatial environmental epidemiology has many remaining research problems that come from the same challenges faced in this dissertation. Namely, challenges are introduced due to spatial heterogeneity of data, spatial dependency, and spatial confounders. In modeling, these items can lead to specious results and incorrect interpretations if models are applied indiscriminately. Assumptions of spatial models must be carefully considered if they are to be used to make causal

claims. No unmeasured confounding and isotropy are the biggest and perhaps most challenging assumptions for causal spatial models.

This does not suggest however that no work has been done to account for these challenges. Inference with spatial data is relatively new but a few major contributions have been made in a variety of fields. These contributions constitute partial solutions to the challenge of spatial confounding and the spatial heterogeneity of the data. This can be accounted for in a variety of ways. Contrarily, inference can be done with the use of spatial case-control matching methods, a version is applied in Chapter 1. Furthermore, autoregressive models like the simultaneous autoregressive model (SAR) can potentially account for spatial confounding by not modeling directly on the response but first subtracting regional means. And finally, the use of spatial smoothing, by jointly modeling the spatial treatment and the spatial confounder, is popular as a neighborhood adjustment strategy to account for spatial confounding. The above methods are all used to account for some measured spatial confounding that we assume is a continuous process on the spatial domain. These are not guaranteed to work if the spatial confounder is on the same spatial scale as the outcome by biasing the effect estimates.

If spatial confounding is unmeasured, then a possible solution is the use of quantitative bias analysis (VanderWeele & Arah 2011). Quantitative bias analysis is commonly the use of a bias formula to estimate a bias factor. The bias factor is then subtracted from the partially adjusted estimate of the exposure on the outcome (Arah 2017). There are many ways to estimate the bias parameters and extension to the use of fixed or probabilistic bias estimation. Other methods of bias analysis include simulation and imputation of the uncontrolled spatial

confounder, propensity calibration through the use of validation data, intensity scores, negative controls or bounding techniques. Additionally, Monte Carlo simulation methods of bias control have been recently shown in a tutorial paper (Banack et al 2021).

These methods of spatial causal inference in the presence of spatial confounding have all been developed or adapted recently, but do not account for the differing spatial scales of the data used in environmental epidemiology or allow for effect decomposition in observational studies. We also do not have a reliable way to estimate the spatial covariance structure of this type of data when it is anisotropic. Many spatial statistical models require stationarity and/or isotropy. Which is quite often violated if the spatial domain of a research problem is wide (like an entire state) as opposed to a small spatial study of an agricultural field, for instance. In Chapters 1, 3 and 4, we present some work-arounds for this assumption like including the variables that potentially cause the anisotropy in the modeling framework as covariates. This could work in some but not all contexts especially when these variables are unmeasured or unknown.

This dissertation aimed to move the field of spatial environmental epidemiology toward inference. This field is racked with challenges to do just that. Not only is the data messy and not ideal but the modeling procedures therein are not built to account for spatial heterogeneity and confounding. With the literature and methodology in other areas however, this dissertation takes a few steps in the right direction. I supply a framework to get spatially heterogeneous predictions of an outcome of interest, work toward effect decomposition in the presence of spatial confounding and autocorrelation, and make the data in this field more tractable and useful with downscaling. For this reason, this dissertation is a substantial contribution to the field which I

hope inspires much more research to improve inference in the field of spatial environmental epidemiology.

REFERENCES

Introduction References

Romanello, M., McGushin, A., Di Napoli, C., Drummond, P., Hughes, N., Jamart, L., & Hamilton, I. (2021). The 2021 report of the Lancet Countdown on health and climate change: code red for a healthy future. *The Lancet*, *398*(10311), 1619-1662.

Chapter 1 References

Aguilera, R., Hansen, K., Gershunov, A., Ilango, S. D., Sheridan, P., & Benmarhnia, T. (2020). Respiratory hospitalizations and wildfire smoke: A spatiotemporal analysis of an extreme firestorm in San Diego County, California. *Environmental Epidemiology*, *4*(5). https://doi.org/10.1097/ee9.0000000000000114

Anderson, B., Dominici, F., Wang, Y., McCormack, M., Bell, M. L., & Peng, R. (2013). Heat-related emergency hospitalizations for respiratory diseases in the Medicare population. *ISEE Conference Abstracts*, *2013*(1), 4710. https://doi.org/10.1289/isee.2013.o-2-28-02

Benmarhnia, T., Kihal-Talantikite, W., Ragettli, M. S., & Deguen, S. (2017). Small-area spatiotemporal analysis of heatwave impacts on elderly mortality in Paris: A cluster analysis approach. *Science of The Total Environment*, *592*, 288–294. https://doi.org/10.1016/j.scitotenv.2017.03.102

Bennett, J. E., Blangiardo, M., Fecht, D., Elliott, P., & Ezzati, M. (2014). Vulnerability to the mortality effects of warm temperature in the districts of England and Wales. *Nature Climate Change*, *4*(4), 269–273. https://doi.org/10.1038/nclimate2123

Bobb, J. F., Peng, R. D., Bell, M. L., & Dominici, F. (2014). Heat-related mortality and adaptation to heat in the United States. *Environmental Health Perspectives*, *122*(8), 811–816. https://doi.org/10.1289/ehp.1307392

Bunker, A., Wildenhain, J., Vandenbergh, A., Henschke, N., Rocklöv, J., Hajat, S., & Sauerborn, R. (2016). Effects of air temperature on climate-sensitive mortality and morbidity outcomes in the elderly; a systematic review and meta-analysis of epidemiological evidence. *EBioMedicine*, *6*, 258–268. https://doi.org/10.1016/j.ebiom.2016.02.034

Cal-Adapt - Exploring California's Climate Change Research. Cal. (2015). Retrieved July 1 2020, from https://cal-adapt.org/

California Energy Commission. (2017). *California Energy Commission - California building climate zone areas*. California Energy Commission. Retrieved June 2018, from https://www.energy.ca.gov/

Chen, K., Bi, J., Chen, J., Chen, X., Huang, L., & Zhou, L., (2015). Influence of heat wave definitions to the added effect of heat waves on daily mortality in Nanjing, China. S*ci. Total Environ.* 506–507, 18–25. https://doi.org/10.1016/j.scitotenv.2014.10.092.

Chien, L.-C., Guo, Y., & Zhang, K. (2016). Spatiotemporal analysis of heat and heat wave effects on elderly mortality in Texas, 2006–2011. *Science of The Total Environment, 562, 845–851.*doi:10.1016/j.scitotenv.2016.04.042

Davis, R., & Novicoff, W. (2018). The Impact of Heat Waves on Emergency Department Admissions in Charlottesville, Virginia, U.S.A. *International Journal of Environmental Research and Public Health, 15(7), 1436.* doi:10.3390/ijerph15071436

Díaz, J., Carmona, R., Mirón, I. J., Ortiz, C., León, I., & Linares, C. (2015). Geographical variation in relative risks associated with heat: Update of Spain's Heat Wave Prevention Plan. *Environment International, 85, 273–283.* doi:10.1016/j.envint.2015.09.022

Efron, B., & Tibshirani, R. J. (1994). *An introduction to the bootstrap*. Chapman & Hall/CRC.

Gao, Y., Gao, X., & Zhang, X. (2017). The 2 °C global temperature target and the evolution of the long-term goal of addressing climate change—from the United Nations Framework Convention on Climate Change to the paris agreement. *Engineering*, *3*(2), 272–278. https://doi.org/10.1016/j.eng.2017.01.022

Goin, D. E., M. Gomez, A., Farkas, K., Zimmerman, S. C., Matthay, E. C., & Ahern, J. (2019). Exposure to community homicide during pregnancy and adverse birth outcomes. *Epidemiology*, *30*(5), 713–722. https://doi.org/10.1097/ede.0000000000001044

Guirguis, K., Gershunov, A., Tardy, A., & Basu, R. (2014). The Impact of Recent Heat Waves on Human Health in California. *Journal of Applied Meteorology and Climatology, 53(1), 3–19.* doi:10.1175/jamc-d-13-0130.1

Hondula, D. M., & Barnett, A. G. (2014). Heat-Related Morbidity in Brisbane, Australia: Spatial Variation and Area-Level Predictors. *Environmental Health Perspectives.*doi:10.1289/ehp.1307496

Hondula, D. M., Davis, R. E., Rocklöv, J., & Saha, M. V. (2013). A time series approach for evaluating intra-city heat-related mortality. *Journal of Epidemiology and Community Health, 67(8), 707–712.* doi:10.1136/jech-2012-202157

Hondula, D. M., Davis, R. E., Leisten, M. J., Saha, M. V., Veazey, L. M., & Wegner, C. R. (2012). Fine-scale spatial variability of heat-related mortality in Philadelphia County, USA, from 1983-2008: a case-series analysis. *Environmental Health, 11(1).*doi:10.1186/1476-069x-11-16

Ingole, V., Sheridan, S. C., Juvekar, S., Achebak, H., & Moraga, P. (2022). Mortality risk attributable to high and low ambient temperature in Pune City, India: A time series analysis from 2004 to 2012. *Environmental Research*, *204*, 112304. https://doi.org/10.1016/j.envres.2021.112304

Ingole, V., Marí-Dell'Olmo, M., Deluca, A., Quijal, M., Borrell, C., Rodríguez-Sanz, M., Achebak, H., Lauwaet, D., Gilabert, J., Murage, P., Hajat, S., Basagaña, X., & Ballester, J. (2020). Spatial variability of heat-related mortality in Barcelona from 1992–2015: A case

crossover study design. *International Journal of Environmental Research and Public Health*, *17*(7), 2553. https://doi.org/10.3390/ijerph17072553

Jänicke, B., Holtmann, A., Kim, K. R., Kang, M., Fehrenbach, U., & Scherer, D. (2018). Quantification and evaluation of intra-urban heat-stress variability in Seoul, Korea. *International Journal of Biometeorology.* doi:10.1007/s00484-018-1631-2

Knowlton, K., Rotkin-Ellman, M., King, G., Margolis, H. G., Smith, D., Solomon, G., Trent, R., & English, P. (2009). The 2006 California Heat Wave: Impacts on Hospitalizations and emergency department visits. *Environmental Health Perspectives*, *117*(1), 61–67. https://doi.org/10.1289/ehp.11594

Kulldorff, M., Mostashari, F., Duczmal, L., Katherine Yih, W., Kleinman, K., & Platt, R. (2007). Multivariate scan statistics for disease surveillance. *Statistics in Medicine, 26(8), 1824–1833.* doi:10.1002/sim.2818

Kulldorff, M. & Nagarwalla, N. (1995) Spatial disease clusters: Detection and Inference. *Statistics in Medicine*, **14**, 799–810.

Li, M., Gu, S., Bi, P., Yang, J., & Liu, Q. (2015). Heat Waves and Morbidity: Current Knowledge and Further Direction-A Comprehensive Literature Review. *International Journal of Environmental Research and Public Health, 12(5), 5256–5283.* doi:10.3390/ijerph120505256

Livneh, B., Bohn, T., Pierce, D. Munoz-Arriola, F., Nijssen, B., Vose, R., Cayan, D.R., & Brekke, L . *(2015)* A spatially comprehensive, hydrometeorological data set for Mexico, the U.S., and Southern Canada 1950–2013. *Sci Data* **2,** 150042 doi:10.1038/sdata.2015.42

Mann, M. E., & Gleick, P. H. (2015). Climate change and California drought in the 21st century. *Proceedings of the National Academy of Sciences, 112(13), 3858–3859.*doi:10.1073/pnas.1503667112

Maps of World (2017). California Latitude and Longitude Map. Maps of World. https://www.mapsofworld.com/

Martiello, M. A., & Giacchi, M. V. (2010). Review article: High temperatures and health outcomes: A review of the literature. *Scandinavian Journal of Public Health*, *38*(8), 826–837. https://doi.org/10.1177/1403494810377685

McElroy, S., Schwarz, L., Green, H., Corcos, I., Guirguis, K., Gershunov, A., & Benmarhnia, T. (2020). Defining heat waves and extreme heat events using sub-regional meteorological data to maximize benefits of early warning systems to Population Health. *Science of The Total Environment*, *721*, 137678. https://doi.org/10.1016/j.scitotenv.2020.137678

Murage, P., Kovats, S., Sarran, C., Taylor, J., McInnes, R., & Hajat, S. (2020). What individual and neighbourhood-level factors increase the risk of heat-related mortality? A case-crossover study of over 185,000 deaths in London using high-resolution climate datasets. *Environment International*, *134*, 105292. https://doi.org/10.1016/j.envint.2019.105292

Nitschke, M., Tucker, G. R., Hansen, A. L., Williams, S., Zhang, Y., & Bi, P. (2011). Impact of two recent extreme heat episodes on morbidity and mortality in Adelaide, South Australia: A case-series analysis. *Environmental Health*, *10*(1). https://doi.org/10.1186/1476-069x-10-42

NOAA. (2018) 'Weather Fatalities 2017', Accessed October 19th, 2018. http://www.nws.noaa.gov/om/hazstats.shtml.

Robine, J.-M., Cheung, S. L., Le Roy, S., Van Oyen, H., Griffiths, C., Michel, J.-P., & Herrmann, F. R. (2008). Death toll exceeded 70,000 in Europe during the summer of 2003. *Comptes Rendus Biologies*, *331*(2), 171–178. https://doi.org/10.1016/j.crvi.2007.12.001

Schwarz, L., Hansen, K., Alari, A., Ilango, S. D., Bernal, N., Basu, R., Gershunov, A., & Benmarhnia, T. (2021). Spatial variation in the joint effect of extreme heat events and ozone on respiratory hospitalizations in California. *Proceedings of the National Academy of Sciences, 118*(22). doi:10.1073/pnas.2023078118

Sherbakov, T., Malig, B., Guirguis, K., Gershunov, A., & Basu, R. (2018). Ambient temperature and added heat wave effects on hospitalizations in California from 1999 to 2009. *Environmental Research*, 160, 83–90. doi:10.1016/j.envres.2017.08.052

Smargiassi, A., Goldberg, M. S., Plante, C., Fournier, M., Baudouin, Y., & Kosatsky, T. (2009). Variation of daily warm season mortality as a function of micro-urban heat islands. *Journal of Epidemiology & Community Health, 63(8), 659–664.* doi:10.1136/jech.2008.078147

Song, J., Yu, H., & Lu, Y. (2021). Spatial-scale dependent risk factors of heat-related mortality: A multiscale geographically weighted regression analysis. *Sustainable Cities and Society*, *74*, 103159. https://doi.org/10.1016/j.scs.2021.103159

Uejio, C. K., Wilhelmi, O. V., Golden, J. S., Mills, D. M., Gulino, S. P., & Samenow, J. P. (2011). Intra-urban societal vulnerability to extreme heat: The role of heat exposure and the built environment, socioeconomics, and neighborhood stability. *Health & Place*, 17(2), 498–507. doi:10.1016/j.healthplace.2010.12.005

Vaneckova, P., Beggs, P. J., & Jacobson, C. R. (2010). Spatial analysis of heat-related mortality among the elderly between 1993 and 2004 in Sydney, Australia. *Social Science & Medicine, 70(2), 293–304.*doi:10.1016/j.socscimed.2009.09.058

Whitman, S., Good, G., Donoghue, E. R., Benbow, N., Shou, W., & Mou, S. (1997). Mortality in Chicago attributed to the July 1995 heat wave. *American Journal of Public Health*, *87*(9), 1515–1518. https://doi.org/10.2105/ajph.87.9.1515

Wilcox, R. R. (2022). *Introduction to robust estimation and hypothesis testing*. Academic Press.

Chapter 2 References

Aguilera, R., Hansen, K., Gershunov, A., Ilango, S. D., Sheridan, P., & Benmarhnia, T. (2020, October). Respiratory hospitalizations and wildfire smoke: a spatiotemporal analysis of an extreme firestorm in San Diego County, California. *Environmental Epidemiology*, *4*(5), e114. https://doi.org/10.1097/ee9.0000000000000114

Analitis, A., Michelozzi, P., D'Ippoliti, D., de'Donato, F., Menne, B., Matthies, F., Atkinson, R. W., Iñiguez, C., Basagaña, X., Schneider, A., Lefranc, A., Paldy, A., Bisanti, L., & Katsouyanni, K. (2014, January). Effects of Heat Waves on Mortality. *Epidemiology*, *25*(1), 15–22. https://doi.org/10.1097/ede.0b013e31828ac01b

Anderson, B., Dominici, F., Wang, Y., McCormack, M., Bell, M. L., & Peng, R. (2013, September 19). Heat-related emergency hospitalizations for respiratory diseases in the Medicare population. *ISEE Conference Abstracts*, *2013*(1), 4710. https://doi.org/10.1289/isee.2013.o-2-28-02

Atkinson*, R., Butland, B., Dimitroulopoulou, S., Heal, M., Stedman, J., Carslaw, N., Jarvis, D., Heaviside, C., Vardoulakis, S., Walton, H., & Anderson, H. R. (2016, August 17). Long-term exposure to ambient ozone and mortality: a quantitative systematic review and meta-analysis of evidence from cohort studies. *ISEE Conference Abstracts*, *2016*(1). https://doi.org/10.1289/isee.2016.3644

Babla, K., Lau, S., Akindolie, O., Radia, T., Modi, N., Kingdon, C., Bush, A., & Gupta, A. (2021, March). Racial microaggressions within respiratory and critical care medicine. *The Lancet Respiratory Medicine*, *9*(3), e27–e28. https://doi.org/10.1016/s2213-2600(21)00001-1

Basu, R., Feng, W. Y., & Ostro, B. D. (2008, January). Characterizing Temperature and Mortality in Nine California Counties. *Epidemiology*, *19*(1), 138–145. https://doi.org/10.1097/ede.0b013e31815c1da7

Basu, R., & Ostro, B. D. (2008, July 15). A Multicounty Analysis Identifying the Populations Vulnerable to Mortality Associated with High Ambient Temperature in California. *American Journal of Epidemiology*, *168*(6), 632–637. https://doi.org/10.1093/aje/kwn170

Basu, R., Pearson, D., Malig, B., Broadwin, R., & Green, R. (2012, November). The Effect of High Ambient Temperature on Emergency Room Visits. *Epidemiology*, *23*(6), 813–820. https://doi.org/10.1097/ede.0b013e31826b7f97

Bell, M. L., Zanobetti, A., & Dominici, F. (2014, May 28). Who is More Affected by Ozone Pollution? A Systematic Review and Meta-Analysis. *American Journal of Epidemiology*, *180*(1), 15–28. https://doi.org/10.1093/aje/kwu115

Benmarhnia, T., Bailey, Z., Kaiser, D., Auger, N., King, N., & Kaufman, J. S. (2016, November). A Difference-in-Differences Approach to Assess the Effect of a Heat Action Plan on Heat-Related Mortality, and Differences in Effectiveness According to Sex, Age, and Socioeconomic Status (Montreal, Quebec). *Environmental Health Perspectives*, *124*(11), 1694–1699. https://doi.org/10.1289/ehp203

Benmarhnia, T., Deguen, S., Kaufman, J. S., & Smargiassi, A. (2015, November). Review Article. *Epidemiology*, *26*(6), 781–793. https://doi.org/10.1097/ede.0000000000000375

Benmarhnia, T., Hajat, A., & Kaufman, J. S. (2021, January 12). Inferential challenges when assessing racial/ethnic health disparities in environmental research. *Environmental Health*, *20*(1). https://doi.org/10.1186/s12940-020-00689-5

Benmarhnia, T., Schwarz, L., Nori-Sarma, A., & Bell, M. L. (2019, October 22). Quantifying the impact of changing the threshold of New York City heat emergency plan in reducing heat-related illnesses. *Environmental Research Letters*, *14*(11), 114006. https://doi.org/10.1088/1748-9326/ab402e

Bouchama, A., Aziz, M. A., Mahri, S. A., Gabere, M. N., Dlamy, M. A., Mohammad, S., Abbad, M. A., & Hussein, M. (2017, August 25). A Model of Exposure to Extreme Environmental Heat Uncovers the Human Transcriptome to Heat Stress. *Scientific Reports*, *7*(1). https://doi.org/10.1038/s41598-017-09819-5

Cal-Adapt. (n.d.). Retrieved September 5, 2022, from https://cal-adapt.org/

Clemesha, R. E. S., Guirguis, K., Gershunov, A., Small, I. J., & Tardy, A. (2017, October 10). California heat waves: their spatial evolution, variation, and coastal modulation by low clouds. *Climate Dynamics*, *50*(11–12), 4285–4301. https://doi.org/10.1007/s00382-017-3875-7

Evans, G. W., & Kantrowitz, E. (2002, May). Socioeconomic Status and Health: The Potential Role of Environmental Risk Exposure. *Annual Review of Public Health*, *23*(1), 303–331. https://doi.org/10.1146/annurev.publhealth.23.112001.112349

Filleul, L., Cassadou, S., Médina, S., Fabres, P., Lefranc, A., Eilstein, D., Le Tertre, A., Pascal, L., Chardon, B., Blanchard, M., Declercq, C., Jusot, J. F., Prouvost, H., & Ledrans, M. (2006, September). The Relation Between Temperature, Ozone, and Mortality in Nine French Cities During the Heat Wave of 2003. *Environmental Health Perspectives*, *114*(9), 1344–1347. https://doi.org/10.1289/ehp.8328

Finley, A. O., Banerjee, S., & Carlin, B. P. (2007). **spBayes**: An*R*Package for Univariate and Multivariate Hierarchical Point-referenced Spatial Models. *Journal of Statistical Software*, *19*(4). https://doi.org/10.18637/jss.v019.i04

Finley, A. O., & Banerjee, S. (2020). Bayesian spatially varying coefficient models in the spBayes R package. *Environmental Modelling & Software*, *125*, 104608. https://doi.org/10.1016/j.envsoft.2019.104608

Fischer, P. H., Brunekreef, B., & Lebret, E. (2004, March). Air pollution related deaths during the 2003 heat wave in the Netherlands. *Atmospheric Environment*, *38*(8), 1083–1085. https://doi.org/10.1016/j.atmosenv.2003.11.010

Forouzanfar, M. H., Afshin, A., Alexander, L. T., Anderson, H. R., Bhutta, Z. A., Biryukov, S., Brauer, M., Burnett, R., Cercy, K., Charlson, F. J., Cohen, A. J., Dandona, L., Estep, K., Ferrari, A. J., Frostad, J. J., Fullman, N., Gething, P. W., Godwin, W. W., Griswold, M., . . . Murray, C. J. L. (2016, October). Global, regional, and national comparative risk assessment of 79 behavioural, environmental and occupational, and metabolic risks or clusters of risks, 1990–2015: a systematic analysis for the Global Burden of Disease Study 2015. *The Lancet*, *388*(10053), 1659–1724. https://doi.org/10.1016/s0140-6736(16)31679-8

Gershengorn, H. B., Patel, S., Shukla, B., Warde, P. R., Bhatia, M., Parekh, D., & Ferreira, T. (2021, August). Association of Race and Ethnicity with COVID-19 Test Positivity and Hospitalization Is Mediated by Socioeconomic Factors. *Annals of the American Thoracic Society*, *18*(8), 1326–1334. https://doi.org/10.1513/annalsats.202011-1448oc

Gershunov, A., Cayan, D. R., & Iacobellis, S. F. (2009, December 1). The Great 2006 Heat Wave over California and Nevada: Signal of an Increasing Trend. *Journal of Climate*, *22*(23), 6181–6203. https://doi.org/10.1175/2009jcli2465.1

Gershunov, A., & Guirguis, K. (2012, September). California heat waves in the present and future. *Geophysical Research Letters*, *39*(18). https://doi.org/10.1029/2012gl052979

Gong, H., Linn, W. S., & McManus, M. S. (1997, January). Attenuated Response to Repeated Daily Ozone Exposures in Asthmatic Subjects. *Archives of Environmental Health: An International Journal*, *52*(1), 34–41. https://doi.org/10.1080/00039899709603797

Grabow, M. L., Spak, S. N., Holloway, T., Stone, B., Mednick, A. C., & Patz, J. A. (2012, January). Air Quality and Exercise-Related Health Benefits from Reduced Car Travel in the Midwestern United States. *Environmental Health Perspectives*, *120*(1), 68–76. https://doi.org/10.1289/ehp.1103440

Green, R. S., Basu, R., Malig, B., Broadwin, R., Kim, J. J., & Ostro, B. (2009, September 22). The effect of temperature on hospital admissions in nine California counties. *International Journal of Public Health*, *55*(2), 113–121. https://doi.org/10.1007/s00038-009-0076-0

Gronlund, C. J. (2014, July 1). Racial and Socioeconomic Disparities in Heat-Related Health Effects and Their Mechanisms: a Review. *Current Epidemiology Reports*, *1*(3), 165–173. https://doi.org/10.1007/s40471-014-0014-4

Gronlund, C. J., Zanobetti, A., Schwartz, J. D., Wellenius, G. A., & O'Neill, M. S. (2014, November). Heat, Heat Waves, and Hospital Admissions among the Elderly in the United States, 1992–2006. *Environmental Health Perspectives*, *122*(11), 1187–1192. https://doi.org/10.1289/ehp.1206132

Ground-level Ozone Pollution. (2022, August 24). US EPA. Retrieved September 5, 2022, from https://www.epa.gov/ground-level-ozone-pollution/

Guirguis, K., Gershunov, A., Tardy, A., & Basu, R. (2014, January). The Impact of Recent Heat Waves on Human Health in California. *Journal of Applied Meteorology and Climatology*, *53*(1), 3–19. https://doi.org/10.1175/jamc-d-13-0130.1

Hackbarth, A. D., Romley, J. A., & Goldman, D. P. (2011, October). Racial and ethnic disparities in hospital care resulting from air pollution in excess of federal standards. *Social Science &Amp; Medicine*, *73*(8), 1163–1168. https://doi.org/10.1016/j.socscimed.2011.08.008

Harlan, S. L., Brazel, A. J., Prashad, L., Stefanov, W. L., & Larsen, L. (2006, December). Neighborhood microclimates and vulnerability to heat stress. *Social Science & Medicine*, *63*(11), 2847–2863. https://doi.org/10.1016/j.socscimed.2006.07.030

Hosmer, D. W., & Lemeshow, S. (1992, September). Confidence Interval Estimation of Interaction. *Epidemiology*, *3*(5), 452–456. https://doi.org/10.1097/00001648-199209000-00012

Jhun, I., Coull, B. A., Zanobetti, A., & Koutrakis, P. (2014, July 25). The impact of nitrogen oxides concentration decreases on ozone trends in the USA. *Air Quality, Atmosphere & Health*, *8*(3), 283–292. https://doi.org/10.1007/s11869-014-0279-2

Jhun, I., Fann, N., Zanobetti, A., & Hubbell, B. (2014, December). Effect modification of ozone-related mortality risks by temperature in 97 US cities. *Environment International*, *73*, 128–134. https://doi.org/10.1016/j.envint.2014.07.009

KELLY, F. J., FULLER, G. W., WALTON, H. A., & FUSSELL, J. C. (2011, December 21). Monitoring air pollution: Use of early warning systems for public health. *Respirology*, *17*(1), 7–19. https://doi.org/10.1111/j.1440-1843.2011.02065.x

Lin, C. M., & Liao, C. M. (2009, June). Temperature-dependent association between mortality rate and carbon monoxide level in a subtropical city: Kaohsiung, Taiwan. *International Journal of Environmental Health Research*, *19*(3), 163–174. https://doi.org/10.1080/09603120802460384

Lindsay, G., Macmillan, A., & Woodward, A. (2010, November 25). Moving urban trips from cars to bicycles: impact on health and emissions. *Australian and New Zealand Journal of Public Health*, *35*(1), 54–60. https://doi.org/10.1111/j.1753-6405.2010.00621.x

Liu, H., Liu, S., Xue, B., Lv, Z., Meng, Z., Yang, X., Xue, T., Yu, Q., & He, K. (2018, January). Ground-level ozone pollution and its health impacts in China. *Atmospheric Environment*, *173*, 223–230. https://doi.org/10.1016/j.atmosenv.2017.11.014

Livneh, B., Bohn, T. J., Pierce, D. W., Munoz-Arriola, F., Nijssen, B., Vose, R., Cayan, D. R., & Brekke, L. (2015, August 18). A spatially comprehensive, hydrometeorological data set for Mexico, the U.S., and Southern Canada 1950–2013. *Scientific Data*, *2*(1). https://doi.org/10.1038/sdata.2015.42

Lowe, D., Ebi, K. L., & Forsberg, B. (2011, December 12). Heatwave Early Warning Systems and Adaptation Advice to Reduce Human Health Consequences of Heatwaves. *International Journal of Environmental Research and Public Health*, *8*(12), 4623–4648. https://doi.org/10.3390/ijerph8124623

Luo, K., Li, R., Wang, Z., Zhang, R., & Xu, Q. (2017, November). Effect modification of the association between temperature variability and daily cardiovascular mortality by air pollutants in three Chinese cities. *Environmental Pollution*, *230*, 989–999. https://doi.org/10.1016/j.envpol.2017.07.045

Madrigano, J., Jack, D., Anderson, G. B., Bell, M. L., & Kinney, P. L. (2015, January 7). Temperature, ozone, and mortality in urban and non-urban counties in the northeastern United States. *Environmental Health*, *14*(1). https://doi.org/10.1186/1476-069x-14-3

Magzamen, S., Moore, B. F., Yost, M. G., Fenske, R. A., & Karr, C. J. (2017, July). Ozone-Related Respiratory Morbidity in a Low-Pollution Region. *Journal of Occupational & Environmental Medicine*, *59*(7), 624–630. https://doi.org/10.1097/jom.0000000000001042

Mahmud, A., Tyree, M., Cayan, D., Motallebi, N., & Kleeman, M. J. (2008, November 7). Statistical downscaling of climate change impacts on ozone concentrations in California. *Journal of Geophysical Research*, *113*(D21). https://doi.org/10.1029/2007jd009534

Maizlish, N., Delaney, T., Dowling, H., Chapman, D. A., Sabo, R., Woolf, S., Orndahl, C., Hill, L., & Snellings, L. (2019, May 16). California Healthy Places Index: Frames Matter. *Public Health Reports*, *134*(4), 354–362. https://doi.org/10.1177/0033354919849882

Maizlish, N., Linesch, N. J., & Woodcock, J. (2017, September). Health and greenhouse gas mitigation benefits of ambitious expansion of cycling, walking, and transit in California. *Journal of Transport &Amp; Health*, *6*, 490–500. https://doi.org/10.1016/j.jth.2017.04.011

Malig, B. J., Pearson, D. L., Chang, Y. B., Broadwin, R., Basu, R., Green, R. S., & Ostro, B. (2016, June). A Time-Stratified Case-Crossover Study of Ambient Ozone Exposure and Emergency Department Visits for Specific Respiratory Diagnoses in California (2005–2008). *Environmental Health Perspectives*, *124*(6), 745–753. https://doi.org/10.1289/ehp.1409495

Marmor, M. (1975, March). Heat Wave Mortality in New York City, 1949 to 1970. *Archives of Environmental Health: An International Journal*, *30*(3), 130–136. https://doi.org/10.1080/00039896.1975.10666661

Medina-Ramón, M., & Schwartz, J. (2008, September). Who is More Vulnerable to Die From Ozone Air Pollution? *Epidemiology*, *19*(5), 672–679. https://doi.org/10.1097/ede.0b013e3181773476

Meng, Y. Y., Rull, R. P., Wilhelm, M., Lombardi, C., Balmes, J., & Ritz, B. (2010, January 7). Outdoor air pollution and uncontrolled asthma in the San Joaquin Valley, California. *Journal of Epidemiology & Community Health*, *64*(2), 142–147. https://doi.org/10.1136/jech.2009.083576

Michelozzi, P., Accetta, G., De Sario, M., D'Ippoliti, D., Marino, C., Baccini, M., Biggeri, A., Anderson, H. R., Katsouyanni, K., Ballester, F., Bisanti, L., Cadum, E., Forsberg, B., Forastiere, F., Goodman, P. G., Hojs, A., Kirchmayer, U., Medina, S., Paldy, A., . . . Perucci, C. A. (2009, March 1). High Temperature and Hospitalizations for Cardiovascular and Respiratory Causes in 12 European Cities. *American Journal of Respiratory and Critical Care Medicine*, *179*(5), 383–389. https://doi.org/10.1164/rccm.200802-217oc

Nuvolone, D., Petri, D., & Voller, F. (2017, May 25). The effects of ozone on human health. *Environmental Science and Pollution Research*, *25*(9), 8074–8088. https://doi.org/10.1007/s11356-017-9239-3

NWS HeatRisk. (n.d.). Retrieved September 5, 2022, from https://www.wrh.noaa.gov/wrh/heatrisk/?wfo=sgx

Pascal, M., Wagner, V., Chatignoux, E., Falq, G., Corso, M., Blanchard, M., Host, S., Larrieu, S., Pascal, L., & Declercq, C. (2012, December). Ozone and short-term mortality in nine French cities: Influence of temperature and season. *Atmospheric Environment*, *62*, 566–572. https://doi.org/10.1016/j.atmosenv.2012.09.009

Pattenden, S., Armstrong, B., Milojevic, A., Heal, M. R., Chalabi, Z., Doherty, R., Barratt, B., Kovats, R. S., & Wilkinson, P. (2010, August 25). Ozone, heat and mortality: acute effects in 15 British conurbations. *Occupational and Environmental Medicine*, *67*(10), 699–707. https://doi.org/10.1136/oem.2009.051714

Phung, D., Thai, P. K., Guo, Y., Morawska, L., Rutherford, S., & Chu, C. (2016, April). Ambient temperature and risk of cardiovascular hospitalization: An updated systematic review and meta-analysis. *Science of the Total Environment*, *550*, 1084–1102. https://doi.org/10.1016/j.scitotenv.2016.01.154

Qian, Z., He, Q., Lin, H. M., Kong, L., Bentley, C. M., Liu, W., & Zhou, D. (2008, September). High Temperatures Enhanced Acute Mortality Effects of Ambient Particle Pollution in

the “Oven” City of Wuhan, China. *Environmental Health Perspectives*, *116*(9), 1172–1178. https://doi.org/10.1289/ehp.10847

Ren, C., Williams, G. M., Mengersen, K., Morawska, L., & Tong, S. (2008, May). Does temperature modify short-term effects of ozone on total mortality in 60 large eastern US communities? — An assessment using the NMMAPS data. *Environment International*, *34*(4), 451–458. https://doi.org/10.1016/j.envint.2007.10.001

Ren, C., Williams, G. M., Mengersen, K., Morawska, L., & Tong, S. (2009, October 19). Temperature Enhanced Effects of Ozone on Cardiovascular Mortality in 95 Large US Communities, 1987–2000: Assessment Using the NMMAPS Data. *Archives of Environmental & Occupational Health*, *64*(3), 177–184. https://doi.org/10.1080/19338240903240749

Richardson, D. B., & Kaufman, J. S. (2009, February 11). Estimation of the Relative Excess Risk Due to Interaction and Associated Confidence Bounds. *American Journal of Epidemiology*, *169*(6), 756–760. https://doi.org/10.1093/aje/kwn411

ROTHMAN, K. J., GREENLAND, S., & WALKER, A. M. (1980, October). CONCEPTS OF INTERACTION. *American Journal of Epidemiology*, *112*(4), 467–470. https://doi.org/10.1093/oxfordjournals.aje.a113015

Schnell, J. L., & Prather, M. J. (2017, February 27). Co-occurrence of extremes in surface ozone, particulate matter, and temperature over eastern North America. *Proceedings of the National Academy of Sciences*, *114*(11), 2854–2859. https://doi.org/10.1073/pnas.1614453114

Schnittker, J. (2004, September). Education and the Changing Shape of the Income Gradient in Health. *Journal of Health and Social Behavior*, *45*(3), 286–305. https://doi.org/10.1177/002214650404500304

Scortichini, M., De Sario, M., de’Donato, F., Davoli, M., Michelozzi, P., & Stafoggia, M. (2018, August 17). Short-Term Effects of Heat on Mortality and Effect Modification by Air Pollution in 25 Italian Cities. *International Journal of Environmental Research and Public Health*, *15*(8), 1771. https://doi.org/10.3390/ijerph15081771

Semenza, J. C., Wilson, D. J., Parra, J., Bontempo, B. D., Hart, M., Sailor, D. J., & George, L. A. (2008, July). Public perception and behavior change in relationship to hot weather and air pollution. *Environmental Research*, *107*(3), 401–411. https://doi.org/10.1016/j.envres.2008.03.005

Shi, W., Sun, Q., Du, P., Tang, S., Chen, C., Sun, Z., Wang, J., Li, T., & Shi, X. (2020, February 5). Modification Effects of Temperature on the Ozone–Mortality Relationship: A Nationwide Multicounty Study in China. *Environmental Science &Amp; Technology*, *54*(5), 2859–2868. https://doi.org/10.1021/acs.est.9b05978

Su, J. G., Morello-Frosch, R., Jesdale, B. M., Kyle, A. D., Shamasunder, B., & Jerrett, M. (2009, October 15). An Index for Assessing Demographic Inequalities in Cumulative Environmental Hazards with Application to Los Angeles, California. *Environmental Science & Technology*, *43*(20), 7626–7634. https://doi.org/10.1021/es901041p

Toloo, G., FitzGerald, G., Aitken, P., Verrall, K., & Tong, S. (2013, April 7). Evaluating the effectiveness of heat warning systems: systematic review of epidemiological evidence. *International Journal of Public Health*, *58*(5), 667–681. https://doi.org/10.1007/s00038-013-0465-2

Tong, S., Ren, C., & Becker, N. (2010, January 5). Excess deaths during the 2004 heatwave in Brisbane, Australia. *International Journal of Biometeorology*, *54*(4), 393–400. https://doi.org/10.1007/s00484-009-0290-8

Tong, S., Wang, X. Y., & Guo, Y. (2012, May 24). Assessing the Short-Term Effects of Heatwaves on Mortality and Morbidity in Brisbane, Australia: Comparison of Case-Crossover and Time Series Analyses. *PLoS ONE*, *7*(5), e37500. https://doi.org/10.1371/journal.pone.0037500

VanderWeele, T. J., & Knol, M. J. (2014, January 1). A Tutorial on Interaction. *Epidemiologic Methods*, *3*(1). https://doi.org/10.1515/em-2013-0005

VanderWeele, T. J., & Robinson, W. R. (2014, July). On the Causal Interpretation of Race in Regressions Adjusting for Confounding and Mediating Variables. *Epidemiology*, *25*(4), 473–484. https://doi.org/10.1097/ede.0000000000000105

Wang, J., Zhang, X., Guo, Z., & Lu, H. (2017, October). Developing an early-warning system for air quality prediction and assessment of cities in China. *Expert Systems With Applications*, *84*, 102–116. https://doi.org/10.1016/j.eswa.2017.04.059

Wilson, A., Reich, B., Neas, L. M., & Rappold, A. (2013, September 19). Modeling the Effect of Temperature on Ozone-Related Mortality. *ISEE Conference Abstracts*, *2013*(1), 3932. https://doi.org/10.1289/isee.2013.p-3-03-25

Xu, Z., FitzGerald, G., Guo, Y., Jalaludin, B., & Tong, S. (2016, April). Impact of heatwave on mortality under different heatwave definitions: A systematic review and meta-analysis. *Environment International*, *89–90*, 193–203. https://doi.org/10.1016/j.envint.2016.02.007

Zahran, S., Brody, S. D., Maghelal, P., Prelog, A., & Lacy, M. (2008, October). Cycling and walking: Explaining the spatial distribution of healthy modes of transportation in the United States. *Transportation Research Part D: Transport and Environment*, *13*(7), 462–470. https://doi.org/10.1016/j.trd.2008.08.001

Chapter 3 References

Aalen, O. O., Stensrud, M. J., Didelez, V., Daniel, R., Roysland, K., & Strohmaier, S. (2019). Time-dependent mediators in survival analysis: Modeling direct and indirect effects with the additive hazards model. *Biometrical Journal*. doi:10.1002/bimj.201800263

Atkinson, P. M., German, S. E., Sear, D. A., & Clark, M. J. (2003). Exploring the Relations Between Riverbank Erosion and Geomorphological Controls Using Geographically Weighted Logistic Regression. *Geographical Analysis*, *35*(1), 58–82. doi:10.1111/j.1538-4632.2003.tb01101.x

Baron, R. M., & Kenny, D. A. (1986). The moderator\textendashmediator variable distinction in social psychological research: Conceptual, strategic, and statistical considerations. *Journal of Personality and Social Psychology*, *51*(6), 1173–1182. doi:10.1037/0022-3514.51.6.1173

Bellavia, A., & Valeri, L. (2017). Decomposition of the Total Effect in the Presence of Multiple Mediators and Interactions. *American Journal of Epidemiology*, *187*(6), 1311–1318. doi:10.1093/aje/kwx355

Benmarhnia, T., Grenier, P., Brand, A., Fournier, M., Deguen, S., & Smargiassi, A. (2015). Quantifying Vulnerability to Extreme Heat in Time Series Analyses: A Novel Approach Applied to Neighborhood Social Disparities under Climate Change. *International Journal of Environmental Research and Public Health*, *12*(9), 11869–11879. doi:10.3390/ijerph120911869

Benmarhnia, T., Hajat, A., & Kaufman, J. S. (2021). Inferential challenges when assessing racial/ethnic health disparities in environmental research. *Environmental Health: A Global Access Science Source*, *20*. doi:10.1186/s12940-020-00689-5

Bind, M. A. C., Vanderweele, T. J., Coull, B. A., & Schwartz, J. D. (2016). Causal mediation analysis for longitudinal data with exogenous exposure. *Biostatistics*, *17*. doi:10.1093/biostatistics/kxv029

Brunsdon, C., Fotheringham, S., & Charlton, M. (1998). Geographically Weighted Regression. *Journal of the Royal Statistical Society: Series D (The Statistician)*, *47*(3), 431–443. doi:10.1111/1467-9884.00145

Brunsdon, Chris, Fotheringham, A. S., & Charlton, M. E. (2010). Geographically Weighted Regression: A Method for Exploring Spatial Nonstationarity. *Geographical Analysis*, *28*(4), 281–298. doi:10.1111/j.1538-4632.1996.tb00936.x

Cho, S.-H., & Huang, Y.-T. (2018). Mediation analysis with causally ordered mediators using Cox proportional hazards model. *Statistics in Medicine*, *38*(9), 1566–1581. doi:10.1002/sim.8058

Chun, Y., & Griffith, D. A. (2014). A quality assessment of eigenvector spatial filtering based parameter estimates for the normal probability model. *Spatial Statistics*, *10*. doi:10.1016/j.spasta.2014.04.001

Coffman, D. L., & Zhong, W. (2012). Assessing mediation using marginal structural models in the presence of confounding and moderation. *Psychological Methods*, *17*(4), 642–664. doi:10.1037/a0029311

Daniel, R. M., Stavola, B. L. D., Cousens, S. N., & Vansteelandt, S. (2014). Causal mediation analysis with multiple mediators. *Biometrics*, *71*(1), 1–14. doi:10.1111/biom.12248

Davis, M. L., Neelon, B., Nietert, P. J., Burgette, L. F., Hunt, K. J., Lawson, A. B., & Egede, L. E. (2019). Analysis of racial differences in hospital stays in the presence of geographic confounding. *Spatial and Spatio-Temporal Epidemiology*, *30*, 100284. https://doi.org/10.1016/j.sste.2019.100284

Doherty, R. M., Heal, M. R., Wilkinson, P., Pattenden, S., Vieno, M., Armstrong, B., … Stevenson, D. S. (2009). Current and future climate- and air pollution-mediated impacts on human health. *Environmental Health*, *8*(Suppl 1), S8. doi:10.1186/1476-069x-8-s1-s8

Dominici, F., Zanobetti, A., Schwartz, J., Braun, D., Sabath, B., & Wu, X. (2022). Assessing Adverse Health Effects of Long-Term Exposure to Low Levels of Ambient Air Pollution: Implementation of Causal Inference Methods. *Research Report (Health Effects Institute).*, 1–56.

Dray, S., Legendre, P., & Peres-Neto, P. R. (2006). Spatial modelling: a comprehensive framework for principal coordinate analysis of neighbour matrices (PCNM). *Ecological Modelling*, *196*. doi:10.1016/j.ecolmodel.2006.02.015

Drineas, P., & Mahoney, M. W. (2005). On the Nyström method for approximating a Gram matrix for improved kernel-based learning. *Journal of Machine Learning Research*, *6*.

Finkelstein, M. M., Jerrett, M., DeLuca, P., Finkelstein, N., Verma, D. K., Chapman, K., & Sears, M. R. (2003). Relation between income, air pollution and mortality: A cohort study. *CMAJ*, *169*.

Gan, X., Weng, J., Li, W., & Han, M. (2020). Spatial-temporal varying coefficient model for lane-changing behavior in work zone merging areas. *Journal of Transportation Safety & Security*, *14*(6), 949–972. https://doi.org/10.1080/19439962.2020.1864075

Gelfand, A. E., Kim, H.-J., Sirmans, C. F., & Banerjee, S. (2003). Spatial modeling with spatially varying coefficient processes. *Journal of the American Statistical Association*, *98*(462), 387–396. https://doi.org/10.1198/016214503000170

Giffin, A., Reich, B. J., Yang, S., & Rappold, A. G. (2022). Generalized propensity score approach to causal inference with spatial interference. *Biometrics*. https://doi.org/10.1111/biom.13745

Griffith, D. (2003). *Spatial Autocorrelation and Spatial Filtering: Gaining Understanding through Theory and Scientific Visualization*. Springer-Verlag.

Griffith, D. A. (2008). Spatial-filtering-based contributions to a critique of geographically weighted regression (GWR). *Environment and Planning A*, *40*. doi:10.1068/a38218

Holland, P. W., & Rubin, D. B. (1987). CAUSAL INFERENCE IN RETROSPECTIVE STUDIES. *ETS Research Report Series*, *1987*(1), 203–231. doi:10.1002/j.2330-8516.1987.tb00211.x

Hossin, M. Z., Koupil, I., & Falkstedt, D. (2019). Early life socioeconomic position and mortality from cardiovascular diseases: An application of causal mediation analysis in the Stockholm Public Health Cohort. *BMJ Open*, *9*. doi:10.1136/bmjopen-2018-026258

Huang, B., Wu, B., & Barry, M. (2010). Geographically and temporally weighted regression for modeling spatio-temporal variation in house prices. *International Journal of Geographical Information Science*, *24*(3), 383–401. doi:10.1080/13658810802672469

Hystad, P., Larkin, A., Rangarajan, S., AlHabib, K. F., Avezum, Á., Calik, K. B. T., … Brauer, M. (2020). Associations of outdoor fine particulate air pollution and cardiovascular disease in 157 436 individuals from 21 high-income, middle-income, and low-income countries (PURE): a prospective cohort study. *The Lancet Planetary Health*, *4*. doi:10.1016/S2542-5196(20)30103-0

Imai, K., Keele, L., & Tingley, D. (2010). A general approach to causal mediation analysis. *Psychological Methods*, *15*(4), 309–334. doi:10.1037/a0020761

Imbens., G. W., & Rubin, D. B. (2015). *Causal inference For statistics, social, and biomedical sciences: An introduction*. Cambridge Univ. Press.

Jiang, H., Hu, H., Li, B., Zhang, Z., Wang, S., & Lin, T. (2021). Understanding the non-stationary relationships between corn yields and meteorology via a spatiotemporally varying coefficient model. *Agricultural and Forest Meteorology*, *301-302*, 108340. https://doi.org/10.1016/j.agrformet.2021.108340

Kaufman, J. S., MacLehose, R. F., & Kaufman, S. (2004). A further critique of the analytic strategy of adjusting for covariates to identify biologic mediation. *Epidemiologic Perspectives & Innovations*, *1*(1), 4.

Kim, C., Daniels, M. J., Hogan, J. W., Choirat, C., & Zigler, C. M. (2019). BAYESIAN METHODS FOR MULTIPLE MEDIATORS: RELATING PRINCIPAL

STRATIFICATION AND CAUSAL MEDIATION IN THE ANALYSIS OF POWER PLANT EMISSION CONTROLS. *Annals of Applied Statistics*, 1927–1956.

Lange, T., Vansteelandt, S., & Bekaert, M. (2012). A Simple Unified Approach for Estimating Natural Direct and Indirect Effects. *American Journal of Epidemiology*, *176*(3), 190–195. doi:10.1093/aje/kwr525

Larsen, A., Yang, S., Reich, B. J., & Rappold, A. G. (2022). A spatial causal analysis of wildland fire-contributed PM2.5 using numerical model output. *The Annals of Applied Statistics*, *16*(4). https://doi.org/10.1214/22-aoas1610

Lin, S.-H., Young, J. G., Logan, R., & VanderWeele, T. J. (χ.χ.). *Mediation analysis for a survival outcome with time-varying exposures, mediators, and confounders*.

Lu, J., & Tang, G. A. (2011). *The spatial distribution cause analysis of theft crime rate based on GWR Model*. doi:10.1109/ICMT.2011.6002711

Lu, B., Charlton, M., & Fotheringhama, A. S. (2011). Geographically Weighted Regression Using a Non-Euclidean Distance Metric with a Study on London House Price Data. *Procedia Environmental Sciences*, *7*, 92–97. doi:10.1016/j.proenv.2011.07.017

Lu, B., Charlton, M., Harris, P., & Fotheringham, A. S. (2014). Geographically weighted regression with a non-Euclidean distance metric: a case study using hedonic house price data. *International Journal of Geographical Information Science*, *28*(4), 660–681. doi:10.1080/13658816.2013.865739

Mendes, J. J., Viana, J., Cruz, F., Pereira, D., Ferreira, S., Pereira, P., … Delgado, A. S. (2021). Blood pressure and tooth loss: A large cross-sectional study with age mediation analysis. *International Journal of Environmental Research and Public Health*, *18*. doi:10.3390/ijerph18010285

Moran, P. A. (1950). Notes on continuous stochastic phenomena. *Biometrika*, *37*. doi:10.1093/biomet/37.1-2.17

Mosquera, P. A., Sebastian, M. S., Waenerlund, A.-K., Ivarsson, A., Weinehall, L., & Gustafsson, P. E. (1 2016). Income-related inequalities in cardiovascular disease from mid-life to old age in a Northern Swedish cohort: A decomposition analysis. *Social Science and Medicine*, *149*. doi:10.1016/j.socscimed.2015.12.017

Murakami, Daisuke, & Griffith, D. A. (2015). Random effects specifications in eigenvector spatial filtering: a simulation study. *Journal of Geographical Systems*, *17*. doi:10.1007/s10109-015-0213-7

Murakami, D. (2017). spmoran: An R package for Moran's eigenvector-based spatial regression analysis. *arXiv*.

Murakami, Daisuke, & Griffith, D. A. (2019b). Spatially varying coefficient modeling for large datasets: Eliminating N from spatial regressions. *Spatial Statistics*, *30*. doi:10.1016/j.spasta.2019.02.003

Murakami, Daisuke, & Griffith, D. A. (2019a). Eigenvector Spatial Filtering for Large Data Sets: Fixed and Random Effects Approaches. *Geographical Analysis*, *51*. doi:10.1111/gean.12156

Naimi, A. I., Cole, S. R., & Kennedy, E. H. (2016). An Introduction to G Methods. *International Journal of Epidemiology*, dyw323. doi:10.1093/ije/dyw323

Nguyen, Q. C., Osypuk, T. L., Schmidt, N. M., Glymour, M. M., & Tchetgen, E. J. T. (2015). Practical Guidance for Conducting Mediation Analysis With Multiple Mediators Using Inverse Odds Ratio Weighting. *American Journal of Epidemiology*, *181*(5), 349–356. doi:10.1093/aje/kwu278

OEHHA, C. (2018). *CalEnviroScreen*.

Páez, A. (2004a). Anisotropic Variance Functions in Geographically Weighted Regression Models. *Geographical Analysis*, *36*(4), 299–314. doi:10.1111/j.1538-4632.2004.tb01138.x

Páez, A. (2004b). Anisotropic Variance Functions in Geographically Weighted Regression Models. *Geographical Analysis*, *36*(4), 299–314. doi:10.1111/j.1538-4632.2004.tb01138.x

Paulsen, K. D., & Jiang, H. (1995). Spatially varying optical property reconstruction using a finite element diffusion equation approximation. *Medical Physics*, *22*(6), 691–701. https://doi.org/10.1118/1.597488

Pearl, J. (2001). Direct and Indirect Effects. *Proceedings of the Seventeenth Conference on Uncertainty in Artificial Intelligence*, 411–420. Παρουσιάστηκε στο Seattle, Washington. San Francisco, CA, USA: Morgan Kaufmann Publishers Inc.

Reich, B. J., Yang, S., Guan, Y., Giffin, A. B., Miller, M. J., & Rappold, A. (2021). A Review of Spatial Causal Inference Methods for Environmental and Epidemiological Applications. *International Statistical Review*, *89*. doi:10.1111/insr.12452

Richiardi, L., Bellocco, R., & Zugna, D. (2013). Mediation analysis in epidemiology: methods, interpretation and bias. *International Journal of Epidemiology*, *42*(5), 1511–1519. doi:10.1093/ije/dyt127

Robins, J. M., & Greenland, S. (1992). Identifiability and Exchangeability for Direct and Indirect Effects. *Epidemiology*, *3*(2), 143–155.

Rubin, D. B. (1974). Estimating causal effects of treatments in randomized and nonrandomized studies. *Journal of Educational Psychology*, *66*(5), 688–701. doi:10.1037/h0037350

Rubin, D. B. (2005). Causal Inference Using Potential Outcomes. *Journal of the American Statistical Association*, *100*. doi:10.1198/016214504000001880

Rudolph, K., Sofrygin, O., Zheng, W., & Van Der Laan, M. J. (2018). Robust and flexible estimation of stochastic mediation effects: A proposed method and example in a randomized trial setting. *Epidemiologic Methods*, *7*(1). doi:10.1515/em-2017-0007

Rudolph, K. E., Goin, D. E., Paksarian, D., Crowder, R., Merikangas, K. R., & Stuart, E. A. (2018). Causal Mediation Analysis With Observational Data: Considerations and Illustration Examining Mechanisms Linking Neighborhood Poverty to Adolescent Substance Use. *American Journal of Epidemiology*, *188*(3), 598–608. doi:10.1093/aje/kwy248

Rudolph, K. E., Sofrygin, O., & van der Laan, M. J. (2020). Complier Stochastic Direct Effects: Identification and Robust Estimation. *Journal of the American Statistical Association*, 1–11. doi:10.1080/01621459.2019.1704292

Ruppert, D., Sheather, S. J., & Wand, M. P. (1995). An effective bandwidth selector for local least squares regression. *Journal of the American Statistical Association*, *90*. doi:10.1080/01621459.1995.10476630

Southern California, Public Health Alliance of. (2018). *Healthy Places Index*.

Steen, J., Loeys, T., Moerkerke, B., Vansteelandt, S., University, G., University, G., … University, G. (χ.χ.). *Medflex: An R Package for Flexible Mediation Analysis Using Natural Effect Models*.

Syriopoulous, E., Rutherford, M. J., & Lambert, P. C. (2021). Understanding disparities in cancer prognosis: An extension of mediation analysis to the relative survival framework. *Biometrical Journal*, *63*. doi:10.1002/bimj.201900355

Tchetgen, E. J. T. (2013). Inverse odds ratio-weighted estimation for causal mediation analysis. *Statistics in Medicine*, *32*(26), 4567–4580. doi:10.1002/sim.5864

Valeri, L., & VanderWeele, T. J. (2013). Mediation analysis allowing for exposure\textendashmediator interactions and causal interpretation: Theoretical assumptions and implementation with SAS and SPSS macros. *Psychological Methods*, *18*(2), 137–150. doi:10.1037/a0031034

VanderWeele, T. J., & Vansteelandt, S. (2010). Odds Ratios for Mediation Analysis for a Dichotomous Outcome. *American Journal of Epidemiology*, *172*(12), 1339–1348.

Vanderweele, T. J. (2011). Controlled Direct and Mediated Effects: Definition, Identification and Bounds. *Scandinavian Journal of Statistics*, *38*. doi:10.1111/j.1467-9469.2010.00722.x

VanderWeele, Tyler J., Vansteelandt, S., & Robins, J. M. (2014). Effect Decomposition in the Presence of an Exposure-Induced Mediator-Outcome Confounder. *Epidemiology*, *25*(2), 300–306. doi:10.1097/ede.0000000000000034

Wang, N., Mei, C.-L., & Yan, X.-D. (2008). Local linear estimation of spatially varying coefficient models: An improvement on the geographically weighted regression technique. *Environment and Planning A: Economy and Space*, *40*(4), 986–1005. https://doi.org/10.1068/a3941

Wheeler, D. C. (2013). Geographically Weighted Regression. Στο *Handbook of Regional Science* (σσ. 1435–1459). doi:10.1007/978-3-642-23430-9_77

Wodtke, G. T., & Zhou, X. (2020). Effect Decomposition in the Presence of Treatment-induced Confounding. *Epidemiology*, *31*(3), 369–375. doi:10.1097/ede.0000000000001168

Ye, Y., Huang, X., & Liu, Y. (2021). Social support and academic burnout among university students: A moderated mediation model. *Psychology Research and Behavior Management*, *14*. doi:10.2147/PRBM.S300797

Zang, Z., Ji, R., Feng, Z., Chen, C., Li, S., & Davis, C. S. (2021). Spatially varying phytoplankton seasonality on the northwest Atlantic Shelf: A model-based assessment of patterns, drivers, and implications. *ICES Journal of Marine Science*, *78*(5), 1920–1934. https://doi.org/10.1093/icesjms/fsab102

Chapter 4 References

Atkinson, P. M. (2013). Downscaling in remote sensing. *International Journal of Applied Earth Observation and Geoinformation*, *22*. https://doi.org/10.1016/j.jag.2012.04.012

Bartlett, P., Freund, Y., Lee, W. S., & Schapire, R. E. (1998). Boosting the margin: A new explanation for the effectiveness of voting methods. *The Annals of Statistics*, *26*(5). https://doi.org/10.1214/aos/1024691352

Bedia, J., Baño-Medina, J., Legasa, M., Iturbide, M., Manzanas, R., Herrera, S., Casanueva, A., San-Martín, D., Cofiño, A., & Gutiérrez, J. M. (2019). Statistical downscaling with the downscaleR package: Contribution to the VALUE intercomparison experiment. *Geoscientific Model Development Discussions*. https://doi.org/10.5194/gmd-2019-224

Dibike, Y. B., & Coulibaly, P. (2006). Temporal neural networks for downscaling climate variability and extremes. *Neural Networks*, *19*(2). https://doi.org/10.1016/j.neunet.2006.01.003

Fan, X., Jiang, L., & Gou, J. (2021). Statistical downscaling and projection of future temperatures across the Loess Plateau, China. *Weather and Climate Extremes*, *32*. https://doi.org/10.1016/j.wace.2021.100328

Gotway, C. A., & Young, L. J. (2002). Combining incompatible spatial data. *Journal of the American Statistical Association*, *97*(458), 632–648. https://doi.org/10.1198/016214502760047140

Hanigan, I. C., Chaston, T. B., Hinze, B., Dennekamp, M., Jalaludin, B., Kinfu, Y., & Morgan, G. G. (2019). A statistical downscaling approach for generating high spatial resolution health risk maps: a case study of road noise and ischemic heart disease mortality in Melbourne, Australia. *International Journal of Health Geographics*, *18*(1). https://doi.org/10.1186/s12942-019-0184-x

Matisziw, T. C., Grubesic, T. H., & Wei, H. (2008). Downscaling spatial structure for the analysis of epidemiological data. *Computers, Environment and Urban Systems*, *32*(1). https://doi.org/10.1016/j.compenvurbsys.2007.06.002

Nicolas, G., Robinson, T. P., Wint, G. R. W., Conchedda, G., Cinardi, G., & Gilbert, M. (2016). Using Random Forest to improve the downscaling of global livestock census data. *PLoS ONE*, *11*(3). https://doi.org/10.1371/journal.pone.0150424

Pouteau, R., Rambal, S., Ratte, J.-P., Gogé, F., Joffre, R., & Winkel, T. (2011). Downscaling MODIS-derived maps using GIS and boosted regression trees: The case of frost occurrence over the arid Andean highlands of Bolivia. *Remote Sensing of Environment*, *115*(1). https://doi.org/10.1016/j.rse.2010.08.011

Serifi, A., Günther, T., & Ban, N. (2021). Spatio-Temporal Downscaling of Climate Data Using Convolutional and Error-Predicting Neural Networks. *Frontiers in Climate*, *3*. https://doi.org/10.3389/fclim.2021.656479

Shen, Z., & Yong, B. (2021). Downscaling the GPM-based satellite precipitation retrievals using gradient boosting decision tree approach over Mainland China. *Journal of Hydrology*, *602*. https://doi.org/10.1016/j.jhydrol.2021.126803

Wei, Z., Meng, Y., Zhang, W., Peng, J., & Meng, L. (2019). Downscaling SMAP soil moisture estimation with gradient boosting decision tree regression over the Tibetan Plateau. *Remote Sensing of Environment*, *225*. https://doi.org/10.1016/j.rse.2019.02.022

Zhang, J., Liu, K., & Wang, M. (2021). Downscaling groundwater storage data in China to a 1-km resolution using machine learning methods. *Remote Sensing*, *13*(3). https://doi.org/10.3390/rs13030523

Conclusion References

Akbari, K., Winter, S. & Tomko, M. (2021). Spatial Causality: A Systematic Review on Spatial Causal Inference. *GEOGRAPHICAL ANALYSIS*, pp. 34-. doi:10.1111/gean.12312

Arah, O. A. (2017). Bias analysis for uncontrolled confounding in the health sciences. *Annual review of public health*, *38*, 23-38.

Banack, H. R., Hayes-Larson, E., & Mayeda, E. R. (2021). Monte Carlo simulation approaches for quantitative bias analysis: a tutorial. *Epidemiologic Reviews*, *43*(1), 106-117.

Christiansen, R., Baumann, M., Kuemmerle, T., Mahecha, M. D., & Peters, J. (2022). Toward causal inference for spatio-temporal data: Conflict and forest loss in Colombia. *Journal of the American Statistical Association*, *117*(538), 591–601. https://doi.org/10.1080/01621459.2021.2013241

Gao, B., Wang, J., Stein, A., & Chen, Z. (2022). Causal inference in spatial statistics. *Spatial Statistics*, *50*, 100621. https://doi.org/10.1016/j.spasta.2022.100621

Reich, B. J., Yang, S., Guan, Y., Giffin, A. B., Miller, M. J., & Rappold, A. (2021). A review of spatial causal inference methods for environmental and epidemiological applications. *International Statistical Review*, *89*(3), 605–634. https://doi.org/10.1111/insr.12452

VanderWeele, T. J., & Arah, O. A. (2011). Bias formulas for sensitivity analysis of unmeasured confounding for general outcomes, treatments, and confounders. *Epidemiology*, 42-52.